EUROPEAN ORGANISATION FOR NUCLEAR RESEARCH (CERN)

JHEP 05 (2019) 164
DOI: 10.1007/JHEP05(2019)164

CERN-EP-2018-226
19th August 2019

Search for single production of vector-like quarks decaying into Wb in pp collisions at $\sqrt{s}$ = 13 TeV with the ATLAS detector

The ATLAS Collaboration

A search for singly produced vector-like quarks Q, where Q can be either a T quark with charge $+2/3$ or a Y quark with charge $-4/3$, is performed in proton–proton collision data at a centre-of-mass energy of 13 TeV corresponding to an integrated luminosity of 36.1 fb^{-1}, recorded with the ATLAS detector at the LHC in 2015 and 2016. The analysis targets $Q \to Wb$ decays where the W boson decays leptonically. No significant deviation from the expected Standard Model background is observed. Upper limits are set on the QWb coupling strength and the mixing between the Standard Model sector and a singlet T quark or a Y quark from a (B, Y) doublet or a (T, B, Y) triplet, taking into account the interference effects with the Standard Model background. The upper limits set on the mixing angle are as small as $|\sin\theta_{\mathrm{L}}| = 0.18$ for a singlet T quark of mass 800 GeV, $|\sin\theta_{\mathrm{R}}| = 0.17$ for a Y quark of mass 800 GeV in a (B, Y) doublet model and $|\sin\theta_{\mathrm{L}}| = 0.16$ for a Y quark of mass 800 GeV in a (T, B, Y) triplet model. Within a (B, Y) doublet model, the limits set on the mixing parameter $|\sin\theta_{\mathrm{R}}|$ are comparable with the exclusion limits from electroweak precision observables in the mass range between about 900 GeV and 1250 GeV.

Contents

1 Introduction

Vector-like quarks (VLQs) are hypothetical spin-$1/2$ coloured particles with left-handed and right-handed components that transform in the same way under the Standard Model (SM) gauge group. Therefore, their masses are not generated by a Yukawa coupling to the Higgs boson [1]. While the discovery of the Higgs boson (H) at the Large Hadron Collider (LHC) [2, 3] excludes a perturbative, fourth generation of chiral quarks [4], since their contribution to loop-mediated Higgs boson couplings would significantly alter the production cross-section and the decay rates of the Higgs boson, the effects on Higgs boson production and decay rates from loop diagrams including VLQs are much smaller than the uncertainty in the current measurements [1]. In many models, VLQs mix mainly with the SM quarks of the third generation due to the large masses of the bottom and top quarks [5, 6]. Vector-like quarks appear in several extensions of the SM that address the hierarchy problem, such as extra dimensions [7], composite Higgs [8, 9] and Little Higgs [10] models, where they are added to the SM in multiplets. They can also appear in supersymmetric models [11] and are able to stabilise the electroweak vacuum [12].

This analysis concentrates on searches for single production of heavy vector-like quarks Q produced in proton–proton (pp) collisions via Wb fusion, $pp \to Qqb + X$, with a subsequent decay $Q \to Wb$. Here Q can be either a T quark with charge $+2/3$ or a Y quark with charge $-4/3$ or their antiquarks. An example of a leading-order Feynman diagram is presented in Figure 1.

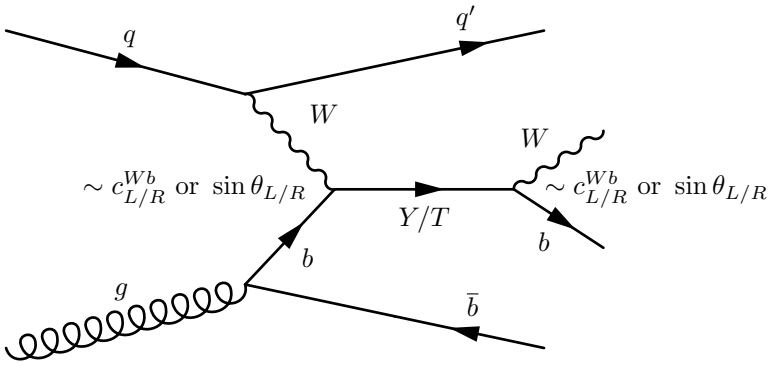

Figure 1: Leading-order Feynman diagram for single Y/T production in Wb fusion and subsequent decay into Wb. The production amplitude scales with $\sin\theta_{\mathrm{L,R}}$ [1] or $c_{\mathrm{L,R}}^{Wb}$ [13, 14] as described in the text.

Vector-like T quarks can belong to any weak-isospin multiplet, while Y quarks cannot exist as singlets. The interpretation used in this analysis focuses on Y quarks from a (B, Y) doublet or a (T, B, Y) triplet, and on singlet T quarks, since T quarks in a (T, B, Y) triplet do not couple to Wb [1]. For singlet T quarks, the branching ratios ($\mathcal{B}$s) are model- and mass-dependent, but in the high-mass limit, which is considered in this analysis, they converge towards 2:1:1 (Wb:Zt:Ht) [1]. Due to its charge, the Y quark can decay only into Wb and therefore $\mathcal{B}(Y \to Wb) = 100\%$. As a consequence, Y quarks can be singly produced in pp collisions only via Wb fusion, while T quarks can be produced not only by Wb fusion but also by Zt and Ht fusion.

Single production of vector-like quarks is enabled by their coupling to SM quarks. As a result, searches for singly produced VLQs in pp collisions can be used to probe these couplings as a function of the VLQ mass, whereas searches for pair-produced VLQs allow limits to be set on VLQ masses; these mass limits are rather insensitive to the couplings. because the signals are produced through strong couplings. At high VLQ masses, single VLQ production can become the dominant production mechanism at the LHC, depending on the strength of the Qqb coupling. Results are presented here for two different models that use different formulations of the Lagrangian that describes these new particles and their interactions. In the model discussed in Ref. [1] (renormalisable theory), a mixing term between the SM and vector-like quarks is introduced in a renormalisable extension of the SM, while Refs. [13, 14] (non-renormalisable theory) use a phenomenological Lagrangian that is parameterised with coupling terms, but is non-renormalisable. The main difference between these approaches is that the Lagrangian in Refs. [13, 14] has additional terms that allow larger production cross-sections, while the Lagrangian in Ref. [1] gives a complete description of the dependence of the $\mathcal{B}$ on the multiplet dimension, with left- and right-handed mixing angles θ_{L} and θ_{R} as model parameters. Within a given multiplet, θ_{L} and θ_{R} are functionally related. Therefore, a given value of either the left- or right-handed mixing angle fully determines all $\mathcal{B}$s for any given heavy-quark mass. For the interpretation in terms of coupling parameters c_{L}^{Wb} and c_{R}^{Wb} as introduced in Refs. [13, 14], assumptions must be made about the $Q \to Wb$, $Q \to Zt$ and $Q \to Ht$ $\mathcal{B}$s in case of $Q = T$. The relative contribution of the left- and right-handed components of the mixing and coupling also depends on the dimension of the VLQ multiplet. For T singlets, only the left-handed component ($\sin\theta_{\mathrm{L}}$ or c_{L}^{Wb}) contributes. For a (B, Y) doublet model, results are interpreted in terms of the dominant right-handed ($\sin\theta_{\mathrm{R}}$) component; for a (T, B, Y) triplet model, results are interpreted in terms of the dominant left-handed ($\sin\theta_{\mathrm{L}}$) component [1]. The formulation of Ref. [1] also allows within a certain multiplet model a comparison of the mixing angles with constraints from electroweak precision observables, such as the ratio R_b of the partial width for

$Z \to b\bar{b}$ to the total hadronic Z-boson width and the oblique parameters S and T [15]. A comparison of the respective Lagrangians of the renormalisable models described in Ref. [1] and the non-renormalisable models described in Refs. [13, 14] yields a simple relation between $\sin\theta_{\mathrm{L,R}}$ and $c^{Wb}_{\mathrm{L,R}}$: $c^{Wb}_{\mathrm{L,R}} = \sqrt{2}\sin\theta_{\mathrm{L,R}}$ for the T singlet model and (B, Y) doublet model and $c^{Wb}_{\mathrm{L}} = 2\sin\theta_{\mathrm{L}}$ for the (T, B, Y) triplet model. This relationship is only true within the regime of validity of the renormalisable formulation, and if one considers only the interactions between Q, W and b.

The ATLAS and CMS Collaborations have published searches for single and pair production of vector-like T quarks in all three decay channels [16–34] and set 95% confidence level (CL) lower limits on T- and Y-quark masses. Assuming a $\mathcal{B}$ of 100% for the corresponding decay channel, the best observed T-quark mass limits are $m_T > 1430$ GeV for $T \to Ht$ [23], 1340 GeV for $T \to Zt$ [33] and 1350 GeV for $T \to Wb$ [20], independent of the size of the c^{Wb} coupling strengths. In Ref. [34], seven individual analyses searching for $B\bar{B}$ or $T\bar{T}$ pair production were combined improving model-independent cross-section limits significantly over individual analyses. T quarks with a mass lower than 1310 GeV are excluded for any combination of decays into SM particles by this analysis. The observed lower limit on the pair-produced Y-quark mass is 1350 GeV [26]. These searches also report limits as a function of the assumed $\mathcal{B}$s. The best observed limits are $m_T > 1310$ GeV and $m_T > 1280$ GeV for a weak-isospin doublet [23] and singlet [27] respectively. Searches for single production of T quarks with decays into Zt [31] and single T/Y-quark production with decays into Wb [22] were carried out by the ATLAS Collaboration using the Run-1 pp dataset a centre-of-mass energy $\sqrt{s} = 8$ TeV. In the $T \to Zt$ decay channel, assuming a mixing parameter $\sin\theta_{\mathrm{L}}$ as low as 0.7, T quarks with masses between 450 GeV and 650 GeV are excluded [31], while for a QWb coupling strength of $\sqrt{(c^{Wb}_{\mathrm{L}})^2 + (c^{Wb}_{\mathrm{R}})^2} = 1$, the observed lower limit on the T-quark mass assuming $\mathcal{B}(T \to Wb) = 0.5$ is 950 GeV [22]. The CMS Collaboration studied single T- and Y-quark production using the Run-2 dataset at $\sqrt{s} = 13$ TeV collected in 2015 [25, 28–30, 32] and set upper limits on the single-T-quark production cross-section times $\mathcal{B}(T \to Ht)$ that vary between 0.31 pb and 0.93 pb for T-quark masses in the range 1000–1800 GeV [32], as well as on the single-T-quark production cross-section times $\mathcal{B}(T \to Zt)$ that vary between 0.98 pb and 0.15 pb (0.6 pb and 0.13 pb) for T-quark masses in the range 700–1700 GeV in the right-handed (left-handed) Tb (Tt) production channel [25]. For a mass of 1000 GeV, a T-quark production cross-section times branching fraction above 0.8 pb (0.7 pb) is excluded for the $T \to Ht$ decay channel assuming left-handed (right-handed) coupling of the T quark to SM particles [28]. For Y quarks with a coupling of 0.5 and $\mathcal{B}(Y \to Wb) = 1$, the observed (expected) lower mass limit is 1.40 (1.0) TeV [29].

This paper describes a search for $Q \to Wb$ ($Q = T$ or Y) production, with the prompt W boson decaying leptonically, giving a lepton + jets signature characterised by the presence of exactly one electron or muon[1], three or more jets and missing transverse momentum from the escaping neutrino. It is assumed that T quarks are produced in Wb fusion only. For single production of a T quark, Zt fusion could in principle contribute as well, but can be neglected for this T-singlet search. For equal values of the TZt and TWb couplings, the cross-section for Zt fusion is about one order of magnitude smaller than for Wb fusion [14]. For the T-singlet case, the TZt coupling is about a factor of $\sqrt{2}$ smaller than the TWb coupling and as a result $\mathcal{B}(T \to Zt)$ is about a factor of two smaller than $\mathcal{B}(T \to Wb)$. Since the single-VLQ production cross-section scales with coupling squared, the Zt fusion cross-section is lowered by another factor of two compared to the Wb fusion cross-section. In addition, the selection efficiency for $tZ \to T \to Wb$ events in the search presented here is about a factor of two smaller than for $bW \to T \to Wb$, because in $tZ \to T \to Wb$ the accompanying top quark from the gluon splitting leads to additional jets in the final state.

[1] Electrons and muons from decays of τ-leptons from $W \to \tau\nu$ are taken into account in the selection.

The analysis is optimised to search for massive VLQs with a high-momentum b-jet in the final state. The b-jet and the charged lepton originating from the Q decay are approximately back-to-back in the transverse plane since both originate from the decay of a heavy object. The outgoing light quark in the process depicted in Figure 1 often produces a jet in the forward region of the detector. The second b-jet from the gluon splitting may be observed in either the forward or central region. Since this b-jet is typically of low energy, it often falls outside the detector acceptance.

The main background processes with a single-lepton signature arise from top-quark pair ($t\bar{t}$) production, single-top-quark production and W-boson production in association with jets (W+jets), with smaller contributions from Z-boson production in association with jets (Z+jets) and from diboson (WW, WZ, ZZ) production. Multijet events also contribute to the selected sample via the misidentification of a jet or a photon as an electron or the presence of a non-prompt electron or muon. To estimate the backgrounds from $t\bar{t}$ and W+jets events in a consistent and robust fashion, two control regions (CRs) are defined. They are chosen to be orthogonal to the signal region (SR) in order to provide independent data samples enriched in particular background sources. The reconstructed mass of the heavy-quark candidate is used as the discriminating variable in a binned likelihood fit to test for the presence of a signal, taking into account the interference with SM background processes. A background-only fit to the SR and CRs is also performed to determine whether the observed event yield in the SR is compatible with the corresponding SM background expectation. The results of the binned profile likelihood fits are used to estimate the Y/T $c_{\mathrm{L,R}}^{Wb}$ coupling limits. In the case of the right-handed Y quark in a (Y, B) doublet model, where the interference effect with the SM is much smaller than for the other models under consideration, a limit on the production cross-section is also quoted.

2 ATLAS detector

The ATLAS detector [35] at the LHC is a multipurpose particle detector with a forward–backward symmetric cylindrical geometry that covers nearly the entire solid angle around the collision point.[2] It consists of an inner tracking detector (ID) surrounded by a thin superconducting solenoid magnet producing an axial 2 T magnetic field, fine-granularity electromagnetic (EM) and hadronic calorimeters, and a muon spectrometer (MS) incorporating three large air-core toroid magnet assemblies. The ID consists of a high-granularity silicon pixel detector, including an insertable B-layer [36, 37] added in 2014, and a silicon microstrip tracker, together providing charged-particle tracking information in the pseudorapidity region $|\eta| < 2.5$. It is surrounded by a transition radiation tracker, which enhances electron identification information in the region $|\eta| < 2.0$. The EM calorimeter is a lead/liquid-argon sampling detector, divided into a barrel region ($|\eta| < 1.475$) and two endcap regions ($1.375 < |\eta| < 3.2$), which provides energy measurements of electromagnetic showers. Hadron calorimetry is also based on the sampling technique, with either scintillator tiles or liquid argon as the active medium and with steel, copper, or tungsten as the absorber material. The calorimeters cover the region $|\eta| < 4.9$. The MS measures the deflection of muons within $|\eta| < 2.7$ using three layers of high-precision tracking chambers located in a toroidal field of approximately 0.5 T and 1 T in the central and endcap regions respectively. The MS is also instrumented with separate trigger chambers covering $|\eta| < 2.4$. A two-level trigger system [38], using custom hardware

[2] ATLAS uses a right-handed coordinate system with its origin at the nominal interaction point (IP) in the centre of the detector. The positive x-axis is defined by the direction from the IP to the centre of the LHC ring, with the positive y-axis pointing upwards, while the beam direction defines the z-axis. Cylindrical coordinates (r, ϕ) are used in the transverse plane, ϕ being the azimuthal angle around the z-axis. The pseudorapidity η is defined in terms of the polar angle θ by $\eta = -\ln\tan(\theta/2)$. The transverse momentum (p_{T}) is defined relative to the beam axis and is calculated as $p_{\mathrm{T}} = p\sin(\theta)$.

followed by a software-based level, is used to reduce the trigger rate to a maximum of around 1 kHz for offline data storage.

3 Physics object reconstruction

The data used in this search correspond to an integrated luminosity of 36.1 fb^{-1} of pp collisions at a centre-of-mass energy of $\sqrt{s}$ = 13 TeV recorded in 2015 and 2016 with the ATLAS detector. Only data-taking periods with stable beam collisions and all relevant ATLAS detector components functioning normally are considered. In this dataset, the average number of simultaneous pp interactions per bunch crossing, or 'pile-up', is approximately 24.

The final states considered in this search require the presence of one charged lepton (electron or muon) candidate and multiple hadronic jets. Single-electron and single-muon triggers with low transverse-momentum (p_{T}) thresholds and lepton isolation requirements (in 2016 only) are combined in a logical OR with higher-threshold triggers without any isolation requirements to give maximum efficiency. For electrons, triggers with a p_{T} threshold of 24 (26) GeV in 2015 (2016) and isolation requirements (in 2016 only) are used along with triggers with a 60 GeV threshold and no isolation requirement, and with a 120 (140) GeV threshold with looser identification criteria. For muons, triggers with p_{T} thresholds of 20 (26) GeV and isolation requirements in 2015 (2016) are combined with a trigger that has a p_{T} threshold of 50 GeV and no isolation requirements in both years. In addition, events must have at least one reconstructed vertex with two or more tracks with p_{T} above 0.4 GeV that is consistent with the beam-collision region in the x–y plane. If multiple vertices are reconstructed, the vertex with the largest sum of the squared p_{T} of its associated tracks is taken as the primary vertex. For the final states considered in this analysis, the vertex reconstruction and selection efficiency is close to 100%.

Electron candidates [39–41] are reconstructed from isolated energy deposits (clusters) in the EM calorimeter, each matched to a reconstructed ID track, within the fiducial region of $|\eta_{\mathrm{cluster}}| < 2.47$, where η_{cluster} is the pseudorapidity of the centroid of the calorimeter energy deposit associated with the electron candidate. A veto is placed on electrons in the transition region between the barrel and endcap electromagnetic calorimeters, $1.37 < |\eta_{\mathrm{cluster}}| < 1.52$. Electrons must satisfy the tight likelihood identification criterion, based on shower-shape and track–cluster matching variables, and must have a transverse energy $E_{\mathrm{T}} = E_{\mathrm{cluster}}/\cosh(\eta_{\mathrm{track}}) > 25\,\mathrm{GeV}$, where E_{cluster} is the electromagnetic cluster energy and η_{track} the track pseudorapidity. Muons are reconstructed [42] by combining a track reconstructed in the ID with one in the MS, using the complete track information from both detectors and accounting for the effects of energy loss and multiple scattering in the material of the detector structure. The muon candidates must satisfy the medium selection criteria [42] and are required to be in the central region of $|\eta| < 2.5$. To reduce the contribution of leptons from hadronic decays (non-prompt leptons), electrons and muons must satisfy isolation criteria that include both track and calorimeter information, and are tuned to give an overall efficiency of 98%, independent of the p_{T} of the lepton. Electron and muon candidates are required to be isolated from additional tracks within a cone around their directions with a radius of $\Delta R \equiv \sqrt{(\Delta\eta)^2 + (\Delta\phi)^2}$ with $\Delta R = \min(0.2, 10\ \mathrm{GeV}/p_{\mathrm{T}})$ [40] for electrons and $\Delta R = \min(0.3, 10\ \mathrm{GeV}/p_{\mathrm{T}})$ for muons [42]. The lepton calorimeter-based isolation variable is defined as the sum of the calorimeter transverse energy deposits in a cone of size $\Delta R = 0.2$, after subtracting the contribution from the energy deposit of the lepton itself and correcting for pile-up effects, divided by the lepton p_{T}. The significance of the transverse impact parameter d_0, calculated relative to the measured beam-line position, is required to satisfy $|d_0/\sigma(d_0)| < 5$ for electrons and $|d_0/\sigma(d_0)| < 3$ for muons, where $\sigma(d_0)$ is the uncertainty in d_0. Finally, the lepton tracks

are matched to the primary vertex of the event by requiring the longitudinal impact parameter z_0 to satisfy $|z_0 \sin\theta_{\text{track}}| < 0.5$ mm, where θ_{track} is the polar angle of the track.[3]

The leptons satisfying the criteria described above are used in the selection of events in the signal and control regions. The estimation of background from non-prompt and fake leptons with the Matrix Method [43], described in Section 5.2, uses 'loose' leptons in addition to the above 'tight' leptons, where the tight sample is a subset of the loose sample. The 'loose' selection requires that the muon (electron) satisfies the medium (likelihood medium) requirements, but does not need to satisfy isolation criteria as defined in Refs. [40, 42].

Jets are reconstructed from three-dimensional topological calorimeter energy clusters [44] using the anti-k_t algorithm [45, 46] with a radius parameter of 0.4 [47]. Each topological cluster is calibrated to the electromagnetic energy scale prior to jet reconstruction. The reconstructed jets from the clusters are then calibrated to the particle level by the application of corrections derived from simulation and from dedicated calibration samples of pp collision data at $\sqrt{s} = 13$ TeV [48, 49]. Data quality criteria are imposed to identify jets arising from non-collision sources or detector noise, and any event containing at least one such jet is removed [50]. Finally, jets considered in this analysis are required to have $p_{\text{T}} > 25$ GeV. The pseudorapidity acceptance for jets differs between different selections: central jets are required to have $|\eta| < 2.5$, while forward jets are defined to have $2.5 < |\eta| < 4.5$. Furthermore, jets with a $p_{\text{T}} < 60$ GeV and $|\eta| < 2.4$ are required to satisfy criteria implemented in the jet vertex tagger algorithm [51] designed to select jets that originate from the hard scattering and reduce the effect of in-time pile-up.

The identification of jets from b-quark decays (b-tagging) is beneficial in this analysis. To identify (tag) jets containing b-hadrons (henceforth referred to as b-jets), a multivariate discriminant is used that combines information about the impact parameters of inner-detector tracks associated with the jet, the presence of displaced secondary vertices, and the reconstructed flight paths of b- and c-hadrons inside the jet [52–55]. Jets are considered to be b-tagged if the value of the multivariate discriminant is larger than a certain threshold. The criterion in use is only calculated for central jets ($|\eta| < 2.5$) with $p_{\text{T}} > 25$ GeV and has an efficiency of approximately 85% for b-jets in simulated $t\bar{t}$ events. The rejection factor against jets originating from light quarks and gluons (henceforth referred to as light-flavour jets) is about 34, and that against jets originating from charm quarks (c-jets) is about 3 [54], determined in simulated $t\bar{t}$ events. Correction factors are defined to correct the tagging rates in the simulation to match the efficiencies measured in the data control samples [54, 56].

To avoid counting a single detector response as two objects, an overlap removal procedure is used. Jets overlapping with identified electron candidates within a cone of $\Delta R = 0.2$ are removed, as the jet and the electron are very likely to be the same physics object. If the nearest jet surviving this requirement is within $\Delta R = 0.4$ of an electron, the electron is discarded, to ensure it is sufficiently separated from nearby jet activity. Muons are removed if they are separated from the nearest jet by $\Delta R < 0.4$, to reduce the background from muons from heavy-flavour hadron decays inside jets. However, if this jet has fewer than three associated tracks, the muon is kept and the jet is removed instead; this avoids an inefficiency for high-energy muons undergoing significant energy loss in the calorimeter.

The missing transverse momentum $\vec{E}_{\text{T}}^{\text{miss}}$ (with magnitude $E_{\text{T}}^{\text{miss}}$) is a measure of the momentum of the escaping neutrinos. It is defined as the negative vector sum of the transverse momenta of all selected and calibrated objects (electrons, muons, photons, hadronically decaying τ-leptons and jets) in the event, including a term to account for energy from soft particles which are not associated with any of the selected

[3] The longitudinal impact parameter z_0 is the difference between the longitudinal position of the track along the beam line at the point where the transverse impact parameter (d_0) is measured and the longitudinal position of the primary vertex.

objects [57]. This soft term is calculated from inner-detector tracks matched to the selected primary vertex to make it resilient to contamination from pile-up interactions [57].

4 Background and signal modelling

Monte Carlo (MC) simulation samples are used to model the expected signal and SM background distributions. The MC samples were processed either through the full ATLAS detector simulation [58] based on GEANT4 [59] or through a faster simulation making use of parameterised showers in the calorimeters [60]. Effects of both in-time and out-of-time pile-up, from additional pp collisions in the same and nearby bunch crossings, were modelled by overlaying minimum-bias interactions generated with PYTHIA 8.186 [61] according to the luminosity profile of the recorded data. The distribution of the number of additional pp interactions in the MC samples was reweighted to match the pile-up conditions observed in data. All simulated samples used EVTGEN [62] to model the decays of heavy-flavour hadrons, except for processes modelled using the SHERPA generator [63]. All simulated events were processed using the same reconstruction algorithms and analysis selection requirements as for the data, but small corrections, obtained from comparisons of simulated events with data in dedicated control regions, were applied to trigger and object reconstruction efficiencies, as well as detector resolutions, to better model the observed response. The main parameters of the MC samples used in this search are summarised in Table 1. Samples for all SM background processes were generated with the full GEANT4 model of the ATLAS detector.

4.1 Background modelling

Top-quark pair events were generated with the next-to-leading-order (NLO) generator POWHEG-BOX 2.0 [64–66] using the CT10 parton distribution function (PDF) set [67], interfaced to PYTHIA 6.428 [68] with the CTEQ6L PDF set [69] and the Perugia 2012 (P2012) set of tuned parameters for the underlying event (UE) [70]. The hard-process factorisation scale μ_{F} and renormalisation scale μ_{R} were set to the default POWHEG-BOX values $\mu = (m_t^2 + p_{\mathrm{T,top}}^2)^{1/2}$, where m_t is the top-quark mass, $m_t = 172.5$ GeV, and $p_{\mathrm{T,top}}$ is the top-quark transverse momentum evaluated for the underlying Born configuration. The h_{damp} parameter, which controls the transverse momentum of the first additional gluon emission beyond the Born configuration, is set equal to the mass of the top quark. The main effect of this choice is to regulate the high-p_T emission against which the $t\bar{t}$ system recoils. The sample was generated assuming that the top quark decays exclusively through $t \to Wb$.

Alternative $t\bar{t}$ samples were produced to model uncertainties in this process. The effects of initial- and final-state radiation (ISR/FSR) were explored using two alternative POWHEG-BOX 2.0 + PYTHIA 6.428 samples: one with h_{damp} set to $2m_t$, the renormalisation and factorisation scales set to half the nominal value and using the P2012 high-variation UE tuned parameters, giving more radiation, and another with P2012 low-variation UE tuned parameters, $h_{\mathrm{damp}} = m_t$ and the renormalisation and factorisation scales set to twice the nominal value, giving less radiation [71]. The values of μ_{R}, μ_{F} and h_{damp} were varied together because these two variations were found to cover the full set of uncertainties obtained by changing the scales and the h_{damp} parameter independently. To provide a comparison with a different parton-shower model, an additional $t\bar{t}$ sample was generated using the same POWHEG-BOX settings as the nominal POWHEG-BOX 2.0 + PYTHIA 6.428 sample, but with parton showering, hadronisation, and the UE simulated with Herwig++ 2.7.1 [72] with the UEEE5 tuned parameters [73] and the corresponding CTEQ6L1 PDF set. Additional $t\bar{t}$ simulation samples were generated using MADGRAPH5_aMC@NLO 2.2.1 [74] interfaced to Herwig++

2.7.1 to determine the systematic uncertainties related to the use of different models for the hard-scattering generation, while maintaining the same parton shower model.

The $t\bar{t}$ prediction was normalised to the theoretical cross-section for the inclusive $t\bar{t}$ process of 832^{+46}_{-51} pb obtained with Top++ [75], calculated at next-to-next-to-leading order (NNLO) in QCD and including resummation of next-to-next-to-leading logarithmic (NNLL) soft gluon terms [76–80]. Theoretical uncertainties result from variations of the factorisation and renormalisation scales, as well as from uncertainties in the PDF and strong coupling constant α_S. The latter two represent the largest contribution to the overall theoretical uncertainty in the cross-section and are calculated using the PDF4LHC prescription [81].

Single-top-quark background processes corresponding to the Wt and s-channel production mechanisms were generated with Powheg-Box 1.0 at NLO [82] using the CT10 PDF set. Overlaps between the $t\bar{t}$ and Wt final states were removed using the "diagram removal" scheme (DR) [83, 84]. The "diagram subtraction" scheme (DS) [84] was considered as an alternative method, and the full difference between the two methods assigned as a shape and normalisation uncertainty [85]. Events from t-channel single-top-quark production were generated using the Powheg-Box 1.0 [82] NLO generator, which uses the four-flavour scheme. The fixed four-flavour PDF set CT10f4 was used for the matrix-element calculations. All single-top-quark samples were normalised to the approximate NNLO theoretical cross-sections [86–88]. Pythia 6.428 with the P2012 set of tuned parameters was used to model the parton shower, hadronisation and underlying event. Additional single-top-quark samples were generated using the same Powheg-Box settings as the nominal sample, while parton showering, hadronisation, and the UE were simulated with Herwig++ 2.7.1. The ISR/FSR effects were explored using alternative Powheg-Box 2.0 + Pythia 6.428 samples with a set of P2012 high- and low-variation UE tuned parameters. Another set of single-top-quark samples was generated using Madgraph5_aMC@NLO 2.2.1 interfaced to Herwig++ 2.7.1 to determine the systematic uncertainties associated with the choice of NLO generator.

Samples of W/Z+jets events were generated with the Sherpa 2.2.0 generator. The matrix-element calculation was performed with up to two partons at NLO and up to four partons at leading order (LO) using Comix [89] and OpenLoops [90]. The matrix-element calculation was merged with the Sherpa parton shower [91] using the ME+PS@NLO prescription [92]. The PDF set used for the matrix-element calculation was CT10 with a dedicated parton shower tuning developed by the Sherpa authors. The W+jets and Z+jets samples were normalised to the NNLO theoretical cross-sections for inclusive W and Z production calculated with FEWZ [93]. Samples generated with Madgraph5_aMC@NLO 2.2.1+ Pythia 8.186 were compared with the nominal W+jets samples to determine the systematic uncertainties associated with the choice of generator.

Diboson events ($WW/WZ/ZZ$+jets) with one of the bosons decaying hadronically and the other leptonically were generated with the NLO generator Sherpa 2.1.1 and include processes containing up to four electroweak vertices. The matrix element included up to one (ZZ) or zero (WW, WZ) additional partons at NLO and up to three partons at LO using the same procedure as for W/Z+jets. All diboson samples were normalised to their NLO theoretical cross-sections provided by Sherpa. Processes producing smaller backgrounds are also considered, and include $t\bar{t}V$ ($V = W,Z$) and $t\bar{t}H$. The $t\bar{t}V$ processes were simulated with Madgraph5_aMC@NLO generator using the NNPDF2.3 PDF set, interfaced to Pythia8 [94] with the A14 UE tune. The $t\bar{t}H$ process was modelled using Madgraph5_aMC@NLO interfaced to Herwig++ 2.7.1.

Table 1: Generators used to model the signals and different background processes. The parameter tune for the underlying event, PDF set, and the highest-order perturbative QCD (pQCD) accuracy used for the normalisation of each sample is given. All processes, except for Yqb signals, were generated at NLO in QCD. The LO cross-sections calculated for the Yqb signal processes in the simulation were normalised to the NLO theoretical cross-section taken from Ref. [14].

Process	Generator + parton showering/hadronisation	Tuned parameters	PDF set	Inclusive cross-section order in pQCD
$\boldsymbol{Yqb}$	MADGRAPH5_aMC@NLO 2.2.3 + PYTHIA 8.210	A14	NNPDF2.3	NLO
$\boldsymbol{t\bar{t}}$	POWHEG-BOX 2.0 + PYTHIA 6.428	P2012	CT10	NNLO+NNLL
Single top	POWHEG-BOX 1.0 + PYTHIA 6.428	P2012	CT10	NNLO+NNLL
Dibosons WW, WZ, ZZ	SHERPA 2.1.1	Default	CT10	NLO
$\boldsymbol{W/Z}$ **+ jets**	SHERPA 2.2.0	Default	CT10	NNLO
$\boldsymbol{t\bar{t}V}$	MADGRAPH5_aMC@NLO 2.2.3 + PYTHIA 8.210	A14	NNPDF2.3	NLO
$\boldsymbol{t\bar{t}H}$	MADGRAPH5_aMC@NLO 2.2.3 + Herwig++ 2.7.1	CTEQ6L1	CT10	NLO

4.2 Signal modelling

Simulated events for signal processes were generated at LO in the four-flavour scheme with the MADGRAPH5_aMC@NLO 2.2.3 generator using the NNPDF2.3 PDF set, interfaced to PYTHIA8 for parton showering and hadronisation. Samples of Yqb signals were produced for masses ranging from 800 GeV to 2000 GeV in steps of 100 GeV with equal left-handed and right-handed coupling strengths of $\kappa_T = 0.5$ [95]. The coupling parameter κ_T in the model described in Ref. [95] used for the signal production is related to the coupling parameters $c_{\mathrm{L,R}}^{Wb}$ in Ref. [14] via $\kappa_T f(m) = c_{\mathrm{L,R}}^{Wb}/\sqrt{2}$, where $f(m) \approx \sqrt{1/(1+O(m_Q^{-4}))}$ with m_Q the VLQ mass in GeV, and therefore $\kappa_T \approx c_{\mathrm{L,R}}^{Wb}/\sqrt{2}$ to a very good approximation. These samples were processed either through the full detector simulation or through the faster simulation. The normalisation of signal events produced with the faster simulation was scaled up by 7.2% to correct for efficiency differences.

Since the kinematic distributions of the decay products for the T quark and Y quark in the Wb decay channel are the same, only Y signal samples were generated and they were used to derive the results also for the Tqb signals. Other possible decay modes of the T quark ($T \to Zt$, $T \to Ht$) have negligible acceptance in this search. The kinematics of the final-state particles are very similar for left-handed and right-handed couplings, and hence the acceptances for the two chiralities are found to be equal. The LO cross-sections calculated for the signal processes in the simulation were normalised to the next-to-leading-order benchmark

calculation from Ref. [14], which is performed in the narrow-width approximation (NWA). The single-VLQ production cross-sections and the decay widths of the VLQ resonances are mass- and coupling-dependent. The VLQ width increases with increasing mass and coupling values such that, for sufficiently large masses and couplings, the NWA is no longer valid. The ratio of the single-VLQ production cross-section without the NWA to that with the NWA, calculated at LO using MADGRAPH5_aMC@NLO 2.2.3, was used to correct the NLO cross-section from Ref. [14] as function of VLQ mass and coupling.

Sizeable interference effects between the amplitude for VLQ signal production and the SM are possible. In the analysis, two scenarios are considered:

1. T-quark production in a T singlet model, in which the T quark has only a left-handed coupling [1]. The SM process that interferes in this case is t-channel single-top-quark production where the top quark is far off-shell as illustrated in Figure 2(a).

2. Y-quark production in a (T, B, Y) triplet or (B, Y) doublet model, in which the Y quark has only a left-handed coupling or right-handed coupling. The SM process that interferes with Y-quark production is electroweak W^-bq production[4] as shown in Figure 2(b). Two cases are considered: a) the Y quark has only a left-handed coupling, which is realised e.g. in a (T, B, Y) triplet model, in which the right-handed coupling is heavily suppressed [1]. Since in the (T, B, Y) triplet model the T quark does not couple to Wb, T-quark production does not contribute to the final state under consideration; b) the Y quark has only a right-handed coupling, which is realised e.g. in a (B, Y) doublet model, in which the left-handed coupling is heavily suppressed. The interference effect for the Y quark with a right-handed coupling is much smaller than that for the Y quark with a left-handed coupling.

These SM contributions (i. e. σ_{SM}) were not modelled in the ATLAS MC simulations.

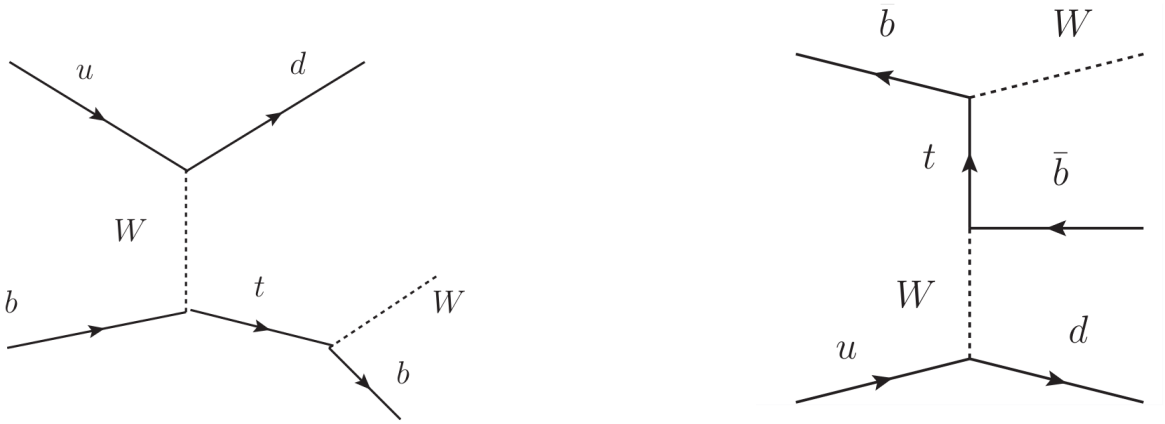

Figure 2: Leading-order Feynman diagrams for the SM processes that interfere with T-quark or Y-quark production, respectively, as described in the text: (a) t-channel single-top-quark production where the top quark is far off-shell and (b) electroweak W^-bq production.

In order to determine the signal yield and acceptance for different signal couplings, the samples of simulated signal events produced with the nominal coupling strength of $\kappa_T = 0.5$ are corrected on an event-by-event

[4] The charge-conjugated state $W^+\bar{b}q$ interferes with the $\bar{Y}$ quark.

basis using reweighting factors. These factors are obtained by comparing the target VLQ mass distribution in generated signal samples, at particle level, with the nominal one. The reweighting takes three effects into account: 1) the effect of interference calculated at LO, 2) the change in cross-section when going from LO to NLO, 3) the effect from the variation of the coupling strength. The method is validated with fully reconstructed signal samples with varied coupling strengths. The matrix-element squared for the process $pp \rightarrow Wbq$ is given by

$$|M|^2 = |M_{\mathrm{SM}}|^2 + |M_{\mathrm{VLQ}}|^2 + 2Re(M^*_{\mathrm{SM}} M_{\mathrm{VLQ}}).$$

As a result, the total cross-section for $pp \rightarrow Wbq$ at LO can be written as $\sigma^{\mathrm{LO}}_{\mathrm{tot}} = \sigma^{\mathrm{LO}}_{\mathrm{SM}} + \sigma^{\mathrm{LO}}_{\mathrm{VLQ}} + \sigma^{\mathrm{LO}}_{\mathrm{I}}$ with the LO SM cross-section $\sigma^{\mathrm{LO}}_{\mathrm{SM}}$, the LO VLQ cross-section $\sigma^{\mathrm{LO}}_{\mathrm{VLQ}}$ and the interference-term cross-section $\sigma^{\mathrm{LO}}_{\mathrm{I}}$. Since the K-factor quantifying the ratio between NLO and LO cross-sections is significantly larger than one for VLQ production, the interference effect has to be modelled at NLO. This modelling uses the K-factors for SM production, K_{SM}, and for VLQ production, K_{VLQ}, writing the total cross-section for $pp \rightarrow Wbq$ at NLO as

$$\sigma^{\mathrm{NLO}}_{\mathrm{tot}} = K_{\mathrm{SM}}\sigma^{\mathrm{LO}}_{\mathrm{SM}} + K_{\mathrm{VLQ}}\sigma^{\mathrm{LO}}_{\mathrm{VLQ}} + \sqrt{K_{\mathrm{SM}} \cdot K_{\mathrm{VLQ}}}\sigma^{\mathrm{LO}}_{\mathrm{I}}. \tag{1}$$

The K_{VLQ} values as a function of the VLQ mass are taken from Ref. [14]. There is no dedicated NLO calculation available for the K_{SM} factor for t-channel single-top-quark production with t-quarks far off-shell. This K_{SM} factor is set to unity since the K-factor for t-channel single-top-quark production for on-shell t-quarks is very close to one [96]. Since there is no dedicated NLO calculation in the literature for electroweak SM W^-bq production interfering with the Y production amplitude, K_{SM} is set to unity in this case as well. No systematic uncertainties are assigned to any of the K_{VLQ} or K_{SM} factors, because it is assumed that they correspond to the particular model assumptions. To obtain the reweighting factors r, events were generated at LO using MADGRAPH5_aMC@NLO 2.2.3 and r calculated as

$$r(m_{Wb}; c, c_0) = \frac{K_{\mathrm{VLQ}} f_{\mathrm{VLQ}}(m_{Wb}; c) + \sqrt{K_{\mathrm{SM}} \cdot K_{\mathrm{VLQ}}} f_{\mathrm{I}}(m_{Wb}; c)}{f_{\mathrm{VLQ}}(m_{Wb}; c_0)}, \tag{2}$$

where c_0 is the nominal coupling used in the simulation, c is the coupling value of interest, and the functions $f_{\mathrm{VLQ}}(m_{Wb}; c)$ and $f_{\mathrm{I}}(m_{Wb}; c)$ describe the Wb invariant mass distributions at particle level scaled to the LO cross-sections $\sigma^{\mathrm{LO}}_{\mathrm{SM}}$ and $\sigma^{\mathrm{LO}}_{\mathrm{I}}$ respectively. The reweighting assumes that the phase change as a function of m_{Wb} for the VLQ and SM amplitudes at NLO is the same as at LO.

Figure 3 shows the generated mass distribution at particle level for a Y quark with a mass of 900 GeV, produced with a coupling strength of 0.5 and scaled to the LO cross-section. It is compared with the generated mass distributions reweighted to a coupling strength of 0.14 with and without the interference term, which is also scaled to the LO cross-section. For the case without interference, it was explicitly checked that events generated with one coupling and reweighted to another target coupling result not only in the same VLQ mass distribution but also in the same distributions of other kinematical variables when generated directly with this target coupling.

5 Event selection and background estimation

This search focuses on final states with a leptonically decaying W boson and a b-quark, originating from the decay of a singly produced Q quark. Events are required to have exactly one isolated identified lepton (electron or muon) with $p_{\mathrm{T}} > 28$ GeV that must be matched to the lepton selected by the trigger, large

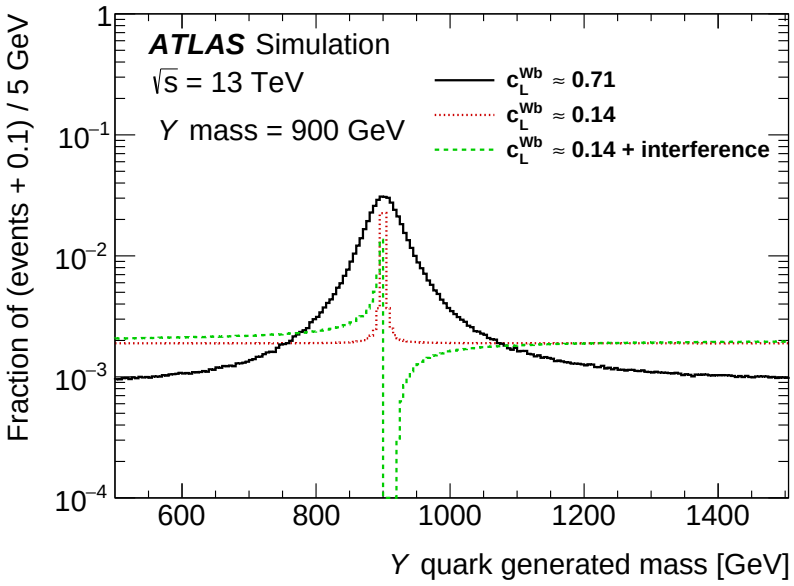

Figure 3: The generated mass distributions at particle level for a Y quark with a mass of 900 GeV, for a coupling strength of $c_0 = \kappa_T \approx 0.5$ and $c_L^{Wb} \approx 1/\sqrt{2}$ ($c_R^{Wb} = 0$, solid line) and of $c_0 = c_L^{Wb} = 0.14$ (dotted line) as defined in Ref. [95]. The distribution for a right-handed only and left-handed only Y quark (solid line) is the same. The dashed line shows the generated vector-like quark mass distribution at particle level of a left-handed Y signal with a mass of 900 GeV, coupling strength of $c_L^{Wb} = 0.14$ and interference effects with the SM included. The interference effects lead to negative entries in some bins of the distribution. For better visualisation of the tail distribution including the interference effect, the bin contents of all distributions were shifted by +0.1 before normalisation.

missing transverse momentum $E_T^{miss} > 120$ GeV from the escaping neutrino, and at least one central jet with $p_T > 25$ GeV satisfying the quality and kinematic criteria discussed in Section 3. The requirement on the missing transverse momentum reduces the fraction of selected events originating from non-prompt or misidentified leptons as well as diboson events. In the following, unless stated otherwise, only events satisfying this selection, referred to as "preselection", are considered. If there are any forward jets in the event, their transverse momentum is required to be larger than 40 GeV.

5.1 Signal and control regions definition

Events must have at least one b-tagged jet. The highest-p_T jet in the event must be b-tagged and have $p_T > 350$ GeV. To further exploit the low multiplicity of high-p_T jets in the signal process, an additional requirement is applied: events containing any jet with $p_T > 75$ GeV and $|\eta| < 2.5$ and satisfying ΔR(jet, leading jet) < 1.2 or ΔR(jet, leading jet) > 2.7 are rejected. This requirement reduces background from production of $t\bar{t}$ events, which are characterised by a higher multiplicity of high-p_T central jets than in signal events. A requirement on the azimuthal separation between the lepton and the b-tagged leading jet, $|\Delta\phi$ (lepton, leading jet)$| > 2.5$, as well as on the minimum distance ΔR between the lepton and any central jet, ΔR(lepton, jet) > 2.0, increases the signal-to-background ratio because, in signal signatures, leptons from the leptonic W-boson decays should be isolated and recoil against the b-quark jet in the event. Furthermore, similar to t-channel single-top production, the single production of VLQs gives rise to a forward jet ($2.5 < |\eta| < 4.5$). Only events with at least one forward jet with

$p_{\mathrm{T}} > 40$ GeV are considered. For a Y signal with a mass between 800 GeV and 2000 GeV and a coupling strength of $\sqrt{(c_{\mathrm{L}}^{Wb})^2 + (c_{\mathrm{R}}^{Wb})^2} \approx 1/\sqrt{2}$, the signal-to-background ratio (S/B) and the signal-to-background significance ratio ($S/\sqrt{B}$) in the SR are in the range 1.0–0.003 and 22.1–0.3 respectively. The acceptance times efficiency including the leptonic W decay branching fractions[5] for these Y signals ranges from 0.7% to 1.8% in the SR.

The normalisation of W+jets and $t\bar{t}$ processes is partially constrained by fitting the predicted yields to data in CRs enriched in W+jets and $t\bar{t}$ events. Two CRs are defined for this purpose, and also provide samples depleted in expected signal events. The selection requirements for the W+jets CR are the same as for the SR, except that each event is required to have exactly one b-tagged jet and the requirement on the azimuthal separation between the lepton and the b-tagged jet is reversed, $|\Delta\phi$ (lepton, leading jet)$| \leq 2.5$. In addition, the b-tagged jet has a slightly lower transverse momentum requirement of $p_{\mathrm{T}} > 250$ GeV and no hard or forward jet veto is applied. The W+jets CR definition results in a composition of W+light-jets and W+heavy-flavour-jets final states similar to that in the SR. The selection requirements for the $t\bar{t}$ CR are the same as for the SR, except that the leading jet p_{T} must be greater than 200 GeV and there must be at least one high-p_{T} jet with $p_{\mathrm{T}} > 75$ GeV and $|\eta| < 2.5$ fulfilling either ΔR (jet, leading jet) < 1.2 or ΔR (jet, leading jet) > 2.7. Table 2 summarises the main selection criteria in the SR and the orthogonal CRs. For Y/T signals with masses of ≥ 800 GeV and a coupling strength of $\sqrt{(c_{\mathrm{L}}^{Wb})^2 + (c_{\mathrm{R}}^{Wb})^2} \approx 1/\sqrt{2}$, the contamination in the $t\bar{t}$ control region is at most 1% and in the W+jets CR at most 0.6%.

A mismodelling of the W+jets background is observed at high jet p_{T}.

To correct for this mismodelling, the leading jet p_{T} distributions in data and MC-simulated W+jets events are compared after applying the preselection criteria and requiring that the leading jet is a b-tagged jet. The ratio of the distributions is taken as a scaling factor, which is applied to the simulated W+jets events in all kinematic distributions. The correction factors are between approximately 0.9 and 1.1 with statistical uncertainties of 4–10% for a jet p_{T} below 500 GeV, and 0.4–0.8 with a statistical uncertainty of about 11% for higher p_{T} values. These reweighting factors are treated as a systematic uncertainty in the final fit.[6]

5.2 Estimation of non-prompt and fake lepton backgrounds

Multijet production results in hadrons, photons and non-prompt leptons that may satisfy the lepton selection criteria and give rise to so called "non-prompt and fake" lepton backgrounds. The multijet background normalisation and shape in the m_{VLQ} distributions are estimated with a data-driven method, referred to as the Matrix Method [43]. This method uses the efficiencies of leptons selected using loose requirements (loose leptons) to pass the default tight lepton selection requirements. The efficiencies are obtained in dedicated control regions enriched in real leptons or in non-prompt and fake leptons, and applied to events selected with either the loose or tight lepton definition to obtain the fraction of multijet events.
The fake-enriched control regions are defined using the preselection criteria, except that events with electrons are required to have a reconstructed transverse W mass[7] $m_{\mathrm{T}}^{W} < 20$ GeV and to have $E_{\mathrm{T}}^{\mathrm{miss}} + m_{\mathrm{T}}^{W} < 60$ GeV,

[5] Events with leptonic τ decays are included.

[6] The residual difference of about 10% between the data and the SM simulation in the tail of the invariant mass distribution of the reconstructed VLQ candidate after applying the W+jets leading-jet p_{T} correction is included in this systematic uncertainty.

[7] The transverse W mass m_{T}^{W} is computed from the missing transverse momentum $\vec{p}_{\mathrm{T}}^{\,\mathrm{miss}}$ and the charged lepton transverse momentum $\vec{p}_{\mathrm{T}}^{\,\ell}$, and is defined as $m_{\mathrm{T}}^{W} = \sqrt{2p_{\mathrm{T}}^{\ell}E_{\mathrm{T}}^{\mathrm{miss}}(1 - \cos\Delta\phi(\vec{p}_{\mathrm{T}}^{\,\ell}, \vec{p}_{\mathrm{T}}^{\,\mathrm{miss}}))}$, where $\Delta\phi(\vec{p}_{\mathrm{T}}^{\,\ell}, \vec{p}_{\mathrm{T}}^{\,\mathrm{miss}})$ is the azimuthal angle between $\vec{p}_{\mathrm{T}}^{\,\ell}$ and $\vec{p}_{\mathrm{T}}^{\,\mathrm{miss}}$.

Table 2: Summary of common preselection requirements and selection requirements for the SR compared to those for the $t\bar{t}$ and W+jets CRs. All other selection requirements are the same for all three regions.

Requirement \ Region	SR	$t\bar{t}$ CR	W+jets CR
Preselection			
Leptons		1	
$E_{\mathrm{T}}^{\mathrm{miss}}$		> 120 GeV	
Central jets ($p_{\mathrm{T}} > 25$ GeV)		≥ 1	
Selection			
b-tagged jets	≥ 1	≥ 1	1
Leading jet p_{T}	> 350 GeV	> 200 GeV	> 250 GeV
Leading jet is b-tagged	Yes	Yes	Yes
$\lvert\Delta\phi$(lepton, leading jet)$\rvert$	> 2.5	> 2.5	≤ 2.5
Jets ($p_{\mathrm{T}} > 75$ GeV) with ΔR (jet, leading jet) < 1.2 or ΔR (jet, leading jet) > 2.7	0	≥ 1	–
ΔR (lepton, jets)	> 2.0	–	> 2.0
Forward jets ($p_{\mathrm{T}} > 40$ GeV)	≥ 1	≥ 1	–

and for events with muons it is required that the leading muon have $|d_0/\sigma(d_0)| > 5$. The real lepton efficiencies are measured using the tag-and-probe method from $Z \to ee$ and $Z \to \mu\mu$ control regions. Further details can be found in Refs. [22, 43].

5.3 Signal candidate mass reconstruction

In the SR, the invariant mass of the reconstructed VLQ candidate m_{VLQ} is used to discriminate the signal from the background processes. It is calculated from the leading b-tagged jet and the decay products of the leptonically decaying W-boson candidate. The W-boson candidate is reconstructed by summing the four-momenta of the charged lepton and the neutrino. To obtain the z-component of the neutrino momentum ($p_{z,\nu}$), the invariant mass of the lepton–neutrino system is set to the W-boson mass and the resulting quadratic equation is solved. If no real solution exists, the $\vec{E}_{\mathrm{T}}^{\mathrm{miss}}$ vector is varied by the minimum amount required to produce exactly one real solution. If two real solutions are found, the one with the smaller $|p_{z,\nu}|$ is used. The W-boson candidate and the leading b-tagged jet are then used to reconstruct the Q candidate. The mass resolutions for Y signals with masses between 800 GeV and 1600 GeV for a coupling of $\sqrt{(c_{\mathrm{L}}^{Wb})^2 + (c_{\mathrm{R}}^{Wb})^2} \approx 1/\sqrt{2}$ are 150–550 GeV.

Figure 4 shows the VLQ candidate invariant mass distribution in the SR for three simulated left-handed Y signal masses, 900 GeV, 1200 GeV and 1600 GeV, with couplings of $c_{\mathrm{L}}^{Wb} \approx 0.29$, ≈ 0.33 and ≈ 0.91 respectively, without (left figure) and with (right figure) interference included, together with the total SM background. The distribution provides good discrimination between signal and background events in the SR. Depending on the coupling and signal mass it is possible that negative entries occur in some bins of the signal-plus-interference m_{VLQ} distribution due to the interference effect.

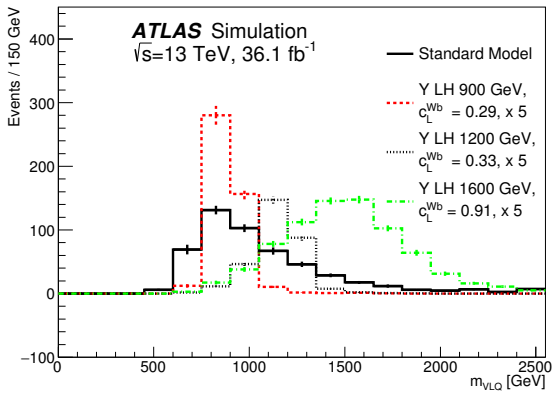

(a)

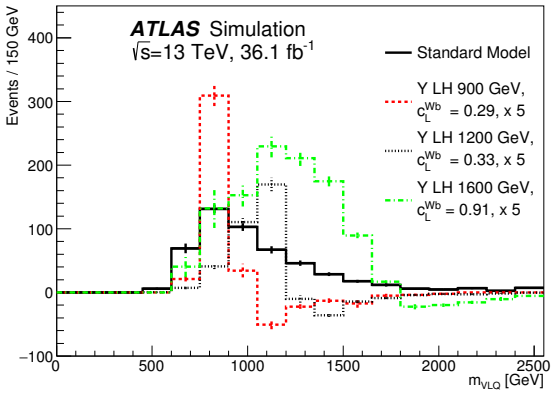

(b)

Figure 4: Distribution of VLQ candidate mass, m_{VLQ}, in the SR for three different signal masses (a) without and (b) with interference effects, for a left-handed Y signal with a mass of 900 GeV (dashed line), 1200 GeV (dotted) and 1600 GeV (dash-dotted line) and a coupling of $c_{\mathrm{L}}^{Wb} \approx 0.29$, ≈ 0.33 and ≈ 0.91 respectively, together with the total SM background (solid line). The error bars represent the statistical uncertainties. The signal event yield is scaled by a factor of five. Depending on the coupling and signal mass it is possible that negative entries occur in some bins of the signal-plus-interference m_{VLQ} distribution due to the interference effect. The distributions for a right-handed and left-handed Y signal without considering any interference effects are the same.

6 Systematic uncertainties

Several sources of systematic uncertainty in this analysis can affect the normalisation of the signal and background and/or their corresponding m_{VLQ} distributions, which are used for the statistical study. They are included as nuisance parameters in the statistical analysis. Sources of uncertainty include the modelling of the detector response, object reconstruction algorithms, uncertainty in the theoretical modelling of the signals and backgrounds, as well as the uncertainty arising from the limited size of the simulated event samples.

The following section describes each of the systematic uncertainties considered in the search. Table 3 presents a summary of all systematic uncertainties considered in the analysis. Leading sources of systematic

uncertainty in the expected SM background are uncertainties that arise from the jet energy scale, flavour-tagging efficiencies (b, c and light) as well as the background modelling, where $t\bar{t}$ generator uncertainties and single-top-quark DS/DR uncertainties are significantly constrained by the fit (see Section 7.1).

Table 3: Systematic uncertainties considered in this analysis. An uncertainty that affects normalisation only (cross-section only) for all processes and channels is denoted by "N", whereas "SN" means that the uncertainty affects both shape and normalisation and "F" means a floating normalisation uncertainty. Some of the systematic uncertainties are split into several components for a more accurate treatment. The relative systematic uncertainties in the inclusive expected SM background yields determined from the VLQ candidate invariant mass distribution after the fit to the background-only hypothesis are given in the last column in percentage. The $t\bar{t}$ and W+jets background scaling-factor uncertainties (last two rows in the table) are the relative systematic uncertainties in the predicted $t\bar{t}$ and W+jets background respectively.

Systematic uncertainty	Type	SM background [%]
Luminosity	N	2.1
Pile-up	SN	0.3
Reconstructed objects:		
Electron efficiency, energy scale, resolution	SN	0.9
Muon efficiency, momentum scale, resolution	SN	0.7
Jet vertex tagger	SN	0.1
Jet energy scale	SN	6.4
Jet energy resolution	SN	2.7
Missing transverse momentum	SN	0.3
b-tagging efficiency for b-jets	SN	0.8
b-tagging efficiency for c-jets	SN	1.8
b-tagging efficiency for light-flavour jets	SN	8.4
Background model:		
$t\bar{t}$ modelling: ISR/FSR	SN	0.2
$t\bar{t}$ modelling: generator	SN	3.8
$t\bar{t}$ modelling: parton shower/hadronisation	SN	4.5
$t\bar{t}$ modelling: interfering background shape	S	0.3
Single-top cross-section	N	0.4
Single-top modelling: ISR/FSR	SN	0.04
Single-top modelling: generator	SN	0.3
Single-top modelling: DS/DR	SN	3.1
Single-top modelling: parton shower/hadronisation	SN	1.6
W+jets modelling: generator	SN	0.8
W+jets modelling: reweighting	S	4.6
W+jets heavy flavour	S	0.04
Diboson + Z+jets normalisation	N	0.2
Multijet normalisation	N	3.8
Multijet reweighting	S	2.1
$t\bar{t}$ background scaling factor	F	26
W+jets background scaling factor	F	19

6.1 Experimental uncertainties

The uncertainty in the combined 2015+2016 integrated luminosity is 2.1%. It is derived, following a methodology similar to that detailed in Ref. [97], and using the LUCID-2 detector for the baseline luminosity measurements [98], from calibration of the luminosity scale using x-y beam-separation scans.

Experimental sources of systematic uncertainty arise from the reconstruction and measurement of jets [49], leptons [40, 42] and $E_{\mathrm{T}}^{\mathrm{miss}}$ [57]. Uncertainties associated with leptons arise from the trigger, reconstruction, identification, and isolation efficiencies, as well as the lepton momentum scale and resolution, and are studied using $Z \to \ell^+\ell^-$ and $J/\psi \to \ell^+\ell^-$ decays in data. Uncertainties associated with jets primarily arise from the jet energy scale, jet energy resolution, and the efficiency of the jet vertex tagger requirement. The largest contribution is from the jet energy scale, where the dependence of the uncertainty on jet p_{T} and η, jet flavour, and pile-up is split into 21 uncorrelated components that are treated independently in the analysis [49]. The systematic uncertainty in the $E_{\mathrm{T}}^{\mathrm{miss}}$ reconstruction is dominated by the uncertainties in the energy calibration and resolution of reconstructed jets and leptons, which are propagated to $E_{\mathrm{T}}^{\mathrm{miss}}$ and thus are included in the uncertainties in the corresponding objects. In addition, uncertainties in the p_{T} scale and resolution of reconstructed tracks that are associated with the hard-scatter vertex but not matched to any reconstructed objects are included.

The efficiency of the flavour-tagging algorithm to correctly tag b-jets, or to mis-tag c-jets or light-flavour jets, is measured for each jet flavour. The efficiencies are measured in control samples of simulated events, and in data samples of $t\bar{t}$ events, D^* mesons, and jets with impact parameters and secondary vertices consistent with a negative lifetime. Correction factors are defined to correct the tagging rates in the simulation to match the efficiencies measured in the data control samples [54, 56]. The uncertainties associated with these measurements are factorised into statistically independent sources and include a total of six independent sources affecting b-jets and four independent sources affecting c-jets. Each of these uncertainties has a different dependence on jet p_{T}. Seventeen sources of uncertainty affecting light-flavour jets are considered, and depend on jet p_{T} and η. These correction factors are only determined up to a jet p_{T} of 300 GeV for b- and c-jets, and p_{T} of 750 GeV for light-flavour jets. Therefore, an additional uncertainty is included to extrapolate these corrections to jets with p_{T} beyond the kinematic reach of the data calibration samples used; it is taken to be correlated among the three jet flavours. This uncertainty is evaluated in the simulation by comparing the tagging efficiencies while varying, e.g., the fraction of tracks with shared hits in the silicon detectors or the fraction of fake tracks resulting from random combinations of hits, both of which typically increase at high jet p_{T} due to growing track multiplicity and density of hits within the jet. Finally, an uncertainty related to the application of c-jet scale factors to τ-jets is considered, but has a negligible impact in this analysis [56].

The flavour-tagging systematic uncertainties are the leading sources of experimental uncertainties (added in quadrature, about 8.7% in the expected background yield in the SR). Other large detector-specific uncertainties arise from jet energy scale uncertainties (about a 6.4% effect on the expected background yield) and jet energy resolution uncertainties (2.7% in the expected background yield). The total systematic uncertainty associated with $E_{\mathrm{T}}^{\mathrm{miss}}$ reconstruction is about 0.3% in the SR. The combined effect of all these uncertainties results in an overall normalisation uncertainty in the SM background of approximately 6.3% taking into account correlations between the different systematic uncertainties.

For the data-driven multijet background, which has a very small contribution in the SR and CRs, a 100% normalisation uncertainty is used, to fully cover discrepancies between the observed data and the SM expectation in multijet-background-enriched regions. The large statistical uncertainties associated with

the multijet background prediction, which are uncorrelated bin-to-bin in the final discriminating variable, do not cover shape differences in the multijet background electron p_{T} distribution. This mismodelling is corrected by determining reweighting factors in a multijet-background-enriched region which are used as additional shape uncertainties in the final discriminant. These reweighting factors are obtained for electrons with $|\eta| < 1.2$ and $|\eta| > 1.2$ separately in a region requiring the same selection requirements as the preselection, but loosening the minimum $E_{\mathrm{T}}^{\mathrm{miss}}$ requirement to 20 GeV and requiring the leading jet is a b-jet.

6.2 Theoretical modelling uncertainties

A number of systematic uncertainties affecting the modelling of $t\bar{t}$ and single-top-quark processes as described in Section 4.1 are considered: uncertainties associated with the modelling of the ISR and FSR, uncertainties associated with the choice of NLO generator, modelling uncertainties in single-top-quark production (for t-channel) based on comparison of the nominal sample with an alternative MC sample described in Section 4.1, differences between single-top-quark Wt samples produced using the diagram subtraction scheme and Wt samples produced using the diagram removal scheme, as well as an uncertainty due to the choice of parton shower and hadronisation model. The $t\bar{t}$ background normalisation is a free parameter in the fit, while the normalisation of the single-top background has an uncertainty of 6.8% [87].

Uncertainties affecting the modelling of the Z+jets background and diboson background processes include a 5% effect from their respective normalisations to the theoretical NNLO cross-sections [93, 99, 100]. Since both these backgrounds are very small, this uncertainty is applied to the sum of the predicted Z+jets and diboson background processes. The W+jets background normalisation is a free parameter in the fit. The W+light-jets and W+heavy-flavour-jets predictions have similar m_{VLQ} distributions in the SR and CRs. Since the predicted ratios of W+light-jets to W+heavy-flavour-jets events in the SR and CRs are similar, but not identical, a systematic uncertainty is derived by comparing the shape of the complete W+jets sample with the W+heavy-flavour-jets portion alone. In addition, alternative W+jets samples were generated using MADGRAPH+PYTHIA8 and compared after applying the preselection criteria plus requiring that the leading jet is a b-tagged jet.

To account for the mismodelling of the leading-jet p_{T} spectrum in W+jets events, reweighting factors are obtained at preselection for W+jet events. The m_{VLQ} distributions with and without these W+jets jet-p_{T} correction factors applied to W+jet events are compared in the SR and CRs and used to quantify the systematic uncertainty in the m_{VLQ} shape of W+jets events in the fit.

All normalisation uncertainties in the different background processes are treated as uncorrelated. For background estimates based on simulations, the largest sources of theoretical modelling uncertainties are due to the choice of parton shower and hadronisation model (2–4%), the choice of generator (about 1–3% in the expected background yield) and varying the parameters controlling the initial- and final-state radiation (about 0.1% in the expected background yield), where the theoretical modelling uncertainties from $t\bar{t}$ contribute the most.

The systematic uncertainties in the modelling of the high-mass Y/T signal sample which correspond to the choice of PDF set are evaluated following the PDF4LHC15 prescription [81]. No further systematic uncertainties in the signal modelling and no uncertainties in the NLO signal production cross-section are considered. In addition, a systematic uncertainty of about 2.5% is applied to cover small differences in the reconstructed VLQ mass between signal samples passed through the full simulation of the detector and signal samples produced with the faster simulation (see Section 4).

The ATLAS MC production used in this analysis does not contain simulated events from the SM contributions that lead to interference with the VLQ signal. Therefore, these SM contributions can not be explicitly considered in the background modelling of the fit. A recent MC production at reconstruction level using the four-flavour scheme for one mass point for a left-handed Y quark shows that the m_{VLQ} distribution of the interfering SM contribution is similar but not identical to that of the other background contributions (W+jets, $t\bar{t}$, single top). To account for the presence of interfering SM contributions in the fit, an additional shape uncertainty is applied to the $t\bar{t}$ m_{VLQ} template, which leads to an uncertainty of 0.2% in the $t\bar{t}$ yield.

7 Results

7.1 Statistical interpretation

A binned maximum-likelihood fit to the data is performed to test for the presence of a signal. A separate fit is performed for each signal hypothesis with given mass and couplings. The inputs to the fit are the distributions of reconstructed VLQ candidate mass m_{VLQ} in the SR and the two CRs. The binned likelihood function $\mathcal{L}(\mu, \theta)$ is constructed as a product of Poisson probability terms over all m_{VLQ} bins considered in the search. It depends on the signal-strength parameter μ, a multiplicative factor to the theoretical signal production cross-section, and θ, a set of nuisance parameters that encode the effect of systematic uncertainties in the signal and background expectations and are implemented in the likelihood function as Gaussian constraints, as well as on the two scale factors for the free-floating $t\bar{t}$ and W+jets SM background normalisations. Uncertainties in each bin of the m_{VLQ} distributions due to the finite numbers of events in the simulation samples are included using dedicated fit parameters and are propagated to μ. The nuisance parameters θ allow variations of the expectations for signal and background according to the corresponding systematic uncertainties, and their fitted values $\hat{\theta}$ correspond to the deviations from the nominal expectations which globally provide the best fit to the data. This procedure reduces the impact of systematic uncertainties on the search sensitivity by taking advantage of the well-populated background-dominated CRs included in the likelihood fit. It also allows the CRs to improve the description of the data.

The test statistic q_μ is defined as the profile log-likelihood ratio: $q_\mu = -2\ln(\mathcal{L}(\mu, \hat{\hat{\theta}}_\mu)/\mathcal{L}(\hat{\mu}, \hat{\theta}))$, where $\hat{\mu}$ and $\hat{\theta}$ are the values of the parameters that maximise the likelihood function (with the constraint $0 \leq \hat{\mu} \leq \mu$), and $\hat{\hat{\theta}}_\mu$ are the values of the nuisance parameters that maximise the likelihood function for a given value of μ. In the absence of any significant deviation from the background expectation, q_μ is used in the $\mathrm{CL_s}$ method [101, 102] to set an upper limit on the signal production cross-section times branching ratio at the 95% CL. For a given signal scenario, values of the production cross-section (parameterised by μ) yielding $\mathrm{CL_s} < 0.05$, where $\mathrm{CL_s}$ is computed using the asymptotic approximation [103], are excluded at 95% CL.

7.2 Fit results

The background-only fit results for the yields in the SR and the two CRs are shown in Figure 5. Figure 6 presents the m_{VLQ} distributions after the background-only fit in the SR and the two CRs with the SR binning as used in the background-only fit. The overall $t\bar{t}$ (W+jets) normalisation is adjusted by a factor of 0.95 ± 0.26 (1.18 ± 0.19), where 0.26 (0.19) is the total uncertainty in the normalisation. An example distribution for a right-handed Y signal and a coupling of $c_{\mathrm{R}}^{Wb} \approx 0.5$ is overlaid, which illustrates what such

a signal would look like. Good agreement between the data and the SM backgrounds is found, in particular in the SR for the m_{VLQ} distribution, where no peak above the expected SM background is observed.

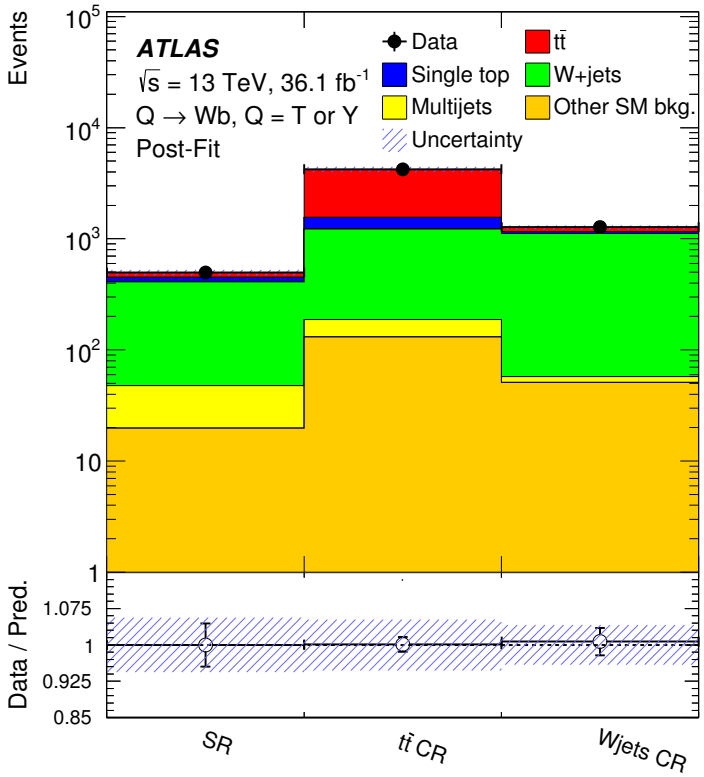

Figure 5: Observed background yields in the SR and in the two CRs after the fit to the data in the control regions and the signal region under the background-only hypothesis. The lower panel shows the ratio of data to the fitted background yields. The error bars, being smaller than the size of the data points and hence not visible in the top part of the plot, represent the statistical uncertainty in the data. The band represents the total (statistical and systematic) uncertainty after the maximum-likelihood fit.

The numbers of data events in the SR and CRs, and the event yields after fitting the background-only hypothesis to data, together with their systematic uncertainties, are listed in Table 4.

Table 4: Event yields in the SR and the $t\bar{t}$ and W+jets CRs after the fit to the background-only hypothesis. The uncertainties include statistical and systematic uncertainties. Due to correlations among the SM backgrounds and the corresponding nuisance parameters, the uncertainties in the individual background components can be larger than the uncertainty in the sum of the background, which is strongly constrained by the data.

Source	SR	$t\bar{t}$ CR	W+jets CR
$t\bar{t}$	58 ± 21	2715 ± 295	100 ± 29
Single top	29 ± 15	271 ± 118	34 ± 18
W+jets	373 ± 45	1052 ± 143	1077 ± 84
Multijet e	22 ± 20	35 ± 40	0 ± 4
Multijet μ	7 ± 7	92 ± 71	26 ± 20
Z+jets, diboson	20 ± 5	102 ± 20	50 ± 8
$t\bar{t}\,V$	0.3 ± 0.1	21 ± 3	1.6 ± 0.3
$t\bar{t}\,H$	0 ± 0	7 ± 1	0.2 ± 0.1
Total	500 ± 30	4300 ± 210	1290 ± 70
Data	497	4227	1274

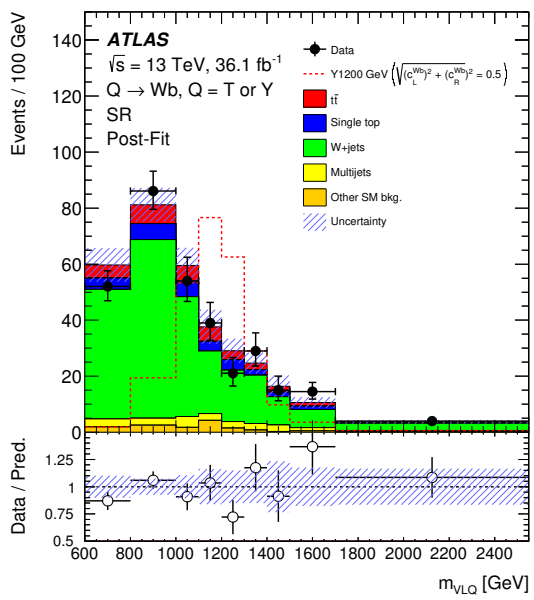

(a)

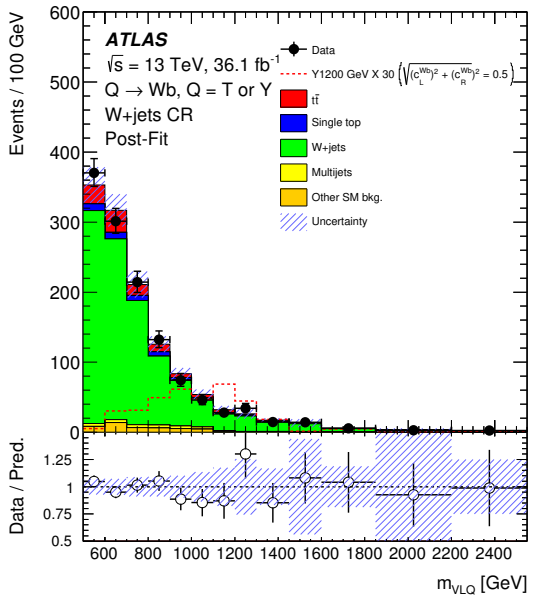

(b)

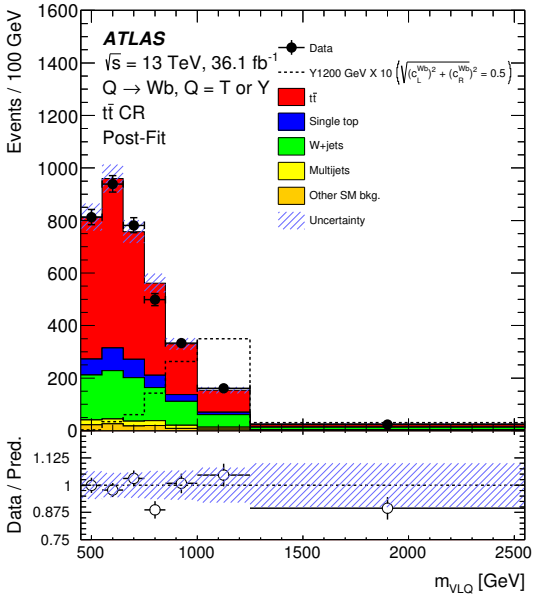

(c)

Figure 6: Distribution of the VLQ candidate mass, m_{VLQ}, in (a) the SR, (b) the W+jets CR, and (c) the $t\bar{t}$ CR, after the fit to the background-only hypothesis. The first and last bin include the underflow and overflow respectively. The lower panels show the ratios of data to the fitted background yields. The error bars represent the statistical uncertainty in the data. The band represents the total systematic uncertainty after the maximum-likelihood fit. An example distribution for a Y signal with a coupling of $\sqrt{(c_{\mathrm{L}}^{Wb})^2 + (c_{\mathrm{R}}^{Wb})^2} \approx 0.5$ without considering any interference effects is overlaid; for better visibility, it is multiplied by a factor of 30 in the W+jets CR and by a factor of 10 in the $t\bar{t}$ CR. While the total uncertainty decreases when performing the fit, the total uncertainty in the bins around 1450-1600 GeV and 1850-2200 GeV in (b) does not decrease due to significant statistical MC uncertainties in these two bins.

7.3 Limits on the VLQ production

When allowing for the signal presence, no significant deviation from the expected SM background is found. In all models considered in this search (T singlet model, right-handed Y in a (B, Y) doublet model, left-handed Y in a (T, B, Y) triplet model), interference effects with SM contributions affect the m_{VLQ} distribution (see Section 4.2). The effects of the interfering SM contributions (σ_{SM}, see Eq. (1)) in the fit are treated as a systematic uncertainty in the background modelling (see Section 6). Therefore, only the interference effect itself (σ_{I}) is explicitly taken into account in the signal template. For the left-handed Y and the T-singlet case, the size and m_{VLQ} distribution of the interfering SM contributions are estimated in three ways:

1. Using the shape of the reweighted template ($\sigma_{\mathrm{VLQ}} + \sigma_{\mathrm{I}}$).
2. Using simulated events in the four- and five-flavour schemes at particle level, with the SR requirements applied.
3. Using the fully-reconstructed MC simulated events mentioned in Section 6.

In the four-flavour scheme, the yield and the m_{VLQ} distribution both agree within statistical uncertainties for the left-handed Y in a (T, B, Y) triplet model and the T singlet model. For the left-handed Y, the yields in the four- and five-flavour schemes differ by a factor of about two, while the m_{VLQ} distributions in both schemes are very similar. A background-only fit in the SR and CRs shows that the interfering SM contribution, the shape of which is taken from the fully reconstructed MC simulation mentioned above, is in agreement with the size used to simulate the interference templates (σ_{I}) and can affect the total postfit background yield by about 4 %. This effect can be accounted for by adding the shape of the interfering SM background as an additional systematic uncertainty in the $t\bar{t}$ template (see Section 6). Studies show that the expected and observed limits change by significantly less than one standard deviation with the addition of this systematic uncertainty. For the right-handed Y in a (B, Y) doublet model, the interfering SM background contributions are much smaller than other background contributions in the SR and the CRs and are therefore negligible. Nonetheless, the non-simulated SM contributions mentionned above, which would lead to interference with a left-handed Y in a (T, B, Y) triplet model or a T singlet quark, are non-negligible and are therefore taken into account in the fit by the same additional systematic uncertainty in the $t\bar{t}$ template. Since the interfering SM contributions are not explicitly taken into account in the fit, upper limits on the total cross-section for $pp \to Wbq$, $\sigma_{\mathrm{tot}} = \sigma_{\mathrm{VLQ}} + \sigma_{\mathrm{I}} + \sigma_{\mathrm{SM}}$, times branching ratio can not be determined, but limits on the coupling value of the vector-like T or Y quark to Wb in a given model based on $\sigma_{\mathrm{VLQ}} + \sigma_{\mathrm{I}}$ are set.

To set a coupling-value limit, the following iterative procedure is performed: for a fixed Q mass hypothesis and for a given coupling value c^{Wb}, a m_{VLQ} signal-plus-interference template $h_{\mathrm{VLQ+I}}(m_{\mathrm{VLQ}}; c^{Wb})$ containing the VLQ (σ_{VLQ}) and the interference contribution (σ_{I}) (but not the interfering SM contribution (σ_{SM})) is constructed by reweighting the default VLQ-only signal template $h_{\mathrm{VLQ}}(m_{\mathrm{VLQ}}; c^{Wb}_{\mathrm{def}})$ for a default coupling value ($c^{Wb}_{\mathrm{def}} = c_0$) using the ratio r (see Eq. (2)) defined in Section 4.2. The maximum-likelihood fit to signal plus background is performed with the signal template $h_{\mathrm{VLQ+I}}(m_{\mathrm{VLQ}}; c^{Wb})$, and an upper limit on $\sigma_{\mathrm{VLQ}} + \sigma_{\mathrm{I}}$ is determined. The T-quark branching ratio is set to $\mathcal{B}(T \to Wb) = 0.5$,[8] whereas $\mathcal{B}(Y \to Wb) = 1$ is used for the Y quark. The theoretical cross-section σ_{VLQ} is taken from Ref. [14], where the NLO Wb fusion cross-section is calculated in the NWA. With rising Q mass and coupling value c^{Wb}, the Q width becomes

[8] For the T singlet model, $\mathcal{B}(T \to Wb) = 0.5$ is a very good approximation in the mass and coupling ranges relevant to this search.

sizeable and the NWA calculation is no longer a good approximation. Therefore, the following correction factor applies to the theoretical cross-section prediction:

$$\frac{\sigma_{\mathrm{LO,noNWA}}}{\sigma_{\mathrm{LO,NWA}}} = C_{\mathrm{NWA}},$$

where $\sigma_{\mathrm{LO,noNWA}}$ is the LO cross-section without the NWA and $\sigma_{\mathrm{LO,NWA}}$ the LO cross-section with the NWA, both calculated with the MADGRAPH5_aMC@NLO 2.2.3 [74] generator. It is assumed that C_{NWA} is the same to a good approximation for the calculation of the NLO cross-section. These correction factors reduce the predicted σ_{VLQ} value. The reduction becomes stronger with increasing mass and coupling value and is about 40% at a Q mass of 1500 GeV and a coupling value of 0.9. From the upper limit on $\sigma_{\mathrm{VLQ}} + \sigma_{\mathrm{I}}$, a corresponding coupling value $c^{Wb\prime}$ is calculated, a new signal template $h_{\mathrm{VLQ+I}}(m_{\mathrm{VLQ}}; c^{Wb\prime})$ is constructed using the reweighting technique described above, and the fit repeated until convergence is observed in the coupling value $c^{Wb\prime}$. It is explicitly checked that the result of the iterative procedure does not depend on the choice of starting value for c^{Wb}, by repeating the full iterative process with a lower or higher starting value than the one at convergence. If the coupling converges to a value smaller than the signal-production value of 0.5, the iterative procedure is repeated with a coupling much lower than the value at convergence. A systematic uncertainty of about 2.5% for the coupling reweighting and a shape uncertainty for the interference contribution are assigned to this procedure.

Depending on the binning of the m_{VLQ} distribution, it is possible that negative entries occur in some bins of the signal-plus-interference template due to the interference effect when large couplings are considered, and this poses a problem in the limit-setting procedure. To avoid this problem, the last bins in the reconstructed m_{VLQ} distribution are merged until no negative bin entries exist. As a result, a different binning in the m_{VLQ} distribution is chosen for each VLQ mass hypothesis for the T-singlet case and for the left-handed Y case, which guarantees (independent of c^{Wb}) that all bins in the signal-plus-interference template have positive values. The rebinning reduces the sensitivity for high-mass T and left-handed Y signals. As an example, Figure 7 shows the fitted VLQ candidate mass distributions for left-handed Y signals with masses of 900 GeV and 1500 GeV and for left-handed T signals with masses of 800 GeV and 1200 GeV. For the T singlet model, the total integral of the signal-plus-interference template at reconstruction level can become negative for VLQ mass hypotheses above 1200 GeV. As a result, no coupling-value limits are set for the T singlet model with masses above 1200 GeV. Tables 5, 6, and 7 summarise the observed and expected 95% $\mathrm{CL_s}$ upper limits on the coupling value and limits on the mixing angle as a function of Q-quark mass, for the T singlet model (assuming $\mathcal{B}(T \to Wb) \approx 0.5$), the right-handed Y in a (B, Y) doublet model, and the left-handed Y in a (T, B, Y) triplet model respectively. The parameterisation of Ref. [1] in terms of right- or left-handed mixing angles is chosen for the coupling limits; these can be easily translated to the parameterisation of Ref. [14] for the models under consideration. In a T singlet model, the upper exclusion limit on $|\sin\theta_{\mathrm{L}}|$ (c_{L}^{Wb}) is 0.18 (0.25) for a T quark of mass of 800 GeV, rising to 0.35 (0.49) for a T quark with a mass of 1200 GeV. For a (B, Y) doublet, the upper exclusion limit on $|\sin\theta_{\mathrm{R}}|$ (c_{R}^{Wb}) is 0.17 (0.24) for a signal with a mass of 800 GeV and 0.55 (0.77) for Y quarks with a mass of 1800 GeV. The observed (expected) lower mass limit for Y quarks is about 1.64 TeV (1.80 TeV) for a right-handed coupling value of $c_{\mathrm{R}}^{Wb} = 1/\sqrt{2}$. For Y signals in a (T, B, Y) triplet the upper exclusion limits on $|\sin\theta_{\mathrm{L}}|$ (c_{L}^{Wb}) vary between 0.16 (0.31) and 0.39 (0.78) for masses between 800 GeV and 1600 GeV.

Table 5: Observed and expected 95% CL upper limits on $|\sin\theta_{\mathrm{L}}|$ and c_{L}^{Wb} for a left-handed T quark in a T singlet model with masses of 800 GeV to 1200 GeV assuming $\mathcal{B}(T \to Wb) = 0.5$. The $\pm1\sigma$ and $\pm2\sigma$ uncertainties in the expected limits are also given.

T mass [GeV]	Observed limit on $\lvert\sin\theta_{\mathrm{L}}\rvert$	Expected limit on $\lvert\sin\theta_{\mathrm{L}}\rvert^{+1\sigma/+2\sigma}_{-1\sigma/-2\sigma}$	Observed limit on c_{L}^{Wb}	Expected limit on $c_{\mathrm{L}}^{Wb\,+1\sigma/+2\sigma}_{\quad-1\sigma/-2\sigma}$
800	0.18	$0.19^{0.04/0.08}_{0.03/0.06}$	0.25	$0.27^{0.06/0.11}_{0.05/0.08}$
900	0.24	$0.20^{0.05/0.09}_{0.05/0.07}$	0.34	$0.29^{0.07/0.13}_{0.07/0.10}$
1000	0.20	$0.21^{0.06/0.08}_{0.07/0.09}$	0.29	$0.30^{0.08/0.12}_{0.10/0.12}$
1100	0.25	$0.27^{0.09/0.11}_{0.13/0.15}$	0.36	$0.38^{0.12/0.15}_{0.18/0.21}$
1200	0.35	$0.35^{0.13/0.14}_{0.22/0.23}$	0.49	$0.49^{0.18/0.20}_{0.31/0.33}$

Table 6: Observed and expected 95% CL upper limits on $|\sin\theta_{\mathrm{R}}|$ and c_{R}^{Wb} for a right-handed Y quark in a (B, Y) doublet model with masses of 800 GeV to 1800 GeV. The $\pm1\sigma$ and $\pm2\sigma$ uncertainties in the expected limits are also given.

Y mass [GeV]	Observed limit on $\lvert\sin\theta_{\mathrm{R}}\rvert$	Expected limit on $\lvert\sin\theta_{\mathrm{R}}\rvert^{+1\sigma/+2\sigma}_{-1\sigma/-2\sigma}$	Observed limit on c_{R}^{Wb}	Expected limit on $c_{\mathrm{R}}^{Wb\,+1\sigma/+2\sigma}_{\quad-1\sigma/-2\sigma}$
800	0.17	$0.20^{0.04/0.08}_{0.03/0.05}$	0.24	$0.28^{0.05/0.12}_{0.04/0.07}$
900	0.18	$0.19^{0.04/0.08}_{0.03/0.05}$	0.26	$0.27^{0.05/0.11}_{0.04/0.07}$
1000	0.17	$0.17^{0.03/0.07}_{0.03/0.05}$	0.25	$0.25^{0.04/0.10}_{0.04/0.07}$
1100	0.17	$0.18^{0.03/0.07}_{0.03/0.05}$	0.24	$0.25^{0.05/0.10}_{0.04/0.07}$
1200	0.17	$0.20^{0.04/0.08}_{0.03/0.05}$	0.25	$0.28^{0.05/0.11}_{0.04/0.08}$
1300	0.19	$0.22^{0.04/0.09}_{0.03/0.06}$	0.27	$0.31^{0.06/0.12}_{0.05/0.08}$
1400	0.24	$0.25^{0.05/0.10}_{0.04/0.07}$	0.35	$0.36^{0.06/0.14}_{0.05/0.10}$
1500	0.31	$0.28^{0.05/0.11}_{0.04/0.07}$	0.44	$0.39^{0.07/0.15}_{0.06/0.11}$
1600	0.45	$0.37^{0.08/0.19}_{0.06/0.10}$	0.64	$0.53^{0.11/0.27}_{0.08/0.14}$
1700	0.59	$0.46^{0.10/0.25}_{0.08/0.13}$	0.83	$0.65^{0.15/0.36}_{0.11/0.18}$
1800	0.55	$0.43^{0.09/0.22}_{0.07/0.12}$	0.77	$0.61^{0.13/0.32}_{0.10/0.17}$

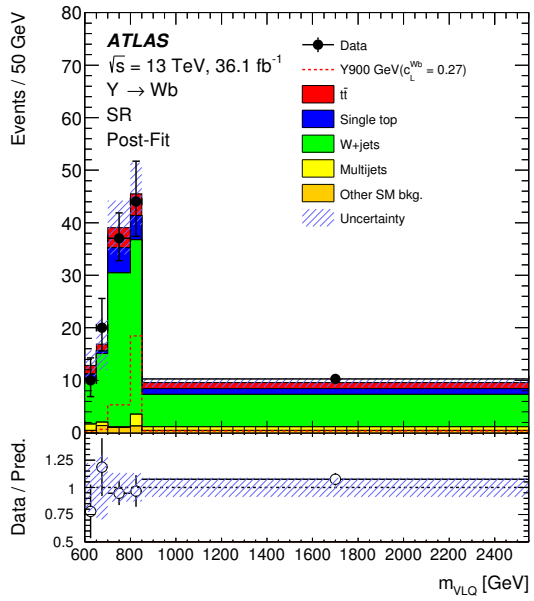

(a)

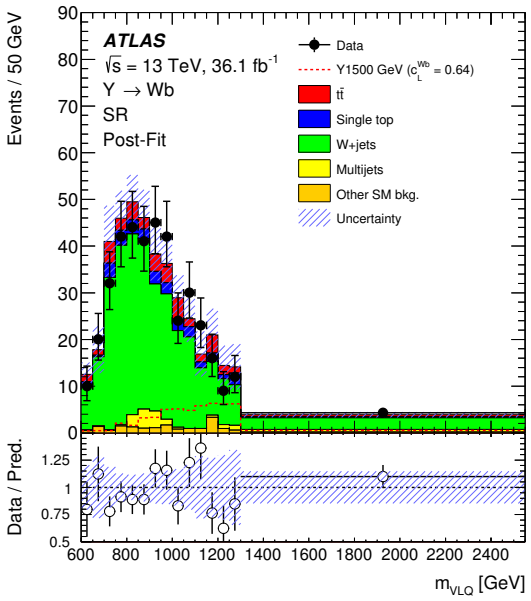

(b)

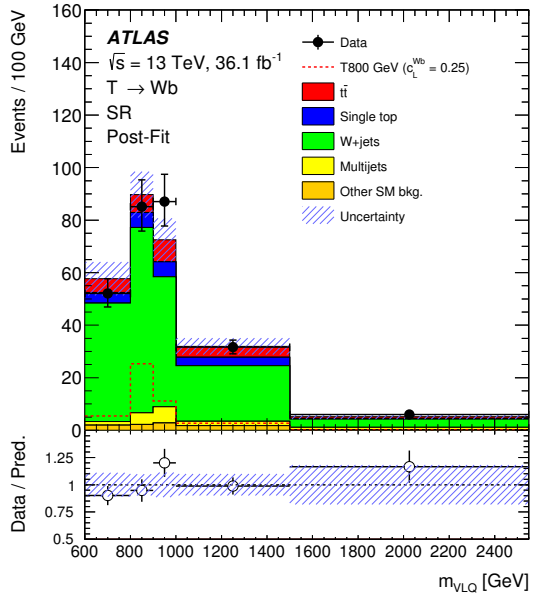

(c)

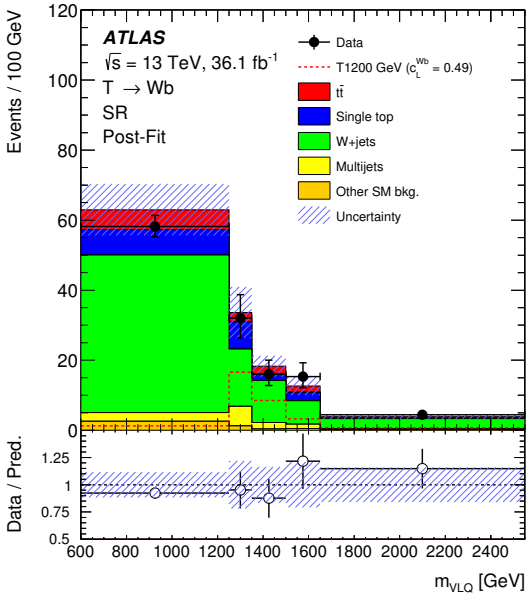

(d)

Figure 7: Distributions of the VLQ candidate mass, m_{VLQ}, after the fit to the background-only hypotheses for four different binnings chosen for four different signal masses. The first and last bin include the underflow and overflow respectively. The VLQ candidate mass distributions for (a) a left-handed Y signal with mass 900 GeV and coupling $c_{\mathrm{L}}^{Wb} = 0.27$, (b) a left-handed Y signal with mass 1500 GeV and coupling $c_{\mathrm{L}}^{Wb} = 0.64$, (c) a left-handed T signal with mass of 800 GeV and coupling $c_{\mathrm{L}}^{Wb} = 0.25$ and (d) a left-handed T signal with mass 1200 GeV and coupling $c_{\mathrm{L}}^{Wb} = 0.49$ are also shown; all signal distributions include interference. The lower panels show the ratio of data to the fitted background yields. The error bars represent the statistical uncertainty in the data. The band represents the total systematic uncertainty after the maximum-likelihood fit.

Table 7: Observed and expected 95% CL upper limits on $|\sin\theta_{\mathrm{L}}|$ and c_{L}^{Wb} for a left-handed Y quark in a (T, B, Y) triplet model with masses of 800 GeV to 1600 GeV. The $\pm1\sigma$ and $\pm2\sigma$ uncertainties in the expected limits are also given.

Y mass [GeV]	Observed limit on $\lvert\sin\theta_{\mathrm{L}}\rvert$	Expected limit on $\lvert\sin\theta_{\mathrm{L}}\rvert^{+1\sigma/+2\sigma}_{-1\sigma/-2\sigma}$	Observed limit on c_{L}^{Wb}	Expected limit on $c_{\mathrm{L}}^{Wb\,+1\sigma/+2\sigma}_{-1\sigma/-2\sigma}$
800	0.16	$0.20^{0.04/0.09}_{0.03/0.05}$	0.31	$0.40^{0.08/0.19}_{0.06/0.11}$
900	0.14	$0.15^{0.03/0.07}_{0.02/0.04}$	0.28	$0.30^{0.06/0.13}_{0.05/0.08}$
1000	0.16	$0.15^{0.03/0.06}_{0.02/0.04}$	0.32	$0.29^{0.05/0.12}_{0.04/0.08}$
1100	0.23	$0.22^{0.03/0.08}_{0.03/0.06}$	0.47	$0.43^{0.07/0.15}_{0.07/0.12}$
1200	0.20	$0.16^{0.03/0.07}_{0.02/0.04}$	0.40	$0.33^{0.06/0.13}_{0.05/0.09}$
1300	0.25	$0.21^{0.04/0.08}_{0.03/0.06}$	0.49	$0.43^{0.08/0.16}_{0.07/0.12}$
1400	0.18	$0.25^{0.05/0.10}_{0.04/0.07}$	0.36	$0.51^{0.09/0.20}_{0.08/0.14}$
1500	0.32	$0.35^{0.08/0.18}_{0.06/0.10}$	0.64	$0.70^{0.16/0.37}_{0.12/0.20}$
1600	0.39	$0.40^{0.11/0.28}_{0.07/0.12}$	0.78	$0.80^{0.21/0.56}_{0.14/0.24}$

In Figure 8, these direct mixing-angle bounds are compared with those from electroweak precision observables taken from Ref. [1], assuming that there are no multiplets other than the one considered. For the (B, Y) doublet model, the bounds presented here are competitive with the indirect constraints for VLQ masses between 800 GeV and 1250 GeV.

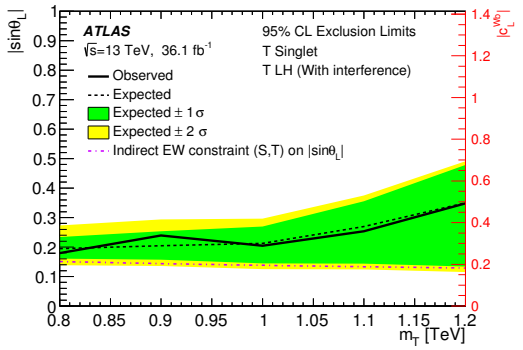

(a)

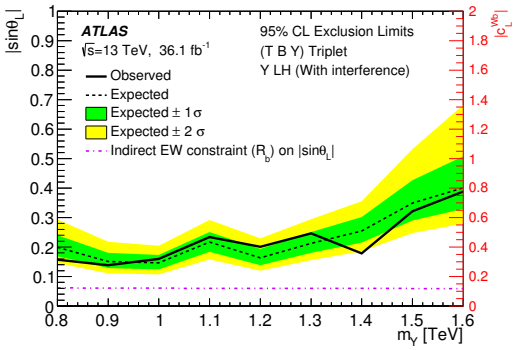

(b)

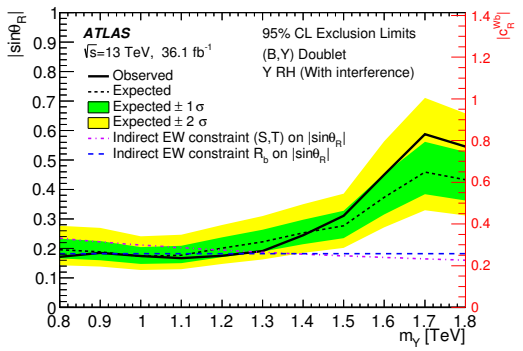

(c)

Figure 8: Observed (solid line) and expected (short-dashed line) 95% CL limits on (a) the mixing angle $|\sin\theta_{\mathrm{L}}|$ and the coupling value c_{L}^{Wb} for a singlet T-quark model assuming $\mathcal{B}(T \to Wb) \approx 0.5$, (b) $|\sin\theta_{\mathrm{L}}|$ and c_{L}^{Wb} for a (T, B, Y) triplet model, and (c) $|\sin\theta_{\mathrm{R}}|$ and c_{R}^{Wb} for a (B, Y) doublet model assuming a branching ratio $\mathcal{B}(Y \to Wb)$ = 1, as a function of the VLQ mass. The surrounding bands correspond to ±1 and ±2 standard deviations around the expected limit. The excluded region is given by the area above the solid line. Constraints from electroweak precision observables, which are only valid for the mixing angles, from either the S and T parameters (dashed-dotted line) or from the R_b values (long-dashed line), are also shown. These constraints are taken from Ref. [1], where they are presented as a function of m_{B} (in the (B, Y) doublet case), respectively, m_{T} (in the (T, B, Y) triplet case) and translated to m_{Y} using the value of the corresponding mixing angle constraint.

Since the interference effect for the case of the right-handed Y quark is very small, and therefore the signal+interference template is very similar to the one of a pure resonance, a limit on $\sigma_{\mathrm{VLQ}} + \sigma_{\mathrm{I}}$ times branching ratio is presented for this case in Figure 9, corresponding to the $|\sin\theta_{\mathrm{R}}|$ and c_{R}^{Wb} limits for a (B, Y) doublet model presented in Figure (c).

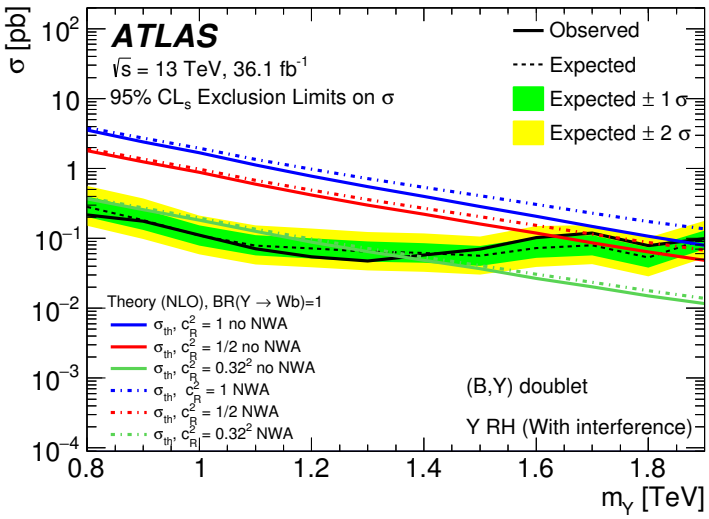

Figure 9: Observed (solid line) and expected (short-dashed line) 95% CL limits on cross-section times branching ratio for the case of the right-handed Y quark for a (B,Y) doublet model as a function of VLQ mass. For the theoretical prediction, the branching ratio $\mathcal{B}(Y \to Wb)$ is set to one. The theoretical NLO cross-sections for different coupling values are shown for the calculation using the narrow-width approximation (dashed-dotted lines) and using no narrow-width approximation (solid lines) as described in the text.

8 Conclusion

A search for the production of a single vector-like quark Q, where Q can be either a T or Y quark, with the subsequent decay into Wb has been carried out with the ATLAS experiment at the CERN LHC. The data used in this search correspond to an integrated luminosity of 36.1 fb^{-1} of pp collisions with a centre-of-mass energy $\sqrt{s}$ = 13 TeV recorded in 2015 and 2016. The selected events have exactly one isolated electron or muon, a high-p_{T} b-tagged jet, missing transverse momentum and at least one forward jet. The Q candidate is fully reconstructed and its mass is used as a discriminating variable in a maximum-likelihood fit. The observed data distributions are compatible with the expected Standard Model background and no significant excess is observed. The search result is interpreted for $Q = T$ in a T singlet model and $Q = Y$ in either a (B, Y) doublet model or in a (T, B, Y) triplet model, taking into account the interference effect with the Standard Model background. Limits at 95% CL are set on the cross-section times branching ratio as a function of the VLQ mass in the case of the (B, Y) doublet model, where interference has the smallest effect. The search results are translated into limits on the QWb mixing angle or coupling. In the T-singlet case, the 95% CL limit on $|\sin\theta_{\mathrm{L}}|$ (c_{L}^{Wb}) varies between 0.18 and 0.35 (0.25 and 0.49) for masses from 800 GeV to 1200 GeV. In the (B, Y) doublet model, exclusion limits on $|\sin\theta_{\mathrm{R}}|$ (c_{R}^{Wb}) vary between 0.17 and 0.55 (0.24 and 0.77) for masses between 800 GeV and 1800 GeV and the $|\sin\theta_{\mathrm{R}}|$ bounds presented here are below the indirect electroweak constraints for masses between about 900 GeV and 1250 GeV where exclusion limits on $|\sin\theta_{\mathrm{R}}|$ are around 0.18–0.19. In the case of the (T, Y, B) triplet, the limits on $|\sin\theta_{\mathrm{L}}|$ (c_{L}^{Wb}) vary between 0.16 and 0.39 (0.31 and 0.78) for masses from 800 GeV to 1600 GeV. For all signal scenarios explored, this analysis is found to significantly improve upon the reach of previous searches.

Acknowledgements

We thank CERN for the very successful operation of the LHC, as well as the support staff from our institutions without whom ATLAS could not be operated efficiently.

We acknowledge the support of ANPCyT, Argentina; YerPhI, Armenia; ARC, Australia; BMWFW and FWF, Austria; ANAS, Azerbaijan; SSTC, Belarus; CNPq and FAPESP, Brazil; NSERC, NRC and CFI, Canada; CERN; CONICYT, Chile; CAS, MOST and NSFC, China; COLCIENCIAS, Colombia; MSMT CR, MPO CR and VSC CR, Czech Republic; DNRF and DNSRC, Denmark; IN2P3-CNRS, CEA-DRF/IRFU, France; SRNSFG, Georgia; BMBF, HGF, and MPG, Germany; GSRT, Greece; RGC, Hong Kong SAR, China; ISF and Benoziyo Center, Israel; INFN, Italy; MEXT and JSPS, Japan; CNRST, Morocco; NWO, Netherlands; RCN, Norway; MNiSW and NCN, Poland; FCT, Portugal; MNE/IFA, Romania; MES of Russia and NRC KI, Russian Federation; JINR; MESTD, Serbia; MSSR, Slovakia; ARRS and MIZŠ, Slovenia; DST/NRF, South Africa; MINECO, Spain; SRC and Wallenberg Foundation, Sweden; SERI, SNSF and Cantons of Bern and Geneva, Switzerland; MOST, Taiwan; TAEK, Turkey; STFC, United Kingdom; DOE and NSF, United States of America. In addition, individual groups and members have received support from BCKDF, CANARIE, CRC and Compute Canada, Canada; COST, ERC, ERDF, Horizon 2020, and Marie Skłodowska-Curie Actions, European Union; Investissements d' Avenir Labex and Idex, ANR, France; DFG and AvH Foundation, Germany; Herakleitos, Thales and Aristeia programmes co-financed by EU-ESF and the Greek NSRF, Greece; BSF-NSF and GIF, Israel; CERCA Programme Generalitat de Catalunya, Spain; The Royal Society and Leverhulme Trust, United Kingdom.

The crucial computing support from all WLCG partners is acknowledged gratefully, in particular from CERN, the ATLAS Tier-1 facilities at TRIUMF (Canada), NDGF (Denmark, Norway, Sweden), CC-IN2P3 (France), KIT/GridKA (Germany), INFN-CNAF (Italy), NL-T1 (Netherlands), PIC (Spain), ASGC (Taiwan), RAL (UK) and BNL (USA), the Tier-2 facilities worldwide and large non-WLCG resource providers. Major contributors of computing resources are listed in Ref. [104].

References

[1] J. A. Aguilar-Saavedra, R. Benbrik, S. Heinemeyer and M. Pérez-Victoria, *Handbook of vectorlike quarks: Mixing and single production*, Phys. Rev. D **88** (2013) 094010, arXiv: 1306.0572 [hep-ph].

[2] ATLAS Collaboration, *Observation of a new particle in the search for the Standard Model Higgs boson with the ATLAS detector at the LHC*, Phys. Lett. B **716** (2012) 1, arXiv: 1207.7214 [hep-ex].

[3] CMS Collaboration, *Observation of a new boson at a mass of 125 GeV with the CMS experiment at the LHC*, Phys. Lett. B **716** (2012) 30, arXiv: 1207.7235 [hep-ex].

[4] O. Eberhardt et al., *Impact of a Higgs Boson at a Mass of 126 GeV on the Standard Model with Three and Four Fermion Generations*, Phys. Rev. Lett. **109** (2012) 241802, arXiv: 1209.1101 [hep-ph].

[5] F. Del Aguila and M. J. Bowick, *The possibility of new fermions with $\Delta I = 0$ mass*, Nucl. Phys. B **224** (1983) 107.

[6] G. Cacciapaglia et al., *Heavy vector-like top partners at the LHC and flavour constraints*, JHEP **03** (2012) 070, arXiv: 1108.6329 [hep-ph].

[7] L. Randall and R. Sundrum, *A Large Mass Hierarchy from a Small Extra Dimension*, Phys. Rev. Lett. **83** (1999) 3370, arXiv: hep-ph/9905221 [hep-ph].

[8] Kaplan, D. B. and Georgi, H. and Dimopoulos, S., *Composite Higgs scalars*, Phys. Lett. B **136** (1984) 187.

[9] N. Vignaroli, *Discovering the composite Higgs through the decay of a heavy fermion*, JHEP **07** (2012) 158, arXiv: 1204.0468 [hep-ph].

[10] M. Schmaltz and D. Tucker-Smith, *Little Higgs Theories*, Ann. Rev. Nucl. Part. Sci. **55** (2005) 229, arXiv: hep-ph/0502182 [hep-ph].

[11] S. P. Martin, *Extra vector-like matter and the lightest Higgs scalar boson mass in low-energy supersymmetry*, Phys. Rev. D **81** (2010) 035004, arXiv: 0910.2732 [hep-ph].

[12] M.-L. Xiao and J.-H. Yu, *Stabilizing electroweak vacuum in a vector-like fermion model*, Phys. Rev. D **90** (2014) 014007, arXiv: 1404.0681 [hep-ph].

[13] A. De Simone, O Matsedonskyi, R. Rattazzi and A. Wulzer, *A first top partner hunter's guide*, JHEP **04** (2013) 004, arXiv: 1211.5663 [hep-ph].

[14] O. Matsedonskyi, G. Panico and A. Wulzer, *On the interpretation of Top Partners searches*, JHEP **12** (2014) 097, arXiv: 1409.0100 [hep-ph],
We would like to thank A. Wulzer for providing us NLO cross-sections for the single VLQ signals and helpful discussion about the NLO cross-section calculations.

[15] M. E. Peskin and T. Takeuchi, *New constraint on a strongly interacting Higgs sector*, Phys. Rev. Lett. **65** (1990) 964.

[16] ATLAS Collaboration, *Search for production of vector-like quark pairs and of four top quarks in the lepton-plus-jets final state in pp collisions at* $\sqrt{s} = 8$ *TeV with the ATLAS detector*, JHEP **08** (2015) 105, arXiv: 1505.04306 [hep-ex].

[17] ATLAS Collaboration, *Search for pair production of vector-like top quarks in events with one lepton, jets, and missing transverse momentum in* $\sqrt{s} = 13$ *TeV pp collisions with the ATLAS detector*, JHEP **08** (2017) 052, arXiv: 1705.10751 [hep-ex].

[18] CMS Collaboration, *Search for vector-like T quarks decaying to top quarks and Higgs bosons in the all-hadronic channel using jet substructure*, JHEP **06** (2015) 080, arXiv: 1503.01952 [hep-ex].

[19] CMS Collaboration, *Inclusive search for a vector-like T quark with charge* $\frac{2}{3}$ *in pp collisions at* $\sqrt{s} = 8$ *TeV*, Phys. Lett. B **729** (2014) 149, arXiv: 1311.7667 [hep-ex].

[20] CMS Collaboration, *Search for pair production of vector-like quarks in the* $bW\bar{b}W$ *channel from proton-proton collisions at* $\sqrt{s} = 13$ *TeV*, Phys. Lett. B **779** (2018) 82, arXiv: 1710.01539 [hep-ex].

[21] ATLAS Collaboration, *Analysis of events with b-jets and a pair of leptons of the same charge in pp collisions at* $\sqrt{s} = 8$ *TeV with the ATLAS detector*, JHEP **10** (2015) 150, arXiv: 1504.04605 [hep-ex].

[22] ATLAS Collaboration, *Search for single production of vector-like quarks decaying into Wb in pp collisions at $\sqrt{s}$ = 8 TeV with the ATLAS detector*, Eur. Phys. J. C **76** (2016) 442, arXiv: 1602.05606 [hep-ex].

[23] ATLAS Collaboration, *Search for pair production of up-type vector-like quarks and for four-top-quark events in final states with multiple b-jets with the ATLAS detector*, JHEP **07** (2018) 089, arXiv: 1803.09678 [hep-ex].

[24] CMS Collaboration, *Search for pair production of vector-like T and B quarks in single-lepton final states using boosted jet substructure in proton-proton collisions at $\sqrt{s}$ = 13 TeV*, JHEP **11** (2017) 085, arXiv: 1706.03408 [hep-ex].

[25] CMS Collaboration, *Search for single production of vector-like quarks decaying to a Z boson and a top or a bottom quark in proton-proton collisions at $\sqrt{s}$ = 13 TeV*, JHEP **05** (2017) 029, arXiv: 1701.07409 [hep-ex].

[26] ATLAS Collaboration, *Search for pair production of heavy vector-like quarks decaying to high-p_{T} W bosons and b quarks in the lepton-plus-jets final state in pp collisions at $\sqrt{s}$=13 TeV with the ATLAS detector*, JHEP **10** (2017) 141, arXiv: 1707.03347 [hep-ex].

[27] CMS Collaboration, *Search for vector-like T and B quark pairs in final states with leptons at $\sqrt{s}$ = 13 TeV*, JHEP **08** (2018) 177, arXiv: 1805.04758 [hep-ex].

[28] CMS Collaboration, *Search for single production of a heavy vector-like T quark decaying to a Higgs boson and a top quark with a lepton and jets in the final state*, Phys. Lett. B **771** (2017) 80, arXiv: 1612.00999 [hep-ex].

[29] CMS Collaboration, *Search for single production of vector-like quarks decaying into a b quark and a W boson in proton–proton collisions at $\sqrt{s}$ = 13 TeV*, Phys. Lett. B **772** (2017) 634, arXiv: 1701.08328 [hep-ex].

[30] CMS Collaboration, *Search for single production of a vector-like T quark decaying to a Z boson and a top quark in proton-proton collisions at $\sqrt{s}$ = 13 TeV*, Phys. Lett. **B781** (2018) 574, arXiv: 1708.01062 [hep-ex].

[31] ATLAS Collaboration, *Search for pair and single production of new heavy quarks that decay to a Z boson and a third-generation quark in pp collisions at $\sqrt{s}$ = 8 TeV with the ATLAS detector*, JHEP **11** (2014) 104, arXiv: 1409.5500 [hep-ex].

[32] CMS Collaboration, *Search for electroweak production of a vector-like quark decaying to a top quark and a Higgs boson using boosted topologies in fully hadronic final states*, JHEP **04** (2017) 136, arXiv: 1612.05336 [hep-ex].

[33] ATLAS Collaboration, *Search for pair- and single-production of vector-like quarks in final states with at least one Z boson decaying into a pair of electrons or muons in pp collision data collected with the ATLAS detector*, (2018), arXiv: 1806.10555 [hep-ex].

[34] ATLAS Collaboration, *Combination of the searches for pair-produced vector-like partners of the third-generation quarks at $\sqrt{s}$ = 13 TeV with the ATLAS detector*, Phys. Rev. Lett. **121** (2018) 211801, arXiv: 1808.02343 [hep-ex].

[35] ATLAS Collaboration, *The ATLAS Experiment at the CERN Large Hadron Collider*, JINST **3** (2008) S08003.

[36] ATLAS Collaboration, *ATLAS Insertable B-Layer Technical Design Report*, ATLAS-TDR-19, 2010, URL: https://cds.cern.ch/record/1291633,
ATLAS Insertable B-Layer Technical Design Report Addendum, ATLAS-TDR-19-ADD-1, 2012, URL: https://cds.cern.ch/record/1451888.

[37] B. Abbott et al., *Production and Integration of the ATLAS Insertable B-Layer*, JINST **13** (2018) T05008, arXiv: 1803.00844 [physics.ins-det].

[38] ATLAS Collaboration, *Performance of the ATLAS trigger system in 2015*, Eur. Phys. J. C **77** (2017) 317, arXiv: 1611.09661 [hep-ex].

[39] ATLAS Collaboration,
Electron and photon energy calibration with the ATLAS detector using LHC Run 1 data, Eur. Phys. J. C **74** (2014) 3071, arXiv: 1407.5063 [hep-ex].

[40] ATLAS Collaboration, *Electron efficiency measurements with the ATLAS detector using the 2015 LHC proton–proton collision data*, ATLAS-CONF-2016-024, 2016, URL: https://cds.cern.ch/record/2157687.

[41] ATLAS Collaboration, *Electron and photon energy calibration with the ATLAS detector using data collected in 2015 at* $\sqrt{s} = 13$ *TeV*, ATL-PHYS-PUB-2016-015, 2016, URL: https://cds.cern.ch/record/2203514.

[42] ATLAS Collaboration, *Muon reconstruction performance of the ATLAS detector in proton–proton collision data at* $\sqrt{s} = 13$ *TeV*, Eur. Phys. J. C **76** (2016) 292, arXiv: 1603.05598 [hep-ex].

[43] ATLAS Collaboration, *Estimation of non-prompt and fake lepton backgrounds in final states with top quarks produced in proton–proton collisions at* $\sqrt{s} = 8$ *TeV with the ATLAS Detector*, ATLAS-CONF-2014-058, 2014, URL: https://cds.cern.ch/record/1951336.

[44] ATLAS Collaboration,
Topological cell clustering in the ATLAS calorimeters and its performance in LHC Run 1, Eur. Phys. J. C **77** (2017) 490, arXiv: 1603.02934 [hep-ex].

[45] M. Cacciari, G. P. Salam and G. Soyez, *The anti-k_t jet clustering algorithm*, JHEP **04** (2008) 063, arXiv: 0802.1189 [hep-ph].

[46] M. Cacciari et al., *FastJet user manual*, Eur. Phys. J. **C72** (2012) 1896, arXiv: 1111.6097 [hep-ph].

[47] ATLAS Collaboration,
Jet energy measurement with the ATLAS detector in proton–proton collisions at $\sqrt{s} = 7$ *TeV*, Eur. Phys. J. C **73** (2013) 2304, arXiv: 1112.6426 [hep-ex].

[48] ATLAS Collaboration, *Monte Carlo Calibration and Combination of In-situ Measurements of Jet Energy Scale, Jet Energy Resolution and Jet Mass in ATLAS*, ATLAS-CONF-2015-037, 2015, URL: https://cds.cern.ch/record/2044941.

[49] ATLAS Collaboration, *Jet energy scale measurements and their systematic uncertainties in proton-proton collisions at* $\sqrt{s} = 13$ *TeV with the ATLAS detector*, Phys. Rev. D **96** (2017) 072002, arXiv: 1703.09665 [hep-ex].

[50] ATLAS Collaboration,
Selection of jets produced in 13 *TeV proton–proton collisions with the ATLAS detector*, ATLAS-CONF-2015-029, 2015, URL: https://cds.cern.ch/record/2037702.

[51] ATLAS Collaboration, *Performance of pile-up mitigation techniques for jets in pp collisions at $\sqrt{s}$ = 8 TeV using the ATLAS detector*, Eur. Phys. J. C **76** (2016) 581, arXiv: 1510.03823 [hep-ex].

[52] ATLAS Collaboration, *Commissioning of the ATLAS b-tagging algorithms using $t\bar{t}$ events in early Run 2 data*, ATL-PHYS-PUB-2015-039, 2015, URL: https://cds.cern.ch/record/2047871.

[53] ATLAS Collaboration, *Calibration of the performance of b-tagging for c and light-flavour jets in the 2012 ATLAS data*, ATLAS-CONF-2014-046, 2014, URL: https://cds.cern.ch/record/1741020.

[54] ATLAS Collaboration, *Performance of b-jet identification in the ATLAS experiment*, JINST **11** (2016) P04008, arXiv: 1512.01094 [hep-ex].

[55] ATLAS Collaboration, *Measurements of b-jet tagging efficiency with the ATLAS detector using $t\bar{t}$ events at $\sqrt{s}$ = 13 TeV*, JHEP **08** (2018) 089, arXiv: 1805.01845 [hep-ex].

[56] ATLAS Collaboration, *Measurements of b-jet tagging efficiency with the ATLAS detector using $t\bar{t}$ events at $\sqrt{s}$ = 13 TeV*, (2018), arXiv: 1805.01845 [hep-ex].

[57] ATLAS Collaboration, *Performance of missing transverse momentum reconstruction with the ATLAS detector using proton-proton collisions at $\sqrt{s}$ = 13 TeV*, Eur. Phys. J. **C78** (2018) 903, arXiv: 1802.08168 [hep-ex].

[58] ATLAS Collaboration, *The ATLAS Simulation Infrastructure*, Eur. Phys. J. C **70** (2010) 823, arXiv: 1005.4568 [physics.ins-det].

[59] GEANT4 Collaboration, *GEANT4 – a simulation toolkit*, Nucl. Instrum. Meth. A **506** (2003) 250.

[60] ATLAS Collaboration, *The simulation principle and performance of the ATLAS fast calorimeter simulation FastCaloSim*, ATL-PHYS-PUB-2010-013, 2010, URL: https://cds.cern.ch/record/1300517.

[61] T. Sjöstrand, S. Mrenna and P. Skands, *A brief introduction to PYTHIA 8.1*, Comput. Phys. Commun. **178** (2008) 852, arXiv: 0710.3820 [hep-ph].

[62] D. J. Lange, *The EvtGen particle decay simulation package*, Nucl. Instrum. Meth. A **462** (2001) 152.

[63] T. Gleisberg et al., *Event generation with SHERPA 1.1*, JHEP **02** (2009) 007, arXiv: 0811.4622 [hep-ph].

[64] P. Nason, *A New method for combining NLO QCD with shower Monte Carlo algorithms*, JHEP **11** (2004) 040, arXiv: hep-ph/0409146 [hep-ph].

[65] S. Alioli, P. Nason, C. Oleari and E. Re, *A general framework for implementing NLO calculations in shower Monte Carlo programs: the POWHEG BOX*, JHEP **06** (2010) 043, arXiv: 1002.2581 [hep-ph].

[66] S. Frixione, G. Ridolfi and P. Nason, *A Positive-weight next-to-leading-order Monte Carlo for heavy flavour hadroproduction*, JHEP **09** (2007) 126, arXiv: 0707.3088 [hep-ph].

[67] H. L. Lai et al., *New parton distributions for collider physics*, Phys. Rev. D **82** (2010) 074024, arXiv: 1007.2241 [hep-ph].

[68] T. Sjöstrand et al., *PYTHIA 6.4 physics and manual*, JHEP **05** (2006) 026, arXiv: hep-ph/0603175 [hep-ph].

[69] J. Pumplin et al., *New Generation of Parton Distributions with Uncertainties from Global QCD Analysis*, JHEP **07** (2002) 012, arXiv: hep-ph/0201195 [hep-ph].

[70] P. Z. Skands, *Tuning Monte Carlo generators: The Perugia tunes*, Phys. Rev. D **82** (2010) 074018, arXiv: 1005.3457 [hep-ph].

[71] ATLAS Collaboration, *Comparison of Monte Carlo generator predictions from Powheg and Sherpa to ATLAS measurements of top pair production at 7 TeV*, ATL-PHYS-PUB-2015-011, 2015, URL: https://cds.cern.ch/record/2020602.

[72] M. Bähr et al., *Herwig++ physics and manual*, Eur. Phys. J. C **58** (2008) 639, arXiv: 0803.0883 [hep-ph].

[73] M. H. Seymour and A. Siódmok, *Constraining MPI models using σ_{eff} and recent Tevatron and LHC Underlying Event data*, JHEP **10** (2013) 113, arXiv: 1307.5015 [hep-ph].

[74] J. Alwall et al., *The automated computation of tree-level and next-to-leading order differential cross sections, and their matching to parton shower simulations*, JHEP **07** (2014) 079, arXiv: 1405.0301 [hep-ph].

[75] M. Czakon and A. Mitov, *Top++: A program for the calculation of the top-pair cross-section at hadron colliders*, Comput. Phys. Commun. **185** (2014) 2930, arXiv: 1112.5675 [hep-ph].

[76] M. Cacciari, M. Czakon, M. Mangano, A. Mitov and P. Nason, *Top-pair production at hadron colliders with next-to-next-to-leading logarithmic soft-gluon resummation*, Phys. Lett. B **710** (2012) 612, arXiv: 1111.5869 [hep-ph].

[77] P. Bärnreuther, M. Czakon and A. Mitov, *Percent Level Precision Physics at the Tevatron: First Genuine NNLO QCD Corrections to $q\bar{q} \to t\bar{t} + X$*, Phys. Rev. Lett. **109** (2012) 132001, arXiv: 1204.5201 [hep-ph].

[78] M. Czakon and A. Mitov, *NNLO corrections to top-pair production at hadron colliders: the all-fermionic scattering channels*, JHEP **12** (2012) 054, arXiv: 1207.0236 [hep-ph].

[79] M. Czakon and A. Mitov, *NNLO corrections to top-pair production at hadron colliders: the quark-gluon reaction*, JHEP **01** (2013) 080, arXiv: 1210.6832 [hep-ph].

[80] M. Czakon, P. Fiedler and A. Mitov, *The Total Top Quark Pair Production Cross Section at Hadron Colliders Through $O(\alpha_S^4)$*, Phys. Rev. Lett. **110** (2013) 252004, arXiv: 1303.6254 [hep-ph].

[81] J. Butterworth et al., *PDF4LHC recommendations for LHC Run II*, J. Phys. G **43** (2016) 023001, arXiv: 1510.03865 [hep-ph].

[82] R. Frederix, E. Re and P. Torrielli, *Single-top t-channel hadroproduction in the four-flavour scheme with POWHEG and aMC@NLO*, JHEP **09** (2012) 130, arXiv: 1207.5391 [hep-ph].

[83] S. Frixione, E. Laenen, P. Motylinski and B. R. Webber, *Single-top production in MC@NLO*, JHEP **03** (2006) 092, arXiv: hep-ph/0512250 [hep-ph].

[84] S. Frixione, E. Laenen, P. Motylinski, C. White and B. R. Webber,
Single-top hadroproduction in association with a W boson, JHEP **07** (2008) 029,
arXiv: 0805.3067 [hep-ph].

[85] C. D. White, S. Frixione, E. Laenen and F. Maltoni, *Isolating Wt production at the LHC*,
JHEP **11** (2009) 074, arXiv: 0908.0631 [hep-ph].

[86] N. Kidonakis, *Next-to-next-to-leading-order collinear and soft gluon corrections for t-channel single top quark production*, Phys. Rev. D **83** (2011) 091503, arXiv: 1103.2792 [hep-ph].

[87] N. Kidonakis,
Two-loop soft anomalous dimensions for single top quark associated production with a W^- or H^-,
Phys. Rev. D **82** (2010) 054018, arXiv: 1005.4451 [hep-ph].

[88] N. Kidonakis,
Next-to-next-to-leading logarithm resummation for s-channel single top quark production,
Phys. Rev. D **81** (2010) 054028, arXiv: 1001.5034 [hep-ph].

[89] T. Gleisberg and S. Höche, *Comix, a new matrix element generator*, JHEP **12** (2008) 039,
arXiv: 0808.3674 [hep-ph].

[90] F. Cascioli, P. Maierhöfer and S. Pozzorini, *Scattering Amplitudes with Open Loops*,
Phys. Rev. Lett. **108** (2012) 111601, arXiv: 1111.5206 [hep-ph].

[91] S. Schumann and F. Krauss,
A Parton shower algorithm based on Catani-Seymour dipole factorisation, JHEP **03** (2008) 038,
arXiv: 0709.1027 [hep-ph].

[92] S. Höche, F. Krauss, M. Schönherr and F. Siegert,
QCD matrix elements + parton showers. The NLO case, JHEP **04** (2013) 027,
arXiv: 1207.5030 [hep-ph].

[93] C. Anastasiou, L. Dixon, K. Melnikov and F. Petriello, *High-precision QCD at hadron colliders: Electroweak gauge boson rapidity distributions at next-to-next-to leading order*,
Phys. Rev. D **69** (2004) 094008, arXiv: hep-ph/0312266 [hep-ph].

[94] T. Sjöstrand, and others, *An introduction to PYTHIA 8.2*, Comput. Phys. Commun. **191** (2015) 159,
arXiv: 1410.3012 [hep-ph].

[95] M. Buchkremer, G. Cacciapaglia, A. Deandrea and L. Panizzi,
Model-independent framework for searches of top partners, Nucl. Phys. B **876** (2013) 376,
arXiv: 1305.4172 [hep-ph].

[96] E. L. Berger, J. Gao, C.-P. Yuan and H. X. Zhu,
NNLO QCD corrections to t-channel single top quark production and decay,
Phys. Rev. D **94** (2016) 071501, arXiv: 1606.08463 [hep-ph].

[97] ATLAS Collaboration,
Luminosity determination in pp collisions at $\sqrt{s} = 8$ TeV using the ATLAS detector at the LHC,
Eur. Phys. J. C **76** (2016) 653, arXiv: 1608.03953 [hep-ex].

[98] G. Avoni et al., *The new LUCID-2 detector for luminosity measurement and monitoring in ATLAS*,
JINST **13** (2018) P07017.

[99] K. Melnikov and F. Petriello,
Electroweak gauge boson production at hadron colliders through $O(\alpha_S^2)$,
Phys. Rev. D **74** (2006) 114017, arXiv: hep-ph/0609070 [hep-ph].

[100] J. M. Campbell and R. K. Ellis, *Update on vector boson pair production at hadron colliders*, Phys. Rev. D **60** (1999) 113006, arXiv: hep-ph/9905386 [hep-ph].

[101] T. Junk, *Confidence level computation for combining searches with small statistics*, Nucl. Instrum. Meth. A **434** (1999) 435, arXiv: hep-ex/9902006 [hep-ex].

[102] A. L. Read, *Presentation of search results: The CL_s technique*, J. Phys. G **28** (2002) 2693.

[103] G. Cowan, K. Cranmer, E. Gross and O. Vitells, *Asymptotic formulae for likelihood-based tests of new physics*, Eur. Phys. J. **C71** (2011) 1554, [Erratum: Eur. Phys. J.C73,2501(2013)], arXiv: 1007.1727 [physics.data-an].

[104] ATLAS Collaboration, *ATLAS Computing Acknowledgements*, ATL-GEN-PUB-2016-002, URL: https://cds.cern.ch/record/2202407.

The ATLAS Collaboration

M. Aaboud[34d], G. Aad[99], B. Abbott[124], O. Abdinov[13,*], B. Abeloos[128], D.K. Abhayasinghe[91], S.H. Abidi[164], O.S. AbouZeid[39], N.L. Abraham[153], H. Abramowicz[158], H. Abreu[157], Y. Abulaiti[6], B.S. Acharya[64a,64b,n], S. Adachi[160], L. Adam[97], L. Adamczyk[81a], J. Adelman[119], M. Adersberger[112], A. Adiguzel[12c,ag], T. Adye[141], A.A. Affolder[143], Y. Afik[157], C. Agheorghiesei[27c], J.A. Aguilar-Saavedra[136f,136a], F. Ahmadov[77,ae], G. Aielli[71a,71b], S. Akatsuka[83], T.P.A. Åkesson[94], E. Akilli[52], A.V. Akimov[108], G.L. Alberghi[23b,23a], J. Albert[173], P. Albicocco[49], M.J. Alconada Verzini[86], S. Alderweireldt[117], M. Aleksa[35], I.N. Aleksandrov[77], C. Alexa[27b], T. Alexopoulos[10], M. Alhroob[124], B. Ali[138], G. Alimonti[66a], J. Alison[36], S.P. Alkire[145], C. Allaire[128], B.M.M. Allbrooke[153], B.W. Allen[127], P.P. Allport[21], A. Aloisio[67a,67b], A. Alonso[39], F. Alonso[86], C. Alpigiani[145], A.A. Alshehri[55], M.I. Alstaty[99], B. Alvarez Gonzalez[35], D. Álvarez Piqueras[171], M.G. Alviggi[67a,67b], B.T. Amadio[18], Y. Amaral Coutinho[78b], A. Ambler[101], L. Ambroz[131], C. Amelung[26], D. Amidei[103], S.P. Amor Dos Santos[136a,136c], S. Amoroso[44], C.S. Amrouche[52], C. Anastopoulos[146], L.S. Ancu[52], N. Andari[142], T. Andeen[11], C.F. Anders[59b], J.K. Anders[20], K.J. Anderson[36], A. Andreazza[66a,66b], V. Andrei[59a], C.R. Anelli[173], S. Angelidakis[37], I. Angelozzi[118], A. Angerami[38], A.V. Anisenkov[120b,120a], A. Annovi[69a], C. Antel[59a], M.T. Anthony[146], M. Antonelli[49], D.J.A. Antrim[168], F. Anulli[70a], M. Aoki[79], J.A. Aparisi Pozo[171], L. Aperio Bella[35], G. Arabidze[104], J.P. Araque[136a], V. Araujo Ferraz[78b], R. Araujo Pereira[78b], A.T.H. Arce[47], R.E. Ardell[91], F.A. Arduh[86], J-F. Arguin[107], S. Argyropoulos[75], A.J. Armbruster[35], L.J. Armitage[90], A Armstrong[168], O. Arnaez[164], H. Arnold[118], M. Arratia[31], O. Arslan[24], A. Artamonov[109,*], G. Artoni[131], S. Artz[97], S. Asai[160], N. Asbah[57], E.M. Asimakopoulou[169], L. Asquith[153], K. Assamagan[29], R. Astalos[28a], R.J. Atkin[32a], M. Atkinson[170], N.B. Atlay[148], K. Augsten[138], G. Avolio[35], R. Avramidou[58a], M.K. Ayoub[15a], G. Azuelos[107,ar], A.E. Baas[59a], M.J. Baca[21], H. Bachacou[142], K. Bachas[65a,65b], M. Backes[131], P. Bagnaia[70a,70b], M. Bahmani[82], H. Bahrasemani[149], A.J. Bailey[171], J.T. Baines[141], M. Bajic[39], C. Bakalis[10], O.K. Baker[180], P.J. Bakker[118], D. Bakshi Gupta[93], S. Balaji[154], E.M. Baldin[120b,120a], P. Balek[177], F. Balli[142], W.K. Balunas[133], J. Balz[97], E. Banas[82], A. Bandyopadhyay[24], S. Banerjee[178,j], A.A.E. Bannoura[179], L. Barak[158], W.M. Barbe[37], E.L. Barberio[102], D. Barberis[53b,53a], M. Barbero[99], T. Barillari[113], M-S. Barisits[35], J. Barkeloo[127], T. Barklow[150], R. Barnea[157], S.L. Barnes[58c], B.M. Barnett[141], R.M. Barnett[18], Z. Barnovska-Blenessy[58a], A. Baroncelli[72a], G. Barone[26], A.J. Barr[131], L. Barranco Navarro[171], F. Barreiro[96], J. Barreiro Guimarães da Costa[15a], R. Bartoldus[150], A.E. Barton[87], P. Bartos[28a], A. Basalaev[134], A. Bassalat[128], R.L. Bates[55], S.J. Batista[164], S. Batlamous[34e], J.R. Batley[31], M. Battaglia[143], M. Bauce[70a,70b], F. Bauer[142], K.T. Bauer[168], H.S. Bawa[150,l], J.B. Beacham[122], T. Beau[132], P.H. Beauchemin[167], P. Bechtle[24], H.C. Beck[51], H.P. Beck[20,q], K. Becker[50], M. Becker[97], C. Becot[44], A. Beddall[12d], A.J. Beddall[12a], V.A. Bednyakov[77], M. Bedognetti[118], C.P. Bee[152], T.A. Beermann[35], M. Begalli[78b], M. Begel[29], A. Behera[152], J.K. Behr[44], A.S. Bell[92], G. Bella[158], L. Bellagamba[23b], A. Bellerive[33], M. Bellomo[157], P. Bellos[9], K. Belotskiy[110], N.L. Belyaev[110], O. Benary[158,*], D. Benchekroun[34a], M. Bender[112], N. Benekos[10], Y. Benhammou[158], E. Benhar Noccioli[180], J. Benitez[75], D.P. Benjamin[47], M. Benoit[52], J.R. Bensinger[26], S. Bentvelsen[118], L. Beresford[131], M. Beretta[49], D. Berge[44], E. Bergeaas Kuutmann[169], N. Berger[5], L.J. Bergsten[26], J. Beringer[18], S. Berlendis[7], N.R. Bernard[100], G. Bernardi[132], C. Bernius[150], F.U. Bernlochner[24], T. Berry[91], P. Berta[97], C. Bertella[15a], G. Bertoli[43a,43b], I.A. Bertram[87], G.J. Besjes[39], O. Bessidskaia Bylund[179], M. Bessner[44], N. Besson[142], A. Bethani[98], S. Bethke[113], A. Betti[24], A.J. Bevan[90], J. Beyer[113], R.M. Bianchi[135], O. Biebel[112], D. Biedermann[19], R. Bielski[35], K. Bierwagen[97], N.V. Biesuz[69a,69b], M. Biglietti[72a], T.R.V. Billoud[107], M. Bindi[51], A. Bingul[12d], C. Bini[70a,70b], S. Biondi[23b,23a], M. Birman[177], T. Bisanz[51], J.P. Biswal[158], C. Bittrich[46], D.M. Bjergaard[47], J.E. Black[150], K.M. Black[25], T. Blazek[28a], I. Bloch[44], C. Blocker[26],

A. Blue[55], U. Blumenschein[90], Dr. Blunier[144a], G.J. Bobbink[118], V.S. Bobrovnikov[120b,120a], S.S. Bocchetta[94], A. Bocci[47], D. Boerner[179], D. Bogavac[112], A.G. Bogdanchikov[120b,120a], C. Bohm[43a], V. Boisvert[91], P. Bokan[169], T. Bold[81a], A.S. Boldyrev[111], A.E. Bolz[59b], M. Bomben[132], M. Bona[90], J.S. Bonilla[127], M. Boonekamp[142], A. Borisov[140], G. Borissov[87], J. Bortfeldt[35], D. Bortoletto[131], V. Bortolotto[71a,71b], D. Boscherini[23b], M. Bosman[14], J.D. Bossio Sola[30], K. Bouaouda[34a], J. Boudreau[135], E.V. Bouhova-Thacker[87], D. Boumediene[37], C. Bourdarios[128], S.K. Boutle[55], A. Boveia[122], J. Boyd[35], D. Boye[32b], I.R. Boyko[77], A.J. Bozson[91], J. Bracinik[21], N. Brahimi[99], A. Brandt[8], G. Brandt[179], O. Brandt[59a], F. Braren[44], U. Bratzler[161], B. Brau[100], J.E. Brau[127], W.D. Breaden Madden[55], K. Brendlinger[44], L. Brenner[44], R. Brenner[169], S. Bressler[177], B. Brickwedde[97], D.L. Briglin[21], D. Britton[55], D. Britzger[59b], I. Brock[24], R. Brock[104], G. Brooijmans[38], T. Brooks[91], W.K. Brooks[144b], E. Brost[119], J.H Broughton[21], P.A. Bruckman de Renstrom[82], D. Bruncko[28b], A. Bruni[23b], G. Bruni[23b], L.S. Bruni[118], S. Bruno[71a,71b], B.H. Brunt[31], M. Bruschi[23b], N. Bruscino[135], P. Bryant[36], L. Bryngemark[44], T. Buanes[17], Q. Buat[35], P. Buchholz[148], A.G. Buckley[55], I.A. Budagov[77], F. Buehrer[50], M.K. Bugge[130], O. Bulekov[110], D. Bullock[8], T.J. Burch[119], S. Burdin[88], C.D. Burgard[118], A.M. Burger[5], B. Burghgrave[119], K. Burka[82], S. Burke[141], I. Burmeister[45], J.T.P. Burr[131], V. Büscher[97], E. Buschmann[51], P. Bussey[55], J.M. Butler[25], C.M. Buttar[55], J.M. Butterworth[92], P. Butti[35], W. Buttinger[35], A. Buzatu[155], A.R. Buzykaev[120b,120a], G. Cabras[23b,23a], S. Cabrera Urbán[171], D. Caforio[138], H. Cai[170], V.M.M. Cairo[2], O. Cakir[4a], N. Calace[52], P. Calafiura[18], A. Calandri[99], G. Calderini[132], P. Calfayan[63], G. Callea[40b,40a], L.P. Caloba[78b], S. Calvente Lopez[96], D. Calvet[37], S. Calvet[37], T.P. Calvet[152], M. Calvetti[69a,69b], R. Camacho Toro[132], S. Camarda[35], P. Camarri[71a,71b], D. Cameron[130], R. Caminal Armadans[100], C. Camincher[35], S. Campana[35], M. Campanelli[92], A. Camplani[39], A. Campoverde[148], V. Canale[67a,67b], M. Cano Bret[58c], J. Cantero[125], T. Cao[158], Y. Cao[170], M.D.M. Capeans Garrido[35], I. Caprini[27b], M. Caprini[27b], M. Capua[40b,40a], R.M. Carbone[38], R. Cardarelli[71a], F.C. Cardillo[146], I. Carli[139], T. Carli[35], G. Carlino[67a], B.T. Carlson[135], L. Carminati[66a,66b], R.M.D. Carney[43a,43b], S. Caron[117], E. Carquin[144b], S. Carrá[66a,66b], G.D. Carrillo-Montoya[35], D. Casadei[32b], M.P. Casado[14,f], A.F. Casha[164], D.W. Casper[168], R. Castelijn[118], F.L. Castillo[171], V. Castillo Gimenez[171], N.F. Castro[136a,136e], A. Catinaccio[35], J.R. Catmore[130], A. Cattai[35], J. Caudron[24], V. Cavaliere[29], E. Cavallaro[14], D. Cavalli[66a], M. Cavalli-Sforza[14], V. Cavasinni[69a,69b], E. Celebi[12b], F. Ceradini[72a,72b], L. Cerda Alberich[171], A.S. Cerqueira[78a], A. Cerri[153], L. Cerrito[71a,71b], F. Cerutti[18], A. Cervelli[23b,23a], S.A. Cetin[12b], A. Chafaq[34a], D Chakraborty[119], S.K. Chan[57], W.S. Chan[118], Y.L. Chan[61a], J.D. Chapman[31], B. Chargeishvili[156b], D.G. Charlton[21], C.C. Chau[33], C.A. Chavez Barajas[153], S. Che[122], A. Chegwidden[104], S. Chekanov[6], S.V. Chekulaev[165a], G.A. Chelkov[77,aq], M.A. Chelstowska[35], C. Chen[58a], C.H. Chen[76], H. Chen[29], J. Chen[58a], J. Chen[38], S. Chen[133], S.J. Chen[15c], X. Chen[15b,ap], Y. Chen[80], Y-H. Chen[44], H.C. Cheng[103], H.J. Cheng[15d], A. Cheplakov[77], E. Cheremushkina[140], R. Cherkaoui El Moursli[34e], E. Cheu[7], K. Cheung[62], L. Chevalier[142], V. Chiarella[49], G. Chiarelli[69a], G. Chiodini[65a], A.S. Chisholm[35,21], A. Chitan[27b], I. Chiu[160], Y.H. Chiu[173], M.V. Chizhov[77], K. Choi[63], A.R. Chomont[128], S. Chouridou[159], Y.S. Chow[118], V. Christodoulou[92], M.C. Chu[61a], J. Chudoba[137], A.J. Chuinard[101], J.J. Chwastowski[82], L. Chytka[126], D. Cinca[45], V. Cindro[89], I.A. Cioară[24], A. Ciocio[18], F. Cirotto[67a,67b], Z.H. Citron[177], M. Citterio[66a], A. Clark[52], M.R. Clark[38], P.J. Clark[48], C. Clement[43a,43b], Y. Coadou[99], M. Cobal[64a,64c], A. Coccaro[53b,53a], J. Cochran[76], H. Cohen[158], A.E.C. Coimbra[177], L. Colasurdo[117], B. Cole[38], A.P. Colijn[118], J. Collot[56], P. Conde Muiño[136a,136b], E. Coniavitis[50], S.H. Connell[32b], I.A. Connelly[98], S. Constantinescu[27b], F. Conventi[67a,as], A.M. Cooper-Sarkar[131], F. Cormier[172], K.J.R. Cormier[164], L.D. Corpe[92], M. Corradi[70a,70b], E.E. Corrigan[94], F. Corriveau[101,ac], A. Cortes-Gonzalez[35], M.J. Costa[171], F. Costanza[5], D. Costanzo[146], G. Cottin[31], G. Cowan[91], B.E. Cox[98], J. Crane[98], K. Cranmer[121], S.J. Crawley[55], R.A. Creager[133], G. Cree[33], S. Crépé-Renaudin[56], F. Crescioli[132], M. Cristinziani[24], V. Croft[121], G. Crosetti[40b,40a], A. Cueto[96], T. Cuhadar Donszelmann[146], A.R. Cukierman[150], S. Czekierda[82], P. Czodrowski[35], M.J. Da Cunha Sargedas De Sousa[58b,136b],

C. Da Via[98], W. Dabrowski[81a], T. Dado[28a,x], S. Dahbi[34e], T. Dai[103], F. Dallaire[107], C. Dallapiccola[100], M. Dam[39], G. D'amen[23b,23a], J. Damp[97], J.R. Dandoy[133], M.F. Daneri[30], N.P. Dang[178,j], N.D Dann[98], M. Danninger[172], V. Dao[35], G. Darbo[53b], S. Darmora[8], O. Dartsi[5], A. Dattagupta[127], T. Daubney[44], S. D'Auria[55], W. Davey[24], C. David[44], T. Davidek[139], D.R. Davis[47], E. Dawe[102], I. Dawson[146], K. De[8], R. De Asmundis[67a], A. De Benedetti[124], M. De Beurs[118], S. De Castro[23b,23a], S. De Cecco[70a,70b], N. De Groot[117], P. de Jong[118], H. De la Torre[104], F. De Lorenzi[76], A. De Maria[51,s], D. De Pedis[70a], A. De Salvo[70a], U. De Sanctis[71a,71b], M. De Santis[71a,71b], A. De Santo[153], K. De Vasconcelos Corga[99], J.B. De Vivie De Regie[128], C. Debenedetti[143], D.V. Dedovich[77], N. Dehghanian[3], M. Del Gaudio[40b,40a], J. Del Peso[96], Y. Delabat Diaz[44], D. Delgove[128], F. Deliot[142], C.M. Delitzsch[7], M. Della Pietra[67a,67b], D. Della Volpe[52], A. Dell'Acqua[35], L. Dell'Asta[25], M. Delmastro[5], C. Delporte[128], P.A. Delsart[56], D.A. DeMarco[164], S. Demers[180], M. Demichev[77], S.P. Denisov[140], D. Denysiuk[118], L. D'Eramo[132], D. Derendarz[82], J.E. Derkaoui[34d], F. Derue[132], P. Dervan[88], K. Desch[24], C. Deterre[44], K. Dette[164], M.R. Devesa[30], P.O. Deviveiros[35], A. Dewhurst[141], S. Dhaliwal[26], F.A. Di Bello[52], A. Di Ciaccio[71a,71b], L. Di Ciaccio[5], W.K. Di Clemente[133], C. Di Donato[67a,67b], A. Di Girolamo[35], G. Di Gregorio[69a,69b], B. Di Micco[72a,72b], R. Di Nardo[100], K.F. Di Petrillo[57], R. Di Sipio[164], D. Di Valentino[33], C. Diaconu[99], M. Diamond[164], F.A. Dias[39], T. Dias Do Vale[136a], M.A. Diaz[144a], J. Dickinson[18], E.B. Diehl[103], J. Dietrich[19], S. Díez Cornell[44], A. Dimitrievska[18], J. Dingfelder[24], F. Dittus[35], F. Djama[99], T. Djobava[156b], J.I. Djuvsland[59a], M.A.B. Do Vale[78c], M. Dobre[27b], D. Dodsworth[26], C. Doglioni[94], J. Dolejsi[139], Z. Dolezal[139], M. Donadelli[78d], J. Donini[37], A. D'onofrio[90], M. D'Onofrio[88], J. Dopke[141], A. Doria[67a], M.T. Dova[86], A.T. Doyle[55], E. Drechsler[51], E. Dreyer[149], T. Dreyer[51], Y. Du[58b], F. Dubinin[108], M. Dubovsky[28a], A. Dubreuil[52], E. Duchovni[177], G. Duckeck[112], A. Ducourthial[132], O.A. Ducu[107,w], D. Duda[113], A. Dudarev[35], A.C. Dudder[97], E.M. Duffield[18], L. Duflot[128], M. Dührssen[35], C. Dülsen[179], M. Dumancic[177], A.E. Dumitriu[27b,d], A.K. Duncan[55], M. Dunford[59a], A. Duperrin[99], H. Duran Yildiz[4a], M. Düren[54], A. Durglishvili[156b], D. Duschinger[46], B. Dutta[44], D. Duvnjak[1], M. Dyndal[44], S. Dysch[98], B.S. Dziedzic[82], C. Eckardt[44], K.M. Ecker[113], R.C. Edgar[103], T. Eifert[35], G. Eigen[17], K. Einsweiler[18], T. Ekelof[169], M. El Kacimi[34c], R. El Kosseifi[99], V. Ellajosyula[99], M. Ellert[169], F. Ellinghaus[179], A.A. Elliot[90], N. Ellis[35], J. Elmsheuser[29], M. Elsing[35], D. Emeliyanov[141], Y. Enari[160], J.S. Ennis[175], M.B. Epland[47], J. Erdmann[45], A. Ereditato[20], S. Errede[170], M. Escalier[128], C. Escobar[171], O. Estrada Pastor[171], A.I. Etienvre[142], E. Etzion[158], H. Evans[63], A. Ezhilov[134], M. Ezzi[34e], F. Fabbri[55], L. Fabbri[23b,23a], V. Fabiani[117], G. Facini[92], R.M. Faisca Rodrigues Pereira[136a], R.M. Fakhrutdinov[140], S. Falciano[70a], P.J. Falke[5], S. Falke[5], J. Faltova[139], Y. Fang[15a], M. Fanti[66a,66b], A. Farbin[8], A. Farilla[72a], E.M. Farina[68a,68b], T. Farooque[104], S. Farrell[18], S.M. Farrington[175], P. Farthouat[35], F. Fassi[34e], P. Fassnacht[35], D. Fassouliotis[9], M. Faucci Giannelli[48], A. Favareto[53b,53a], W.J. Fawcett[31], L. Fayard[128], O.L. Fedin[134,o], W. Fedorko[172], M. Feickert[41], S. Feigl[130], L. Feligioni[99], C. Feng[58b], E.J. Feng[35], M. Feng[47], M.J. Fenton[55], A.B. Fenyuk[140], L. Feremenga[8], J. Ferrando[44], A. Ferrari[169], P. Ferrari[118], R. Ferrari[68a], D.E. Ferreira de Lima[59b], A. Ferrer[171], D. Ferrere[52], C. Ferretti[103], F. Fiedler[97], A. Filipčič[89], F. Filthaut[117], K.D. Finelli[25], M.C.N. Fiolhais[136a,136c,a], L. Fiorini[171], C. Fischer[14], W.C. Fisher[104], N. Flaschel[44], I. Fleck[148], P. Fleischmann[103], R.R.M. Fletcher[133], T. Flick[179], B.M. Flierl[112], L.M. Flores[133], L.R. Flores Castillo[61a], F.M. Follega[73a,73b], N. Fomin[17], G.T. Forcolin[73a,73b], A. Formica[142], F.A. Förster[14], A.C. Forti[98], A.G. Foster[21], D. Fournier[128], H. Fox[87], S. Fracchia[146], P. Francavilla[69a,69b], M. Franchini[23b,23a], S. Franchino[59a], D. Francis[35], L. Franconi[143], M. Franklin[57], M. Frate[168], M. Fraternali[68a,68b], A.N. Fray[90], D. Freeborn[92], S.M. Fressard-Batraneanu[35], B. Freund[107], W.S. Freund[78b], E.M. Freundlich[45], D.C. Frizzell[124], D. Froidevaux[35], J.A. Frost[131], C. Fukunaga[161], E. Fullana Torregrosa[171], T. Fusayasu[114], J. Fuster[171], O. Gabizon[157], A. Gabrielli[23b,23a], A. Gabrielli[18], G.P. Gach[81a], S. Gadatsch[52], P. Gadow[113], G. Gagliardi[53b,53a], L.G. Gagnon[107], C. Galea[27b], B. Galhardo[136a,136c], E.J. Gallas[131], B.J. Gallop[141], P. Gallus[138], G. Galster[39], R. Gamboa Goni[90], K.K. Gan[122], S. Ganguly[177], J. Gao[58a], Y. Gao[88], Y.S. Gao[150,l], C. García[171], J.E. García Navarro[171],

J.A. García Pascual[15a], M. Garcia-Sciveres[18], R.W. Gardner[36], N. Garelli[150], V. Garonne[130], K. Gasnikova[44], A. Gaudiello[53b,53a], G. Gaudio[68a], I.L. Gavrilenko[108], A. Gavrilyuk[109], C. Gay[172], G. Gaycken[24], E.N. Gazis[10], C.N.P. Gee[141], J. Geisen[51], M. Geisen[97], M.P. Geisler[59a], K. Gellerstedt[43a,43b], C. Gemme[53b], M.H. Genest[56], C. Geng[103], S. Gentile[70a,70b], S. George[91], D. Gerbaudo[14], G. Gessner[45], S. Ghasemi[148], M. Ghasemi Bostanabad[173], M. Ghneimat[24], B. Giacobbe[23b], S. Giagu[70a,70b], N. Giangiacomi[23b,23a], P. Giannetti[69a], A. Giannini[67a,67b], S.M. Gibson[91], M. Gignac[143], D. Gillberg[33], G. Gilles[179], D.M. Gingrich[3,ar], M.P. Giordani[64a,64c], F.M. Giorgi[23b], P.F. Giraud[142], P. Giromini[57], G. Giugliarelli[64a,64c], D. Giugni[66a], F. Giuli[131], M. Giulini[59b], S. Gkaitatzis[159], I. Gkialas[9,i], E.L. Gkougkousis[14], P. Gkountoumis[10], L.K. Gladilin[111], C. Glasman[96], J. Glatzer[14], P.C.F. Glaysher[44], A. Glazov[44], M. Goblirsch-Kolb[26], J. Godlewski[82], S. Goldfarb[102], T. Golling[52], D. Golubkov[140], A. Gomes[136a,136b,136d], R. Goncalves Gama[78a], R. Gonçalo[136a], G. Gonella[50], L. Gonella[21], A. Gongadze[77], F. Gonnella[21], J.L. Gonski[57], S. González de la Hoz[171], S. Gonzalez-Sevilla[52], L. Goossens[35], P.A. Gorbounov[109], H.A. Gordon[29], B. Gorini[35], E. Gorini[65a,65b], A. Gorišek[89], A.T. Goshaw[47], C. Gössling[45], M.I. Gostkin[77], C.A. Gottardo[24], C.R. Goudet[128], D. Goujdami[34c], A.G. Goussiou[145], N. Govender[32b,b], C. Goy[5], E. Gozani[157], I. Grabowska-Bold[81a], P.O.J. Gradin[169], E.C. Graham[88], J. Gramling[168], E. Gramstad[130], S. Grancagnolo[19], V. Gratchev[134], P.M. Gravila[27f], F.G. Gravili[65a,65b], C. Gray[55], H.M. Gray[18], Z.D. Greenwood[93,ai], C. Grefe[24], K. Gregersen[94], I.M. Gregor[44], P. Grenier[150], K. Grevtsov[44], N.A. Grieser[124], J. Griffiths[8], A.A. Grillo[143], K. Grimm[150], S. Grinstein[14,y], Ph. Gris[37], J.-F. Grivaz[128], S. Groh[97], E. Gross[177], J. Grosse-Knetter[51], G.C. Grossi[93], Z.J. Grout[92], C. Grud[103], A. Grummer[116], L. Guan[103], W. Guan[178], J. Guenther[35], A. Guerguichon[128], F. Guescini[165a], D. Guest[168], R. Gugel[50], B. Gui[122], T. Guillemin[5], S. Guindon[35], U. Gul[55], C. Gumpert[35], J. Guo[58c], W. Guo[103], Y. Guo[58a,r], Z. Guo[99], R. Gupta[41], S. Gurbuz[12c], G. Gustavino[124], B.J. Gutelman[157], P. Gutierrez[124], C. Gutschow[92], C. Guyot[142], M.P. Guzik[81a], C. Gwenlan[131], C.B. Gwilliam[88], A. Haas[121], C. Haber[18], H.K. Hadavand[8], N. Haddad[34e], A. Hadef[58a], S. Hageböck[24], M. Hagihara[166], H. Hakobyan[181,*], M. Haleem[174], J. Haley[125], G. Halladjian[104], G.D. Hallewell[99], K. Hamacher[179], P. Hamal[126], K. Hamano[173], A. Hamilton[32a], G.N. Hamity[146], K. Han[58a,ah], L. Han[58a], S. Han[15d], K. Hanagaki[79,u], M. Hance[143], D.M. Handl[112], B. Haney[133], R. Hankache[132], P. Hanke[59a], E. Hansen[94], J.B. Hansen[39], J.D. Hansen[39], M.C. Hansen[24], P.H. Hansen[39], K. Hara[166], A.S. Hard[178], T. Harenberg[179], S. Harkusha[105], P.F. Harrison[175], N.M. Hartmann[112], Y. Hasegawa[147], A. Hasib[48], S. Hassani[142], S. Haug[20], R. Hauser[104], L. Hauswald[46], L.B. Havener[38], M. Havranek[138], C.M. Hawkes[21], R.J. Hawkings[35], D. Hayden[104], C. Hayes[152], C.P. Hays[131], J.M. Hays[90], H.S. Hayward[88], S.J. Haywood[141], M.P. Heath[48], V. Hedberg[94], L. Heelan[8], S. Heer[24], K.K. Heidegger[50], J. Heilman[33], S. Heim[44], T. Heim[18], B. Heinemann[44,am], J.J. Heinrich[112], L. Heinrich[121], C. Heinz[54], J. Hejbal[137], L. Helary[35], A. Held[172], S. Hellesund[130], S. Hellman[43a,43b], C. Helsens[35], R.C.W. Henderson[87], Y. Heng[178], S. Henkelmann[172], A.M. Henriques Correia[35], G.H. Herbert[19], H. Herde[26], V. Herget[174], Y. Hernández Jiménez[32c], H. Herr[97], M.G. Herrmann[112], G. Herten[50], R. Hertenberger[112], L. Hervas[35], T.C. Herwig[133], G.G. Hesketh[92], N.P. Hessey[165a], J.W. Hetherly[41], S. Higashino[79], E. Higón-Rodriguez[171], K. Hildebrand[36], E. Hill[173], J.C. Hill[31], K.K. Hill[29], K.H. Hiller[44], S.J. Hillier[21], M. Hils[46], I. Hinchliffe[18], M. Hirose[129], D. Hirschbuehl[179], B. Hiti[89], O. Hladik[137], D.R. Hlaluku[32c], X. Hoad[48], J. Hobbs[152], N. Hod[165a], M.C. Hodgkinson[146], A. Hoecker[35], M.R. Hoeferkamp[116], F. Hoenig[112], D. Hohn[24], D. Hohov[128], T.R. Holmes[36], M. Holzbock[112], M. Homann[45], S. Honda[166], T. Honda[79], T.M. Hong[135], A. Hönle[113], B.H. Hooberman[170], W.H. Hopkins[127], Y. Horii[115], P. Horn[46], A.J. Horton[149], L.A. Horyn[36], J-Y. Hostachy[56], A. Hostiuc[145], S. Hou[155], A. Hoummada[34a], J. Howarth[98], J. Hoya[86], M. Hrabovsky[126], I. Hristova[19], J. Hrivnac[128], A. Hrynevich[106], T. Hryn'ova[5], P.J. Hsu[62], S.-C. Hsu[145], Q. Hu[29], S. Hu[58c], Y. Huang[15a], Z. Hubacek[138], F. Hubaut[99], M. Huebner[24], F. Huegging[24], T.B. Huffman[131], E.W. Hughes[38], M. Huhtinen[35], R.F.H. Hunter[33], P. Huo[152], A.M. Hupe[33], N. Huseynov[77,ae], J. Huston[104], J. Huth[57], R. Hyneman[103], G. Iacobucci[52], G. Iakovidis[29], I. Ibragimov[148], L. Iconomidou-Fayard[128], Z. Idrissi[34e],

P. Iengo[35], R. Ignazzi[39], O. Igonkina[118,aa], R. Iguchi[160], T. Iizawa[52], Y. Ikegami[79], M. Ikeno[79], D. Iliadis[159], N. Ilic[150], F. Iltzsche[46], G. Introzzi[68a,68b], M. Iodice[72a], K. Iordanidou[38], V. Ippolito[70a,70b], M.F. Isacson[169], N. Ishijima[129], M. Ishino[160], M. Ishitsuka[162], W. Islam[125], C. Issever[131], S. Istin[157], F. Ito[166], J.M. Iturbe Ponce[61a], R. Iuppa[73a,73b], A. Ivina[177], H. Iwasaki[79], J.M. Izen[42], V. Izzo[67a], P. Jacka[137], P. Jackson[1], R.M. Jacobs[24], V. Jain[2], G. Jäkel[179], K.B. Jakobi[97], K. Jakobs[50], S. Jakobsen[74], T. Jakoubek[137], D.O. Jamin[125], D.K. Jana[93], R. Jansky[52], J. Janssen[24], M. Janus[51], P.A. Janus[81a], G. Jarlskog[94], N. Javadov[77,ae], T. Javůrek[35], M. Javurkova[50], F. Jeanneau[142], L. Jeanty[18], J. Jejelava[156a,af], A. Jelinskas[175], P. Jenni[50,c], J. Jeong[44], N. Jeong[44], S. Jézéquel[5], H. Ji[178], J. Jia[152], H. Jiang[76], Y. Jiang[58a], Z. Jiang[150,p], S. Jiggins[50], F.A. Jimenez Morales[37], J. Jimenez Pena[171], S. Jin[15c], A. Jinaru[27b], O. Jinnouchi[162], H. Jivan[32c], P. Johansson[146], K.A. Johns[7], C.A. Johnson[63], W.J. Johnson[145], K. Jon-And[43a,43b], R.W.L. Jones[87], S.D. Jones[153], S. Jones[7], T.J. Jones[88], J. Jongmanns[59a], P.M. Jorge[136a,136b], J. Jovicevic[165a], X. Ju[18], J.J. Junggeburth[113], A. Juste Rozas[14,y], A. Kaczmarska[82], M. Kado[128], H. Kagan[122], M. Kagan[150], T. Kaji[176], E. Kajomovitz[157], C.W. Kalderon[94], A. Kaluza[97], S. Kama[41], A. Kamenshchikov[140], L. Kanjir[89], Y. Kano[160], V.A. Kantserov[110], J. Kanzaki[79], B. Kaplan[121], L.S. Kaplan[178], D. Kar[32c], M.J. Kareem[165b], E. Karentzos[10], S.N. Karpov[77], Z.M. Karpova[77], V. Kartvelishvili[87], A.N. Karyukhin[140], L. Kashif[178], R.D. Kass[122], A. Kastanas[43a,43b], Y. Kataoka[160], C. Kato[58d,58c], J. Katzy[44], K. Kawade[80], K. Kawagoe[85], T. Kawamoto[160], G. Kawamura[51], E.F. Kay[88], V.F. Kazanin[120b,120a], R. Keeler[173], R. Kehoe[41], J.S. Keller[33], E. Kellermann[94], J.J. Kempster[21], J. Kendrick[21], O. Kepka[137], S. Kersten[179], B.P. Kerševan[89], R.A. Keyes[101], M. Khader[170], F. Khalil-Zada[13], A. Khanov[125], A.G. Kharlamov[120b,120a], T. Kharlamova[120b,120a], E.E. Khoda[172], A. Khodinov[163], T.J. Khoo[52], E. Khramov[77], J. Khubua[156b], S. Kido[80], M. Kiehn[52], C.R. Kilby[91], Y.K. Kim[36], N. Kimura[64a,64c], O.M. Kind[19], B.T. King[88], D. Kirchmeier[46], J. Kirk[141], A.E. Kiryunin[113], T. Kishimoto[160], D. Kisielewska[81a], V. Kitali[44], O. Kivernyk[5], E. Kladiva[28b,*], T. Klapdor-Kleingrothaus[50], M.H. Klein[103], M. Klein[88], U. Klein[88], K. Kleinknecht[97], P. Klimek[119], A. Klimentov[29], R. Klingenberg[45,*], T. Klingl[24], T. Klioutchnikova[35], F.F. Klitzner[112], P. Kluit[118], S. Kluth[113], E. Kneringer[74], E.B.F.G. Knoops[99], A. Knue[50], A. Kobayashi[160], D. Kobayashi[85], T. Kobayashi[160], M. Kobel[46], M. Kocian[150], P. Kodys[139], P.T. Koenig[24], T. Koffas[33], E. Koffeman[118], N.M. Köhler[113], T. Koi[150], M. Kolb[59b], I. Koletsou[5], T. Kondo[79], N. Kondrashova[58c], K. Köneke[50], A.C. König[117], T. Kono[79], R. Konoplich[121,aj], V. Konstantinides[92], N. Konstantinidis[92], B. Konya[94], R. Kopeliansky[63], S. Koperny[81a], K. Korcyl[82], K. Kordas[159], G. Koren[158], A. Korn[92], I. Korolkov[14], E.V. Korolkova[146], N. Korotkova[111], O. Kortner[113], S. Kortner[113], T. Kosek[139], V.V. Kostyukhin[24], A. Kotwal[47], A. Koulouris[10], A. Kourkoumeli-Charalampidi[68a,68b], C. Kourkoumelis[9], E. Kourlitis[146], V. Kouskoura[29], A.B. Kowalewska[82], R. Kowalewski[173], T.Z. Kowalski[81a], C. Kozakai[160], W. Kozanecki[142], A.S. Kozhin[140], V.A. Kramarenko[111], G. Kramberger[89], D. Krasnopevtsev[58a], M.W. Krasny[132], A. Krasznahorkay[35], D. Krauss[113], J.A. Kremer[81a], J. Kretzschmar[88], P. Krieger[164], K. Krizka[18], K. Kroeninger[45], H. Kroha[113], J. Kroll[137], J. Kroll[133], J. Krstic[16], U. Kruchonak[77], H. Krüger[24], N. Krumnack[76], M.C. Kruse[47], T. Kubota[102], S. Kuday[4b], J.T. Kuechler[179], S. Kuehn[35], A. Kugel[59a], F. Kuger[174], T. Kuhl[44], V. Kukhtin[77], R. Kukla[99], Y. Kulchitsky[105], S. Kuleshov[144b], Y.P. Kulinich[170], M. Kuna[56], T. Kunigo[83], A. Kupco[137], T. Kupfer[45], O. Kuprash[158], H. Kurashige[80], L.L. Kurchaninov[165a], Y.A. Kurochkin[105], M.G. Kurth[15d], E.S. Kuwertz[35], M. Kuze[162], J. Kvita[126], T. Kwan[101], A. La Rosa[113], J.L. La Rosa Navarro[78d], L. La Rotonda[40b,40a], F. La Ruffa[40b,40a], C. Lacasta[171], F. Lacava[70a,70b], J. Lacey[44], D.P.J. Lack[98], H. Lacker[19], D. Lacour[132], E. Ladygin[77], R. Lafaye[5], B. Laforge[132], T. Lagouri[32c], S. Lai[51], S. Lammers[63], W. Lampl[7], E. Lançon[29], U. Landgraf[50], M.P.J. Landon[90], M.C. Lanfermann[52], V.S. Lang[44], J.C. Lange[14], R.J. Langenberg[35], A.J. Lankford[168], F. Lanni[29], K. Lantzsch[24], A. Lanza[68a], A. Lapertosa[53b,53a], S. Laplace[132], J.F. Laporte[142], T. Lari[66a], F. Lasagni Manghi[23b,23a], M. Lassnig[35], T.S. Lau[61a], A. Laudrain[128], M. Lavorgna[67a,67b], A.T. Law[143], M. Lazzaroni[66a,66b], B. Le[102], O. Le Dortz[132], E. Le Guirriec[99], E.P. Le Quilleuc[142], M. LeBlanc[7], T. LeCompte[6], F. Ledroit-Guillon[56], C.A. Lee[29],

G.R. Lee[144a], L. Lee[57], S.C. Lee[155], B. Lefebvre[101], M. Lefebvre[173], F. Legger[112], C. Leggett[18], K. Lehmann[149], N. Lehmann[179], G. Lehmann Miotto[35], W.A. Leight[44], A. Leisos[159,v], M.A.L. Leite[78d], R. Leitner[139], D. Lellouch[177], B. Lemmer[51], K.J.C. Leney[92], T. Lenz[24], B. Lenzi[35], R. Leone[7], S. Leone[69a], C. Leonidopoulos[48], G. Lerner[153], C. Leroy[107], R. Les[164], A.A.J. Lesage[142], C.G. Lester[31], M. Levchenko[134], J. Levêque[5], D. Levin[103], L.J. Levinson[177], D. Lewis[90], B. Li[103], C-Q. Li[58a], H. Li[58b], L. Li[58c], M. Li[15a], Q. Li[15d], Q.Y. Li[58a], S. Li[58d,58c], X. Li[58c], Y. Li[148], Z. Liang[15a], B. Liberti[71a], A. Liblong[164], K. Lie[61c], S. Liem[118], A. Limosani[154], C.Y. Lin[31], K. Lin[104], T.H. Lin[97], R.A. Linck[63], J.H. Lindon[21], B.E. Lindquist[152], A.L. Lionti[52], E. Lipeles[133], A. Lipniacka[17], M. Lisovyi[59b], T.M. Liss[170,ao], A. Lister[172], A.M. Litke[143], J.D. Little[8], B. Liu[76], B.L Liu[6], H.B. Liu[29], H. Liu[103], J.B. Liu[58a], J.K.K. Liu[131], K. Liu[132], M. Liu[58a], P. Liu[18], Y. Liu[15a], Y.L. Liu[58a], Y.W. Liu[58a], M. Livan[68a,68b], A. Lleres[56], J. Llorente Merino[15a], S.L. Lloyd[90], C.Y. Lo[61b], F. Lo Sterzo[41], E.M. Lobodzinska[44], P. Loch[7], T. Lohse[19], K. Lohwasser[146], M. Lokajicek[137], B.A. Long[25], J.D. Long[170], R.E. Long[87], L. Longo[65a,65b], K.A. Looper[122], J.A. Lopez[144b], I. Lopez Paz[14], A. Lopez Solis[146], J. Lorenz[112], N. Lorenzo Martinez[5], M. Losada[22], P.J. Lösel[112], A. Lösle[50], X. Lou[44], X. Lou[15a], A. Lounis[128], J. Love[6], P.A. Love[87], J.J. Lozano Bahilo[171], H. Lu[61a], M. Lu[58a], N. Lu[103], Y.J. Lu[62], H.J. Lubatti[145], C. Luci[70a,70b], A. Lucotte[56], C. Luedtke[50], F. Luehring[63], I. Luise[132], L. Luminari[70a], B. Lund-Jensen[151], M.S. Lutz[100], P.M. Luzi[132], D. Lynn[29], R. Lysak[137], E. Lytken[94], F. Lyu[15a], V. Lyubushkin[77], H. Ma[29], L.L. Ma[58b], Y. Ma[58b], G. Maccarrone[49], A. Macchiolo[113], C.M. Macdonald[146], J. Machado Miguens[133,136b], D. Madaffari[171], R. Madar[37], W.F. Mader[46], A. Madsen[44], N. Madysa[46], J. Maeda[80], K. Maekawa[160], S. Maeland[17], T. Maeno[29], A.S. Maevskiy[111], V. Magerl[50], C. Maidantchik[78b], T. Maier[112], A. Maio[136a,136b,136d], O. Majersky[28a], S. Majewski[127], Y. Makida[79], N. Makovec[128], B. Malaescu[132], Pa. Malecki[82], V.P. Maleev[134], F. Malek[56], U. Mallik[75], D. Malon[6], C. Malone[31], S. Maltezos[10], S. Malyukov[35], J. Mamuzic[171], G. Mancini[49], I. Mandić[89], J. Maneira[136a], L. Manhaes de Andrade Filho[78a], J. Manjarres Ramos[46], K.H. Mankinen[94], A. Mann[112], A. Manousos[74], B. Mansoulie[142], J.D. Mansour[15a], M. Mantoani[51], S. Manzoni[66a,66b], A. Marantis[159], G. Marceca[30], L. March[52], L. Marchese[131], G. Marchiori[132], M. Marcisovsky[137], C.A. Marin Tobon[35], M. Marjanovic[37], D.E. Marley[103], F. Marroquim[78b], Z. Marshall[18], M.U.F Martensson[169], S. Marti-Garcia[171], C.B. Martin[122], T.A. Martin[175], V.J. Martin[48], B. Martin dit Latour[17], M. Martinez[14,y], V.I. Martinez Outschoorn[100], S. Martin-Haugh[141], V.S. Martoiu[27b], A.C. Martyniuk[92], A. Marzin[35], L. Masetti[97], T. Mashimo[160], R. Mashinistov[108], J. Masik[98], A.L. Maslennikov[120b,120a], L.H. Mason[102], L. Massa[71a,71b], P. Massarotti[67a,67b], P. Mastrandrea[5], A. Mastroberardino[40b,40a], T. Masubuchi[160], P. Mättig[179], J. Maurer[27b], B. Maček[89], S.J. Maxfield[88], D.A. Maximov[120b,120a], R. Mazini[155], I. Maznas[159], S.M. Mazza[143], N.C. Mc Fadden[116], G. Mc Goldrick[164], S.P. Mc Kee[103], A. McCarn[103], T.G. McCarthy[113], L.I. McClymont[92], E.F. McDonald[102], J.A. Mcfayden[35], G. Mchedlidze[51], M.A. McKay[41], K.D. McLean[173], S.J. McMahon[141], P.C. McNamara[102], C.J. McNicol[175], R.A. McPherson[173,ac], J.E. Mdhluli[32c], Z.A. Meadows[100], S. Meehan[145], T.M. Megy[50], S. Mehlhase[112], A. Mehta[88], T. Meideck[56], B. Meirose[42], D. Melini[171,g], B.R. Mellado Garcia[32c], J.D. Mellenthin[51], M. Melo[28a], F. Meloni[44], A. Melzer[24], S.B. Menary[98], E.D. Mendes Gouveia[136a], L. Meng[88], X.T. Meng[103], A. Mengarelli[23b,23a], S. Menke[113], E. Meoni[40b,40a], S. Mergelmeyer[19], C. Merlassino[20], P. Mermod[52], L. Merola[67a,67b], C. Meroni[66a], F.S. Merritt[36], A. Messina[70a,70b], J. Metcalfe[6], A.S. Mete[168], C. Meyer[133], J. Meyer[157], J-P. Meyer[142], H. Meyer Zu Theenhausen[59a], F. Miano[153], R.P. Middleton[141], L. Mijović[48], G. Mikenberg[177], M. Mikestikova[137], M. Mikuž[89], M. Milesi[102], A. Milic[164], D.A. Millar[90], D.W. Miller[36], A. Milov[177], D.A. Milstead[43a,43b], A.A. Minaenko[140], M. Miñano Moya[171], I.A. Minashvili[156b], A.I. Mincer[121], B. Mindur[81a], M. Mineev[77], Y. Minegishi[160], Y. Ming[178], L.M. Mir[14], A. Mirto[65a,65b], K.P. Mistry[133], T. Mitani[176], J. Mitrevski[112], V.A. Mitsou[171], A. Miucci[20], P.S. Miyagawa[146], A. Mizukami[79], J.U. Mjörnmark[94], T. Mkrtchyan[181], M. Mlynarikova[139], T. Moa[43a,43b], K. Mochizuki[107], P. Mogg[50], S. Mohapatra[38], S. Molander[43a,43b], R. Moles-Valls[24], M.C. Mondragon[104],

K. Mönig[44], J. Monk[39], E. Monnier[99], A. Montalbano[149], J. Montejo Berlingen[35], F. Monticelli[86], S. Monzani[66a], N. Morange[128], D. Moreno[22], M. Moreno Llácer[35], P. Morettini[53b], M. Morgenstern[118], S. Morgenstern[46], D. Mori[149], M. Morii[57], M. Morinaga[176], V. Morisbak[130], A.K. Morley[35], G. Mornacchi[35], A.P. Morris[92], J.D. Morris[90], L. Morvaj[152], P. Moschovakos[10], M. Mosidze[156b], H.J. Moss[146], J. Moss[150,m], K. Motohashi[162], R. Mount[150], E. Mountricha[35], E.J.W. Moyse[100], S. Muanza[99], F. Mueller[113], J. Mueller[135], R.S.P. Mueller[112], D. Muenstermann[87], G.A. Mullier[94], F.J. Munoz Sanchez[98], P. Murin[28b], W.J. Murray[175,141], A. Murrone[66a,66b], M. Muškinja[89], C. Mwewa[32a], A.G. Myagkov[140,ak], J. Myers[127], M. Myska[138], B.P. Nachman[18], O. Nackenhorst[45], K. Nagai[131], K. Nagano[79], Y. Nagasaka[60], M. Nagel[50], E. Nagy[99], A.M. Nairz[35], Y. Nakahama[115], K. Nakamura[79], T. Nakamura[160], I. Nakano[123], H. Nanjo[129], F. Napolitano[59a], R.F. Naranjo Garcia[44], R. Narayan[11], D.I. Narrias Villar[59a], I. Naryshkin[134], T. Naumann[44], G. Navarro[22], R. Nayyar[7], H.A. Neal[103], P.Y. Nechaeva[108], T.J. Neep[142], A. Negri[68a,68b], M. Negrini[23b], S. Nektarijevic[117], C. Nellist[51], M.E. Nelson[131], S. Nemecek[137], P. Nemethy[121], M. Nessi[35,e], M.S. Neubauer[170], M. Neumann[179], P.R. Newman[21], T.Y. Ng[61c], Y.S. Ng[19], H.D.N. Nguyen[99], T. Nguyen Manh[107], E. Nibigira[37], R.B. Nickerson[131], R. Nicolaidou[142], D.S. Nielsen[39], J. Nielsen[143], N. Nikiforou[11], V. Nikolaenko[140,ak], I. Nikolic-Audit[132], K. Nikolopoulos[21], P. Nilsson[29], Y. Ninomiya[79], A. Nisati[70a], N. Nishu[58c], R. Nisius[113], I. Nitsche[45], T. Nitta[176], T. Nobe[160], Y. Noguchi[83], M. Nomachi[129], I. Nomidis[132], M.A. Nomura[29], T. Nooney[90], M. Nordberg[35], N. Norjoharuddeen[131], T. Novak[89], O. Novgorodova[46], R. Novotny[138], L. Nozka[126], K. Ntekas[168], E. Nurse[92], F. Nuti[102], F.G. Oakham[33,ar], H. Oberlack[113], T. Obermann[24], J. Ocariz[132], A. Ochi[80], I. Ochoa[38], J.P. Ochoa-Ricoux[144a], K. O'Connor[26], S. Oda[85], S. Odaka[79], S. Oerdek[51], A. Oh[98], S.H. Oh[47], C.C. Ohm[151], H. Oide[53b,53a], M.L. Ojeda[164], H. Okawa[166], Y. Okazaki[83], Y. Okumura[160], T. Okuyama[79], A. Olariu[27b], L.F. Oleiro Seabra[136a], S.A. Olivares Pino[144a], D. Oliveira Damazio[29], J.L. Oliver[1], M.J.R. Olsson[36], A. Olszewski[82], J. Olszowska[82], D.C. O'Neil[149], A. Onofre[136a,136e], K. Onogi[115], P.U.E. Onyisi[11], H. Oppen[130], M.J. Oreglia[36], G.E. Orellana[86], Y. Oren[158], D. Orestano[72a,72b], E.C. Orgill[98], N. Orlando[61b], A.A. O'Rourke[44], R.S. Orr[164], B. Osculati[53b,53a,*], V. O'Shea[55], R. Ospanov[58a], G. Otero y Garzon[30], H. Otono[85], M. Ouchrif[34d], F. Ould-Saada[130], A. Ouraou[142], Q. Ouyang[15a], M. Owen[55], R.E. Owen[21], V.E. Ozcan[12c], N. Ozturk[8], J. Pacalt[126], H.A. Pacey[31], K. Pachal[149], A. Pacheco Pages[14], L. Pacheco Rodriguez[142], C. Padilla Aranda[14], S. Pagan Griso[18], M. Paganini[180], G. Palacino[63], S. Palazzo[40b,40a], S. Palestini[35], M. Palka[81b], D. Pallin[37], I. Panagoulias[10], C.E. Pandini[35], J.G. Panduro Vazquez[91], P. Pani[35], G. Panizzo[64a,64c], L. Paolozzi[52], T.D. Papadopoulou[10], K. Papageorgiou[9,i], A. Paramonov[6], D. Paredes Hernandez[61b], S.R. Paredes Saenz[131], B. Parida[163], A.J. Parker[87], K.A. Parker[44], M.A. Parker[31], F. Parodi[53b,53a], J.A. Parsons[38], U. Parzefall[50], V.R. Pascuzzi[164], J.M.P. Pasner[143], E. Pasqualucci[70a], S. Passaggio[53b], F. Pastore[91], P. Pasuwan[43a,43b], S. Pataraia[97], J.R. Pater[98], A. Pathak[178,j], T. Pauly[35], B. Pearson[113], M. Pedersen[130], L. Pedraza Diaz[117], R. Pedro[136a,136b], S.V. Peleganchuk[120b,120a], O. Penc[137], C. Peng[15d], H. Peng[58a], B.S. Peralva[78a], M.M. Perego[142], A.P. Pereira Peixoto[136a], D.V. Perepelitsa[29], F. Peri[19], L. Perini[66a,66b], H. Pernegger[35], S. Perrella[67a,67b], V.D. Peshekhonov[77,*], K. Peters[44], R.F.Y. Peters[98], B.A. Petersen[35], T.C. Petersen[39], E. Petit[56], A. Petridis[1], C. Petridou[159], P. Petroff[128], M. Petrov[131], F. Petrucci[72a,72b], M. Pettee[180], N.E. Pettersson[100], A. Peyaud[142], R. Pezoa[144b], T. Pham[102], F.H. Phillips[104], P.W. Phillips[141], M.W. Phipps[170], G. Piacquadio[152], E. Pianori[18], A. Picazio[100], M.A. Pickering[131], R.H. Pickles[98], R. Piegaia[30], J.E. Pilcher[36], A.D. Pilkington[98], M. Pinamonti[71a,71b], J.L. Pinfold[3], M. Pitt[177], L. Pizzimento[71a,71b], M-A. Pleier[29], V. Pleskot[139], E. Plotnikova[77], D. Pluth[76], P. Podberezko[120b,120a], R. Poettgen[94], R. Poggi[52], L. Poggioli[128], I. Pogrebnyak[104], D. Pohl[24], I. Pokharel[51], G. Polesello[68a], A. Poley[18], A. Policicchio[70a,70b], R. Polifka[35], A. Polini[23b], C.S. Pollard[44], V. Polychronakos[29], D. Ponomarenko[110], L. Pontecorvo[70a], G.A. Popeneciu[27d], D.M. Portillo Quintero[132], S. Pospisil[138], K. Potamianos[44], I.N. Potrap[77], C.J. Potter[31], H. Potti[11], T. Poulsen[94], J. Poveda[35], T.D. Powell[146], M.E. Pozo Astigarraga[35], P. Pralavorio[99], S. Prell[76], D. Price[98], M. Primavera[65a],

S. Prince[101], N. Proklova[110], K. Prokofiev[61c], F. Prokoshin[144b], S. Protopopescu[29], J. Proudfoot[6], M. Przybycien[81a], A. Puri[170], P. Puzo[128], J. Qian[103], Y. Qin[98], A. Quadt[51], M. Queitsch-Maitland[44], A. Qureshi[1], P. Rados[102], F. Ragusa[66a,66b], G. Rahal[95], J.A. Raine[52], S. Rajagopalan[29], A. Ramirez Morales[90], T. Rashid[128], S. Raspopov[5], M.G. Ratti[66a,66b], D.M. Rauch[44], F. Rauscher[112], S. Rave[97], B. Ravina[146], I. Ravinovich[177], J.H. Rawling[98], M. Raymond[35], A.L. Read[130], N.P. Readioff[56], M. Reale[65a,65b], D.M. Rebuzzi[68a,68b], A. Redelbach[174], G. Redlinger[29], R. Reece[143], R.G. Reed[32c], K. Reeves[42], L. Rehnisch[19], J. Reichert[133], D. Reikher[158], A. Reiss[97], C. Rembser[35], H. Ren[15d], M. Rescigno[70a], S. Resconi[66a], E.D. Resseguie[133], S. Rettie[172], E. Reynolds[21], O.L. Rezanova[120b,120a], P. Reznicek[139], E. Ricci[73a,73b], R. Richter[113], S. Richter[44], E. Richter-Was[81b], O. Ricken[24], M. Ridel[132], P. Rieck[113], C.J. Riegel[179], O. Rifki[44], M. Rijssenbeek[152], A. Rimoldi[68a,68b], M. Rimoldi[20], L. Rinaldi[23b], G. Ripellino[151], B. Ristić[87], E. Ritsch[35], I. Riu[14], J.C. Rivera Vergara[144a], F. Rizatdinova[125], E. Rizvi[90], C. Rizzi[14], R.T. Roberts[98], S.H. Robertson[101,ac], D. Robinson[31], J.E.M. Robinson[44], A. Robson[55], E. Rocco[97], C. Roda[69a,69b], Y. Rodina[99], S. Rodriguez Bosca[171], A. Rodriguez Perez[14], D. Rodriguez Rodriguez[171], A.M. Rodríguez Vera[165b], S. Roe[35], C.S. Rogan[57], O. Røhne[130], R. Röhrig[113], C.P.A. Roland[63], J. Roloff[57], A. Romaniouk[110], M. Romano[23b,23a], N. Rompotis[88], M. Ronzani[121], L. Roos[132], S. Rosati[70a], K. Rosbach[50], P. Rose[143], N-A. Rosien[51], B.J. Rosser[133], E. Rossi[44], E. Rossi[72a,72b], E. Rossi[67a,67b], L.P. Rossi[53b], L. Rossini[66a,66b], J.H.N. Rosten[31], R. Rosten[14], M. Rotaru[27b], J. Rothberg[145], D. Rousseau[128], D. Roy[32c], A. Rozanov[99], Y. Rozen[157], X. Ruan[32c], F. Rubbo[150], F. Rühr[50], A. Ruiz-Martinez[171], Z. Rurikova[50], N.A. Rusakovich[77], H.L. Russell[101], J.P. Rutherfoord[7], E.M. Rüttinger[44,k], Y.F. Ryabov[134], M. Rybar[170], G. Rybkin[128], S. Ryu[6], A. Ryzhov[140], G.F. Rzehorz[51], P. Sabatini[51], G. Sabato[118], S. Sacerdoti[128], H.F-W. Sadrozinski[143], R. Sadykov[77], F. Safai Tehrani[70a], P. Saha[119], M. Sahinsoy[59a], A. Sahu[179], M. Saimpert[44], M. Saito[160], T. Saito[160], H. Sakamoto[160], A. Sakharov[121,aj], D. Salamani[52], G. Salamanna[72a,72b], J.E. Salazar Loyola[144b], P.H. Sales De Bruin[169], D. Salihagic[113], A. Salnikov[150], J. Salt[171], D. Salvatore[40b,40a], F. Salvatore[153], A. Salvucci[61a,61b,61c], A. Salzburger[35], J. Samarati[35], D. Sammel[50], D. Sampsonidis[159], D. Sampsonidou[159], J. Sánchez[171], A. Sanchez Pineda[64a,64c], H. Sandaker[130], C.O. Sander[44], M. Sandhoff[179], C. Sandoval[22], D.P.C. Sankey[141], M. Sannino[53b,53a], Y. Sano[115], A. Sansoni[49], C. Santoni[37], H. Santos[136a], I. Santoyo Castillo[153], A. Santra[171], A. Sapronov[77], J.G. Saraiva[136a,136d], O. Sasaki[79], K. Sato[166], E. Sauvan[5], P. Savard[164,ar], N. Savic[113], R. Sawada[160], C. Sawyer[141], L. Sawyer[93,ai], C. Sbarra[23b], A. Sbrizzi[23b,23a], T. Scanlon[92], J. Schaarschmidt[145], P. Schacht[113], B.M. Schachtner[112], D. Schaefer[36], L. Schaefer[133], J. Schaeffer[97], S. Schaepe[35], U. Schäfer[97], A.C. Schaffer[128], D. Schaile[112], R.D. Schamberger[152], N. Scharmberg[98], V.A. Schegelsky[134], D. Scheirich[139], F. Schenck[19], M. Schernau[168], C. Schiavi[53b,53a], S. Schier[143], L.K. Schildgen[24], Z.M. Schillaci[26], E.J. Schioppa[35], M. Schioppa[40b,40a], K.E. Schleicher[50], S. Schlenker[35], K.R. Schmidt-Sommerfeld[113], K. Schmieden[35], C. Schmitt[97], S. Schmitt[44], S. Schmitz[97], J.C. Schmoeckel[44], U. Schnoor[50], L. Schoeffel[142], A. Schoening[59b], E. Schopf[131], M. Schott[97], J.F.P. Schouwenberg[117], J. Schovancova[35], S. Schramm[52], A. Schulte[97], H-C. Schultz-Coulon[59a], M. Schumacher[50], B.A. Schumm[143], Ph. Schune[142], A. Schwartzman[150], T.A. Schwarz[103], Ph. Schwemling[142], R. Schwienhorst[104], A. Sciandra[24], G. Sciolla[26], M. Scornajenghi[40b,40a], F. Scuri[69a], F. Scutti[102], L.M. Scyboz[113], J. Searcy[103], C.D. Sebastiani[70a,70b], P. Seema[19], S.C. Seidel[116], A. Seiden[143], T. Seiss[36], J.M. Seixas[78b], G. Sekhniaidze[67a], K. Sekhon[103], S.J. Sekula[41], N. Semprini-Cesari[23b,23a], S. Sen[47], S. Senkin[37], C. Serfon[130], L. Serin[128], L. Serkin[64a,64b], M. Sessa[58a], H. Severini[124], F. Sforza[167], A. Sfyrla[52], E. Shabalina[51], J.D. Shahinian[143], N.W. Shaikh[43a,43b], L.Y. Shan[15a], R. Shang[170], J.T. Shank[25], M. Shapiro[18], A.S. Sharma[1], A. Sharma[131], P.B. Shatalov[109], K. Shaw[153], S.M. Shaw[98], A. Shcherbakova[134], Y. Shen[124], N. Sherafati[33], A.D. Sherman[25], P. Sherwood[92], L. Shi[155,an], S. Shimizu[79], C.O. Shimmin[180], M. Shimojima[114], I.P.J. Shipsey[131], S. Shirabe[85], M. Shiyakova[77], J. Shlomi[177], A. Shmeleva[108], D. Shoaleh Saadi[107], M.J. Shochet[36], S. Shojaii[102], D.R. Shope[124], S. Shrestha[122], E. Shulga[110], P. Sicho[137], A.M. Sickles[170], P.E. Sidebo[151], E. Sideras Haddad[32c], O. Sidiropoulou[35],

A. Sidoti[23b,23a], F. Siegert[46], Dj. Sijacki[16], J. Silva[136a], M. Silva Jr.[178], M.V. Silva Oliveira[78a], S.B. Silverstein[43a], S. Simion[128], E. Simioni[97], M. Simon[97], R. Simoniello[97], P. Sinervo[164], N.B. Sinev[127], M. Sioli[23b,23a], G. Siragusa[174], I. Siral[103], S.Yu. Sivoklokov[111], J. Sjölin[43a,43b], P. Skubic[124], M. Slater[21], T. Slavicek[138], M. Slawinska[82], K. Sliwa[167], R. Slovak[139], V. Smakhtin[177], B.H. Smart[5], J. Smiesko[28a], N. Smirnov[110], S.Yu. Smirnov[110], Y. Smirnov[110], L.N. Smirnova[111], O. Smirnova[94], J.W. Smith[51], M.N.K. Smith[38], M. Smizanska[87], K. Smolek[138], A. Smykiewicz[82], A.A. Snesarev[108], I.M. Snyder[127], S. Snyder[29], R. Sobie[173,ac], A.M. Soffa[168], A. Soffer[158], A. Søgaard[48], D.A. Soh[155], G. Sokhrannyi[89], C.A. Solans Sanchez[35], M. Solar[138], E.Yu. Soldatov[110], U. Soldevila[171], A.A. Solodkov[140], A. Soloshenko[77], O.V. Solovyanov[140], V. Solovyev[134], P. Sommer[146], H. Son[167], W. Song[141], W.Y. Song[165b], A. Sopczak[138], F. Sopkova[28b], C.L. Sotiropoulou[69a,69b], S. Sottocornola[68a,68b], R. Soualah[64a,64c,h], A.M. Soukharev[120b,120a], D. South[44], B.C. Sowden[91], S. Spagnolo[65a,65b], M. Spalla[113], M. Spangenberg[175], F. Spanò[91], D. Sperlich[19], F. Spettel[113], T.M. Spieker[59a], R. Spighi[23b], G. Spigo[35], L.A. Spiller[102], D.P. Spiteri[55], M. Spousta[139], A. Stabile[66a,66b], R. Stamen[59a], S. Stamm[19], E. Stanecka[82], R.W. Stanek[6], C. Stanescu[72a], B. Stanislaus[131], M.M. Stanitzki[44], B. Stapf[118], S. Stapnes[130], E.A. Starchenko[140], G.H. Stark[36], J. Stark[56], S.H Stark[39], P. Staroba[137], P. Starovoitov[59a], S. Stärz[35], R. Staszewski[82], M. Stegler[44], P. Steinberg[29], B. Stelzer[149], H.J. Stelzer[35], O. Stelzer-Chilton[165a], H. Stenzel[54], T.J. Stevenson[90], G.A. Stewart[55], M.C. Stockton[127], G. Stoicea[27b], P. Stolte[51], S. Stonjek[113], A. Straessner[46], J. Strandberg[151], S. Strandberg[43a,43b], M. Strauss[124], P. Strizenec[28b], R. Ströhmer[174], D.M. Strom[127], R. Stroynowski[41], A. Strubig[48], S.A. Stucci[29], B. Stugu[17], J. Stupak[124], N.A. Styles[44], D. Su[150], J. Su[135], S. Suchek[59a], Y. Sugaya[129], M. Suk[138], V.V. Sulin[108], M.J. Sullivan[88], D.M.S. Sultan[52], S. Sultansoy[4c], T. Sumida[83], S. Sun[103], X. Sun[3], K. Suruliz[153], C.J.E. Suster[154], M.R. Sutton[153], S. Suzuki[79], M. Svatos[137], M. Swiatlowski[36], S.P. Swift[2], A. Sydorenko[97], I. Sykora[28a], T. Sykora[139], D. Ta[97], K. Tackmann[44,z], J. Taenzer[158], A. Taffard[168], R. Tafirout[165a], E. Tahirovic[90], N. Taiblum[158], H. Takai[29], R. Takashima[84], E.H. Takasugi[113], K. Takeda[80], T. Takeshita[147], Y. Takubo[79], M. Talby[99], A.A. Talyshev[120b,120a], J. Tanaka[160], M. Tanaka[162], R. Tanaka[128], B.B. Tannenwald[122], S. Tapia Araya[144b], S. Tapprogge[97], A. Tarek Abouelfadl Mohamed[132], S. Tarem[157], G. Tarna[27b,d], G.F. Tartarelli[66a], P. Tas[139], M. Tasevsky[137], T. Tashiro[83], E. Tassi[40b,40a], A. Tavares Delgado[136a,136b], Y. Tayalati[34e], A.C. Taylor[116], A.J. Taylor[48], G.N. Taylor[102], P.T.E. Taylor[102], W. Taylor[165b], A.S. Tee[87], P. Teixeira-Dias[91], H. Ten Kate[35], P.K. Teng[155], J.J. Teoh[118], S. Terada[79], K. Terashi[160], J. Terron[96], S. Terzo[14], M. Testa[49], R.J. Teuscher[164,ac], S.J. Thais[180], T. Theveneaux-Pelzer[44], F. Thiele[39], D.W. Thomas[91], J.P. Thomas[21], A.S. Thompson[55], P.D. Thompson[21], L.A. Thomsen[180], E. Thomson[133], Y. Tian[38], R.E. Ticse Torres[51], V.O. Tikhomirov[108,al], Yu.A. Tikhonov[120b,120a], S. Timoshenko[110], P. Tipton[180], S. Tisserant[99], K. Todome[162], S. Todorova-Nova[5], S. Todt[46], J. Tojo[85], S. Tokár[28a], K. Tokushuku[79], E. Tolley[122], K.G. Tomiwa[32c], M. Tomoto[115], L. Tompkins[150,p], K. Toms[116], B. Tong[57], P. Tornambe[50], E. Torrence[127], H. Torres[46], E. Torró Pastor[145], C. Tosciri[131], J. Toth[99,ab], F. Touchard[99], D.R. Tovey[146], C.J. Treado[121], T. Trefzger[174], F. Tresoldi[153], A. Tricoli[29], I.M. Trigger[165a], S. Trincaz-Duvoid[132], M.F. Tripiana[14], W. Trischuk[164], B. Trocmé[56], A. Trofymov[128], C. Troncon[66a], M. Trovatelli[173], F. Trovato[153], L. Truong[32b], M. Trzebinski[82], A. Trzupek[82], F. Tsai[44], J.C-L. Tseng[131], P.V. Tsiareshka[105], A. Tsirigotis[159], N. Tsirintanis[9], V. Tsiskaridze[152], E.G. Tskhadadze[156a], I.I. Tsukerman[109], V. Tsulaia[18], S. Tsuno[79], D. Tsybychev[152,163], Y. Tu[61b], A. Tudorache[27b], V. Tudorache[27b], T.T. Tulbure[27a], A.N. Tuna[57], S. Turchikhin[77], D. Turgeman[177], I. Turk Cakir[4b,t], R. Turra[66a], P.M. Tuts[38], E. Tzovara[97], G. Ucchielli[23b,23a], I. Ueda[79], M. Ughetto[43a,43b], F. Ukegawa[166], G. Unal[35], A. Undrus[29], G. Unel[168], F.C. Ungaro[102], Y. Unno[79], K. Uno[160], J. Urban[28b], P. Urquijo[102], P. Urrejola[97], G. Usai[8], J. Usui[79], L. Vacavant[99], V. Vacek[138], B. Vachon[101], K.O.H. Vadla[130], A. Vaidya[92], C. Valderanis[112], E. Valdes Santurio[43a,43b], M. Valente[52], S. Valentinetti[23b,23a], A. Valero[171], L. Valéry[44], R.A. Vallance[21], A. Vallier[5], J.A. Valls Ferrer[171], T.R. Van Daalen[14], H. Van der Graaf[118], P. Van Gemmeren[6], J. Van Nieuwkoop[149], I. Van Vulpen[118], M. Vanadia[71a,71b], W. Vandelli[35], A. Vaniachine[163], P. Vankov[118],

R. Vari[70a], E.W. Varnes[7], C. Varni[53b,53a], T. Varol[41], D. Varouchas[128], K.E. Varvell[154], G.A. Vasquez[144b], J.G. Vasquez[180], F. Vazeille[37], D. Vazquez Furelos[14], T. Vazquez Schroeder[101], J. Veatch[51], V. Vecchio[72a,72b], L.M. Veloce[164], F. Veloso[136a,136c], S. Veneziano[70a], A. Ventura[65a,65b], M. Venturi[173], N. Venturi[35], V. Vercesi[68a], M. Verducci[72a,72b], C.M. Vergel Infante[76], C. Vergis[24], W. Verkerke[118], A.T. Vermeulen[118], J.C. Vermeulen[118], M.C. Vetterli[149,ar], N. Viaux Maira[144b], M. Vicente Barreto Pinto[52], I. Vichou[170,*], T. Vickey[146], O.E. Vickey Boeriu[146], G.H.A. Viehhauser[131], S. Viel[18], L. Vigani[131], M. Villa[23b,23a], M. Villaplana Perez[66a,66b], E. Vilucchi[49], M.G. Vincter[33], V.B. Vinogradov[77], A. Vishwakarma[44], C. Vittori[23b,23a], I. Vivarelli[153], S. Vlachos[10], M. Vogel[179], P. Vokac[138], G. Volpi[14], S.E. von Buddenbrock[32c], E. Von Toerne[24], V. Vorobel[139], K. Vorobev[110], M. Vos[171], J.H. Vossebeld[88], N. Vranjes[16], M. Vranjes Milosavljevic[16], V. Vrba[138], M. Vreeswijk[118], T. Šfiligoj[89], R. Vuillermet[35], I. Vukotic[36], T. Ženiš[28a], L. Živković[16], P. Wagner[24], W. Wagner[179], J. Wagner-Kuhr[112], H. Wahlberg[86], S. Wahrmund[46], K. Wakamiya[80], V.M. Walbrecht[113], J. Walder[87], R. Walker[112], S.D. Walker[91], W. Walkowiak[148], V. Wallangen[43a,43b], A.M. Wang[57], C. Wang[58b,d], F. Wang[178], H. Wang[18], H. Wang[3], J. Wang[154], J. Wang[59b], P. Wang[41], Q. Wang[124], R.-J. Wang[132], R. Wang[58a], R. Wang[6], S.M. Wang[155], W.T. Wang[58a], W. Wang[15c,ad], W.X. Wang[58a,ad], Y. Wang[58a], Z. Wang[58c], C. Wanotayaroj[44], A. Warburton[101], C.P. Ward[31], D.R. Wardrope[92], A. Washbrook[48], P.M. Watkins[21], A.T. Watson[21], M.F. Watson[21], G. Watts[145], S. Watts[98], B.M. Waugh[92], A.F. Webb[11], S. Webb[97], C. Weber[180], M.S. Weber[20], S.A. Weber[33], S.M. Weber[59a], A.R. Weidberg[131], B. Weinert[63], J. Weingarten[45], M. Weirich[97], C. Weiser[50], P.S. Wells[35], T. Wenaus[29], T. Wengler[35], S. Wenig[35], N. Wermes[24], M.D. Werner[76], P. Werner[35], M. Wessels[59a], T.D. Weston[20], K. Whalen[127], N.L. Whallon[145], A.M. Wharton[87], A.S. White[103], A. White[8], M.J. White[1], R. White[144b], D. Whiteson[168], B.W. Whitmore[87], F.J. Wickens[141], W. Wiedenmann[178], M. Wielers[141], C. Wiglesworth[39], L.A.M. Wiik-Fuchs[50], F. Wilk[98], H.G. Wilkens[35], L.J. Wilkins[91], H.H. Williams[133], S. Williams[31], C. Willis[104], S. Willocq[100], J.A. Wilson[21], I. Wingerter-Seez[5], E. Winkels[153], F. Winklmeier[127], O.J. Winston[153], B.T. Winter[24], M. Wittgen[150], M. Wobisch[93], A. Wolf[97], T.M.H. Wolf[118], R. Wolff[99], M.W. Wolter[82], H. Wolters[136a,136c], V.W.S. Wong[172], N.L. Woods[143], S.D. Worm[21], B.K. Wosiek[82], K.W. Woźniak[82], K. Wraight[55], M. Wu[36], S.L. Wu[178], X. Wu[52], Y. Wu[58a], T.R. Wyatt[98], B.M. Wynne[48], S. Xella[39], Z. Xi[103], L. Xia[175], D. Xu[15a], H. Xu[58a], L. Xu[29], T. Xu[142], W. Xu[103], B. Yabsley[154], S. Yacoob[32a], K. Yajima[129], D.P. Yallup[92], D. Yamaguchi[162], Y. Yamaguchi[162], A. Yamamoto[79], T. Yamanaka[160], F. Yamane[80], M. Yamatani[160], T. Yamazaki[160], Y. Yamazaki[80], Z. Yan[25], H.J. Yang[58c,58d], H.T. Yang[18], S. Yang[75], Y. Yang[160], Z. Yang[17], W-M. Yao[18], Y.C. Yap[44], Y. Yasu[79], E. Yatsenko[58c,58d], J. Ye[41], S. Ye[29], I. Yeletskikh[77], E. Yigitbasi[25], E. Yildirim[97], K. Yorita[176], K. Yoshihara[133], C.J.S. Young[35], C. Young[150], J. Yu[8], J. Yu[76], X. Yue[59a], S.P.Y. Yuen[24], B. Zabinski[82], G. Zacharis[10], E. Zaffaroni[52], R. Zaidan[14], A.M. Zaitsev[140,ak], T. Zakareishvili[156b], N. Zakharchuk[33], J. Zalieckas[17], S. Zambito[57], D. Zanzi[35], D.R. Zaripovas[55], S.V. Zeißner[45], C. Zeitnitz[179], G. Zemaityte[131], J.C. Zeng[170], Q. Zeng[150], O. Zenin[140], D. Zerwas[128], M. Zgubič[131], D.F. Zhang[58b], D. Zhang[103], F. Zhang[178], G. Zhang[58a], H. Zhang[15c], J. Zhang[6], L. Zhang[15c], L. Zhang[58a], M. Zhang[170], P. Zhang[15c], R. Zhang[58a], R. Zhang[24], X. Zhang[58b], Y. Zhang[15d], Z. Zhang[128], P. Zhao[47], X. Zhao[41], Y. Zhao[58b,128,ah], Z. Zhao[58a], A. Zhemchugov[77], Z. Zheng[103], D. Zhong[170], B. Zhou[103], C. Zhou[178], L. Zhou[41], M.S. Zhou[15d], M. Zhou[152], N. Zhou[58c], Y. Zhou[7], C.G. Zhu[58b], H.L. Zhu[58a], H. Zhu[15a], J. Zhu[103], Y. Zhu[58a], X. Zhuang[15a], K. Zhukov[108], V. Zhulanov[120b,120a], A. Zibell[174], D. Zieminska[63], N.I. Zimine[77], S. Zimmermann[50], Z. Zinonos[113], M. Zinser[97], M. Ziolkowski[148], G. Zobernig[178], A. Zoccoli[23b,23a], K. Zoch[51], T.G. Zorbas[146], R. Zou[36], M. Zur Nedden[19], L. Zwalinski[35].

[1]Department of Physics, University of Adelaide, Adelaide; Australia.
[2]Physics Department, SUNY Albany, Albany NY; United States of America.
[3]Department of Physics, University of Alberta, Edmonton AB; Canada.

[4(a)]Department of Physics, Ankara University, Ankara;[(b)]Istanbul Aydin University, Istanbul;[(c)]Division of Physics, TOBB University of Economics and Technology, Ankara; Turkey.
[5]LAPP, Université Grenoble Alpes, Université Savoie Mont Blanc, CNRS/IN2P3, Annecy; France.
[6]High Energy Physics Division, Argonne National Laboratory, Argonne IL; United States of America.
[7]Department of Physics, University of Arizona, Tucson AZ; United States of America.
[8]Department of Physics, University of Texas at Arlington, Arlington TX; United States of America.
[9]Physics Department, National and Kapodistrian University of Athens, Athens; Greece.
[10]Physics Department, National Technical University of Athens, Zografou; Greece.
[11]Department of Physics, University of Texas at Austin, Austin TX; United States of America.
[12(a)]Bahcesehir University, Faculty of Engineering and Natural Sciences, Istanbul;[(b)]Istanbul Bilgi University, Faculty of Engineering and Natural Sciences, Istanbul;[(c)]Department of Physics, Bogazici University, Istanbul;[(d)]Department of Physics Engineering, Gaziantep University, Gaziantep; Turkey.
[13]Institute of Physics, Azerbaijan Academy of Sciences, Baku; Azerbaijan.
[14]Institut de Física d'Altes Energies (IFAE), Barcelona Institute of Science and Technology, Barcelona; Spain.
[15(a)]Institute of High Energy Physics, Chinese Academy of Sciences, Beijing;[(b)]Physics Department, Tsinghua University, Beijing;[(c)]Department of Physics, Nanjing University, Nanjing;[(d)]University of Chinese Academy of Science (UCAS), Beijing; China.
[16]Institute of Physics, University of Belgrade, Belgrade; Serbia.
[17]Department for Physics and Technology, University of Bergen, Bergen; Norway.
[18]Physics Division, Lawrence Berkeley National Laboratory and University of California, Berkeley CA; United States of America.
[19]Institut für Physik, Humboldt Universität zu Berlin, Berlin; Germany.
[20]Albert Einstein Center for Fundamental Physics and Laboratory for High Energy Physics, University of Bern, Bern; Switzerland.
[21]School of Physics and Astronomy, University of Birmingham, Birmingham; United Kingdom.
[22]Centro de Investigaciónes, Universidad Antonio Nariño, Bogota; Colombia.
[23(a)]Dipartimento di Fisica e Astronomia, Università di Bologna, Bologna;[(b)]INFN Sezione di Bologna; Italy.
[24]Physikalisches Institut, Universität Bonn, Bonn; Germany.
[25]Department of Physics, Boston University, Boston MA; United States of America.
[26]Department of Physics, Brandeis University, Waltham MA; United States of America.
[27(a)]Transilvania University of Brasov, Brasov;[(b)]Horia Hulubei National Institute of Physics and Nuclear Engineering, Bucharest;[(c)]Department of Physics, Alexandru Ioan Cuza University of Iasi, Iasi;[(d)]National Institute for Research and Development of Isotopic and Molecular Technologies, Physics Department, Cluj-Napoca;[(e)]University Politehnica Bucharest, Bucharest;[(f)]West University in Timisoara, Timisoara; Romania.
[28(a)]Faculty of Mathematics, Physics and Informatics, Comenius University, Bratislava;[(b)]Department of Subnuclear Physics, Institute of Experimental Physics of the Slovak Academy of Sciences, Kosice; Slovak Republic.
[29]Physics Department, Brookhaven National Laboratory, Upton NY; United States of America.
[30]Departamento de Física, Universidad de Buenos Aires, Buenos Aires; Argentina.
[31]Cavendish Laboratory, University of Cambridge, Cambridge; United Kingdom.
[32(a)]Department of Physics, University of Cape Town, Cape Town;[(b)]Department of Mechanical Engineering Science, University of Johannesburg, Johannesburg;[(c)]School of Physics, University of the Witwatersrand, Johannesburg; South Africa.
[33]Department of Physics, Carleton University, Ottawa ON; Canada.

[34(a)]Faculté des Sciences Ain Chock, Réseau Universitaire de Physique des Hautes Energies - Université Hassan II, Casablanca;[(b)]Centre National de l'Energie des Sciences Techniques Nucleaires (CNESTEN), Rabat;[(c)]Faculté des Sciences Semlalia, Université Cadi Ayyad, LPHEA-Marrakech;[(d)]Faculté des Sciences, Université Mohamed Premier and LPTPM, Oujda;[(e)]Faculté des sciences, Université Mohammed V, Rabat; Morocco.
[35]CERN, Geneva; Switzerland.
[36]Enrico Fermi Institute, University of Chicago, Chicago IL; United States of America.
[37]LPC, Université Clermont Auvergne, CNRS/IN2P3, Clermont-Ferrand; France.
[38]Nevis Laboratory, Columbia University, Irvington NY; United States of America.
[39]Niels Bohr Institute, University of Copenhagen, Copenhagen; Denmark.
[40(a)]Dipartimento di Fisica, Università della Calabria, Rende;[(b)]INFN Gruppo Collegato di Cosenza, Laboratori Nazionali di Frascati; Italy.
[41]Physics Department, Southern Methodist University, Dallas TX; United States of America.
[42]Physics Department, University of Texas at Dallas, Richardson TX; United States of America.
[43(a)]Department of Physics, Stockholm University;[(b)]Oskar Klein Centre, Stockholm; Sweden.
[44]Deutsches Elektronen-Synchrotron DESY, Hamburg and Zeuthen; Germany.
[45]Lehrstuhl für Experimentelle Physik IV, Technische Universität Dortmund, Dortmund; Germany.
[46]Institut für Kern- und Teilchenphysik, Technische Universität Dresden, Dresden; Germany.
[47]Department of Physics, Duke University, Durham NC; United States of America.
[48]SUPA - School of Physics and Astronomy, University of Edinburgh, Edinburgh; United Kingdom.
[49]INFN e Laboratori Nazionali di Frascati, Frascati; Italy.
[50]Physikalisches Institut, Albert-Ludwigs-Universität Freiburg, Freiburg; Germany.
[51]II. Physikalisches Institut, Georg-August-Universität Göttingen, Göttingen; Germany.
[52]Département de Physique Nucléaire et Corpusculaire, Université de Genève, Genève; Switzerland.
[53(a)]Dipartimento di Fisica, Università di Genova, Genova;[(b)]INFN Sezione di Genova; Italy.
[54]II. Physikalisches Institut, Justus-Liebig-Universität Giessen, Giessen; Germany.
[55]SUPA - School of Physics and Astronomy, University of Glasgow, Glasgow; United Kingdom.
[56]LPSC, Université Grenoble Alpes, CNRS/IN2P3, Grenoble INP, Grenoble; France.
[57]Laboratory for Particle Physics and Cosmology, Harvard University, Cambridge MA; United States of America.
[58(a)]Department of Modern Physics and State Key Laboratory of Particle Detection and Electronics, University of Science and Technology of China, Hefei;[(b)]Institute of Frontier and Interdisciplinary Science and Key Laboratory of Particle Physics and Particle Irradiation (MOE), Shandong University, Qingdao;[(c)]School of Physics and Astronomy, Shanghai Jiao Tong University, KLPPAC-MoE, SKLPPC, Shanghai;[(d)]Tsung-Dao Lee Institute, Shanghai; China.
[59(a)]Kirchhoff-Institut für Physik, Ruprecht-Karls-Universität Heidelberg, Heidelberg;[(b)]Physikalisches Institut, Ruprecht-Karls-Universität Heidelberg, Heidelberg; Germany.
[60]Faculty of Applied Information Science, Hiroshima Institute of Technology, Hiroshima; Japan.
[61(a)]Department of Physics, Chinese University of Hong Kong, Shatin, N.T., Hong Kong;[(b)]Department of Physics, University of Hong Kong, Hong Kong;[(c)]Department of Physics and Institute for Advanced Study, Hong Kong University of Science and Technology, Clear Water Bay, Kowloon, Hong Kong; China.
[62]Department of Physics, National Tsing Hua University, Hsinchu; Taiwan.
[63]Department of Physics, Indiana University, Bloomington IN; United States of America.
[64(a)]INFN Gruppo Collegato di Udine, Sezione di Trieste, Udine;[(b)]ICTP, Trieste;[(c)]Dipartimento di Chimica, Fisica e Ambiente, Università di Udine, Udine; Italy.
[65(a)]INFN Sezione di Lecce;[(b)]Dipartimento di Matematica e Fisica, Università del Salento, Lecce; Italy.
[66(a)]INFN Sezione di Milano;[(b)]Dipartimento di Fisica, Università di Milano, Milano; Italy.

[67(a)]INFN Sezione di Napoli;[(b)]Dipartimento di Fisica, Università di Napoli, Napoli; Italy.
[68(a)]INFN Sezione di Pavia;[(b)]Dipartimento di Fisica, Università di Pavia, Pavia; Italy.
[69(a)]INFN Sezione di Pisa;[(b)]Dipartimento di Fisica E. Fermi, Università di Pisa, Pisa; Italy.
[70(a)]INFN Sezione di Roma;[(b)]Dipartimento di Fisica, Sapienza Università di Roma, Roma; Italy.
[71(a)]INFN Sezione di Roma Tor Vergata;[(b)]Dipartimento di Fisica, Università di Roma Tor Vergata, Roma; Italy.
[72(a)]INFN Sezione di Roma Tre;[(b)]Dipartimento di Matematica e Fisica, Università Roma Tre, Roma; Italy.
[73(a)]INFN-TIFPA;[(b)]Università degli Studi di Trento, Trento; Italy.
[74]Institut für Astro- und Teilchenphysik, Leopold-Franzens-Universität, Innsbruck; Austria.
[75]University of Iowa, Iowa City IA; United States of America.
[76]Department of Physics and Astronomy, Iowa State University, Ames IA; United States of America.
[77]Joint Institute for Nuclear Research, Dubna; Russia.
[78(a)]Departamento de Engenharia Elétrica, Universidade Federal de Juiz de Fora (UFJF), Juiz de Fora;[(b)]Universidade Federal do Rio De Janeiro COPPE/EE/IF, Rio de Janeiro;[(c)]Universidade Federal de São João del Rei (UFSJ), São João del Rei;[(d)]Instituto de Física, Universidade de São Paulo, São Paulo; Brazil.
[79]KEK, High Energy Accelerator Research Organization, Tsukuba; Japan.
[80]Graduate School of Science, Kobe University, Kobe; Japan.
[81(a)]AGH University of Science and Technology, Faculty of Physics and Applied Computer Science, Krakow;[(b)]Marian Smoluchowski Institute of Physics, Jagiellonian University, Krakow; Poland.
[82]Institute of Nuclear Physics Polish Academy of Sciences, Krakow; Poland.
[83]Faculty of Science, Kyoto University, Kyoto; Japan.
[84]Kyoto University of Education, Kyoto; Japan.
[85]Research Center for Advanced Particle Physics and Department of Physics, Kyushu University, Fukuoka ; Japan.
[86]Instituto de Física La Plata, Universidad Nacional de La Plata and CONICET, La Plata; Argentina.
[87]Physics Department, Lancaster University, Lancaster; United Kingdom.
[88]Oliver Lodge Laboratory, University of Liverpool, Liverpool; United Kingdom.
[89]Department of Experimental Particle Physics, Jožef Stefan Institute and Department of Physics, University of Ljubljana, Ljubljana; Slovenia.
[90]School of Physics and Astronomy, Queen Mary University of London, London; United Kingdom.
[91]Department of Physics, Royal Holloway University of London, Egham; United Kingdom.
[92]Department of Physics and Astronomy, University College London, London; United Kingdom.
[93]Louisiana Tech University, Ruston LA; United States of America.
[94]Fysiska institutionen, Lunds universitet, Lund; Sweden.
[95]Centre de Calcul de l'Institut National de Physique Nucléaire et de Physique des Particules (IN2P3), Villeurbanne; France.
[96]Departamento de Física Teorica C-15 and CIAFF, Universidad Autónoma de Madrid, Madrid; Spain.
[97]Institut für Physik, Universität Mainz, Mainz; Germany.
[98]School of Physics and Astronomy, University of Manchester, Manchester; United Kingdom.
[99]CPPM, Aix-Marseille Université, CNRS/IN2P3, Marseille; France.
[100]Department of Physics, University of Massachusetts, Amherst MA; United States of America.
[101]Department of Physics, McGill University, Montreal QC; Canada.
[102]School of Physics, University of Melbourne, Victoria; Australia.
[103]Department of Physics, University of Michigan, Ann Arbor MI; United States of America.
[104]Department of Physics and Astronomy, Michigan State University, East Lansing MI; United States of America.

[105]B.I. Stepanov Institute of Physics, National Academy of Sciences of Belarus, Minsk; Belarus.
[106]Research Institute for Nuclear Problems of Byelorussian State University, Minsk; Belarus.
[107]Group of Particle Physics, University of Montreal, Montreal QC; Canada.
[108]P.N. Lebedev Physical Institute of the Russian Academy of Sciences, Moscow; Russia.
[109]Institute for Theoretical and Experimental Physics (ITEP), Moscow; Russia.
[110]National Research Nuclear University MEPhI, Moscow; Russia.
[111]D.V. Skobeltsyn Institute of Nuclear Physics, M.V. Lomonosov Moscow State University, Moscow; Russia.
[112]Fakultät für Physik, Ludwig-Maximilians-Universität München, München; Germany.
[113]Max-Planck-Institut für Physik (Werner-Heisenberg-Institut), München; Germany.
[114]Nagasaki Institute of Applied Science, Nagasaki; Japan.
[115]Graduate School of Science and Kobayashi-Maskawa Institute, Nagoya University, Nagoya; Japan.
[116]Department of Physics and Astronomy, University of New Mexico, Albuquerque NM; United States of America.
[117]Institute for Mathematics, Astrophysics and Particle Physics, Radboud University Nijmegen/Nikhef, Nijmegen; Netherlands.
[118]Nikhef National Institute for Subatomic Physics and University of Amsterdam, Amsterdam; Netherlands.
[119]Department of Physics, Northern Illinois University, DeKalb IL; United States of America.
[120(a)]Budker Institute of Nuclear Physics, SB RAS, Novosibirsk;[(b)]Novosibirsk State University Novosibirsk; Russia.
[121]Department of Physics, New York University, New York NY; United States of America.
[122]Ohio State University, Columbus OH; United States of America.
[123]Faculty of Science, Okayama University, Okayama; Japan.
[124]Homer L. Dodge Department of Physics and Astronomy, University of Oklahoma, Norman OK; United States of America.
[125]Department of Physics, Oklahoma State University, Stillwater OK; United States of America.
[126]Palacký University, RCPTM, Joint Laboratory of Optics, Olomouc; Czech Republic.
[127]Center for High Energy Physics, University of Oregon, Eugene OR; United States of America.
[128]LAL, Université Paris-Sud, CNRS/IN2P3, Université Paris-Saclay, Orsay; France.
[129]Graduate School of Science, Osaka University, Osaka; Japan.
[130]Department of Physics, University of Oslo, Oslo; Norway.
[131]Department of Physics, Oxford University, Oxford; United Kingdom.
[132]LPNHE, Sorbonne Université, Paris Diderot Sorbonne Paris Cité, CNRS/IN2P3, Paris; France.
[133]Department of Physics, University of Pennsylvania, Philadelphia PA; United States of America.
[134]Konstantinov Nuclear Physics Institute of National Research Centre "Kurchatov Institute", PNPI, St. Petersburg; Russia.
[135]Department of Physics and Astronomy, University of Pittsburgh, Pittsburgh PA; United States of America.
[136(a)]Laboratório de Instrumentação e Física Experimental de Partículas - LIP;[(b)]Departamento de Física, Faculdade de Ciências, Universidade de Lisboa, Lisboa;[(c)]Departamento de Física, Universidade de Coimbra, Coimbra;[(d)]Centro de Física Nuclear da Universidade de Lisboa, Lisboa;[(e)]Departamento de Física, Universidade do Minho, Braga;[(f)]Departamento de Física Teorica y del Cosmos, Universidad de Granada, Granada (Spain);[(g)]Dep Física and CEFITEC of Faculdade de Ciências e Tecnologia, Universidade Nova de Lisboa, Caparica; Portugal.
[137]Institute of Physics, Academy of Sciences of the Czech Republic, Prague; Czech Republic.
[138]Czech Technical University in Prague, Prague; Czech Republic.

[139]Charles University, Faculty of Mathematics and Physics, Prague; Czech Republic.
[140]State Research Center Institute for High Energy Physics, NRC KI, Protvino; Russia.
[141]Particle Physics Department, Rutherford Appleton Laboratory, Didcot; United Kingdom.
[142]IRFU, CEA, Université Paris-Saclay, Gif-sur-Yvette; France.
[143]Santa Cruz Institute for Particle Physics, University of California Santa Cruz, Santa Cruz CA; United States of America.
[144(a)]Departamento de Física, Pontificia Universidad Católica de Chile, Santiago;[(b)]Departamento de Física, Universidad Técnica Federico Santa María, Valparaíso; Chile.
[145]Department of Physics, University of Washington, Seattle WA; United States of America.
[146]Department of Physics and Astronomy, University of Sheffield, Sheffield; United Kingdom.
[147]Department of Physics, Shinshu University, Nagano; Japan.
[148]Department Physik, Universität Siegen, Siegen; Germany.
[149]Department of Physics, Simon Fraser University, Burnaby BC; Canada.
[150]SLAC National Accelerator Laboratory, Stanford CA; United States of America.
[151]Physics Department, Royal Institute of Technology, Stockholm; Sweden.
[152]Departments of Physics and Astronomy, Stony Brook University, Stony Brook NY; United States of America.
[153]Department of Physics and Astronomy, University of Sussex, Brighton; United Kingdom.
[154]School of Physics, University of Sydney, Sydney; Australia.
[155]Institute of Physics, Academia Sinica, Taipei; Taiwan.
[156(a)]E. Andronikashvili Institute of Physics, Iv. Javakhishvili Tbilisi State University, Tbilisi;[(b)]High Energy Physics Institute, Tbilisi State University, Tbilisi; Georgia.
[157]Department of Physics, Technion, Israel Institute of Technology, Haifa; Israel.
[158]Raymond and Beverly Sackler School of Physics and Astronomy, Tel Aviv University, Tel Aviv; Israel.
[159]Department of Physics, Aristotle University of Thessaloniki, Thessaloniki; Greece.
[160]International Center for Elementary Particle Physics and Department of Physics, University of Tokyo, Tokyo; Japan.
[161]Graduate School of Science and Technology, Tokyo Metropolitan University, Tokyo; Japan.
[162]Department of Physics, Tokyo Institute of Technology, Tokyo; Japan.
[163]Tomsk State University, Tomsk; Russia.
[164]Department of Physics, University of Toronto, Toronto ON; Canada.
[165(a)]TRIUMF, Vancouver BC;[(b)]Department of Physics and Astronomy, York University, Toronto ON; Canada.
[166]Division of Physics and Tomonaga Center for the History of the Universe, Faculty of Pure and Applied Sciences, University of Tsukuba, Tsukuba; Japan.
[167]Department of Physics and Astronomy, Tufts University, Medford MA; United States of America.
[168]Department of Physics and Astronomy, University of California Irvine, Irvine CA; United States of America.
[169]Department of Physics and Astronomy, University of Uppsala, Uppsala; Sweden.
[170]Department of Physics, University of Illinois, Urbana IL; United States of America.
[171]Instituto de Física Corpuscular (IFIC), Centro Mixto Universidad de Valencia - CSIC, Valencia; Spain.
[172]Department of Physics, University of British Columbia, Vancouver BC; Canada.
[173]Department of Physics and Astronomy, University of Victoria, Victoria BC; Canada.
[174]Fakultät für Physik und Astronomie, Julius-Maximilians-Universität Würzburg, Würzburg; Germany.
[175]Department of Physics, University of Warwick, Coventry; United Kingdom.
[176]Waseda University, Tokyo; Japan.
[177]Department of Particle Physics, Weizmann Institute of Science, Rehovot; Israel.

[178]Department of Physics, University of Wisconsin, Madison WI; United States of America.
[179]Fakultät für Mathematik und Naturwissenschaften, Fachgruppe Physik, Bergische Universität Wuppertal, Wuppertal; Germany.
[180]Department of Physics, Yale University, New Haven CT; United States of America.
[181]Yerevan Physics Institute, Yerevan; Armenia.
[a] Also at Borough of Manhattan Community College, City University of New York, NY; United States of America.
[b] Also at Centre for High Performance Computing, CSIR Campus, Rosebank, Cape Town; South Africa.
[c] Also at CERN, Geneva; Switzerland.
[d] Also at CPPM, Aix-Marseille Université, CNRS/IN2P3, Marseille; France.
[e] Also at Département de Physique Nucléaire et Corpusculaire, Université de Genève, Genève; Switzerland.
[f] Also at Departament de Fisica de la Universitat Autonoma de Barcelona, Barcelona; Spain.
[g] Also at Departamento de Física Teorica y del Cosmos, Universidad de Granada, Granada (Spain); Spain.
[h] Also at Department of Applied Physics and Astronomy, University of Sharjah, Sharjah; United Arab Emirates.
[i] Also at Department of Financial and Management Engineering, University of the Aegean, Chios; Greece.
[j] Also at Department of Physics and Astronomy, University of Louisville, Louisville, KY; United States of America.
[k] Also at Department of Physics and Astronomy, University of Sheffield, Sheffield; United Kingdom.
[l] Also at Department of Physics, California State University, Fresno CA; United States of America.
[m] Also at Department of Physics, California State University, Sacramento CA; United States of America.
[n] Also at Department of Physics, King's College London, London; United Kingdom.
[o] Also at Department of Physics, St. Petersburg State Polytechnical University, St. Petersburg; Russia.
[p] Also at Department of Physics, Stanford University; United States of America.
[q] Also at Department of Physics, University of Fribourg, Fribourg; Switzerland.
[r] Also at Department of Physics, University of Michigan, Ann Arbor MI; United States of America.
[s] Also at Dipartimento di Fisica E. Fermi, Università di Pisa, Pisa; Italy.
[t] Also at Giresun University, Faculty of Engineering, Giresun; Turkey.
[u] Also at Graduate School of Science, Osaka University, Osaka; Japan.
[v] Also at Hellenic Open University, Patras; Greece.
[w] Also at Horia Hulubei National Institute of Physics and Nuclear Engineering, Bucharest; Romania.
[x] Also at II. Physikalisches Institut, Georg-August-Universität Göttingen, Göttingen; Germany.
[y] Also at Institucio Catalana de Recerca i Estudis Avancats, ICREA, Barcelona; Spain.
[z] Also at Institut für Experimentalphysik, Universität Hamburg, Hamburg; Germany.
[aa] Also at Institute for Mathematics, Astrophysics and Particle Physics, Radboud University Nijmegen/Nikhef, Nijmegen; Netherlands.
[ab] Also at Institute for Particle and Nuclear Physics, Wigner Research Centre for Physics, Budapest; Hungary.
[ac] Also at Institute of Particle Physics (IPP); Canada.
[ad] Also at Institute of Physics, Academia Sinica, Taipei; Taiwan.
[ae] Also at Institute of Physics, Azerbaijan Academy of Sciences, Baku; Azerbaijan.
[af] Also at Institute of Theoretical Physics, Ilia State University, Tbilisi; Georgia.
[ag] Also at Istanbul University, Dept. of Physics, Istanbul; Turkey.
[ah] Also at LAL, Université Paris-Sud, CNRS/IN2P3, Université Paris-Saclay, Orsay; France.
[ai] Also at Louisiana Tech University, Ruston LA; United States of America.
[aj] Also at Manhattan College, New York NY; United States of America.

[ak] Also at Moscow Institute of Physics and Technology State University, Dolgoprudny; Russia.
[al] Also at National Research Nuclear University MEPhI, Moscow; Russia.
[am] Also at Physikalisches Institut, Albert-Ludwigs-Universität Freiburg, Freiburg; Germany.
[an] Also at School of Physics, Sun Yat-sen University, Guangzhou; China.
[ao] Also at The City College of New York, New York NY; United States of America.
[ap] Also at The Collaborative Innovation Center of Quantum Matter (CICQM), Beijing; China.
[aq] Also at Tomsk State University, Tomsk, and Moscow Institute of Physics and Technology State University, Dolgoprudny; Russia.
[ar] Also at TRIUMF, Vancouver BC; Canada.
[as] Also at Universita di Napoli Parthenope, Napoli; Italy.
[*] Deceased